TECHNISCHE UNIVERSITÄT MÜNCHEN

Fakultät für Medizin

Ewing Sarcoma-Derived Extracellular Vesicles Impair Dendritic Cell Maturation and Function, and Upregulate Endogenous Retroelements

Dr. med. Hendrik Maximilian Gaßmann

Vollständiger Abdruck der von der Fakultät für Medizin der Technischen Universität München zur Erlangung des akademischen Grades eines

Doctors of Philosophy (Ph.D.)

genehmigten Dissertation.

Vorsitz: Prof. Dr. Ruben Portuges

Betreuer: Prof. Dr. Stefan Burdach

Prüfende/-r der Dissertation:

1. Priv.-Doz. Dr. Uwe Thiel
2. Prof. Dr. Elfriede Nößner
3. apl. Prof. Dr. Martin S. Staege

Die Dissertation wurde am 11.10.2022 bei der Fakultät für Medizin der Technischen Universität München eingereicht und durch die Fakultät für Medizin am 25.01.2023 angenommen.

For Caterina and our families

Table of contents

1 Summary

1.1 English abstract

Background and aims: Ewing Sarcoma (EwS) is a non-immunogenic pediatric solid tumor of bone and soft tissues with high metastatic capacity. EwS is scarcely infiltrated by T cells and harbors immunosuppressive M2 macrophages; however, the mechanisms of the immunosuppressive tumor microenvironment (TME) are not fully understood. As extracellular vesicles (EVs) facilitate cancer-host communication, this work hypothesized that EwS EVs may pathologically activate myeloid cells affecting differentiation and functionality.

Methods: EVs were isolated by differential centrifugation or size exclusion chromatography from supernatants of EwS and MRC5 fibroblast cell lines, and from plasma of EwS patients and healthy donors. EV preparations were quantified and characterized using nanoparticle tracking analysis, immunoblotting and flow cytometry. The effect of 0.075–4.0 x 10^{10} EV particles on healthy donor-derived $CD33^+$ and $CD14^+$ myeloid cells *in vitro* was determined by cytokine multiplex assay, flow cytometry, whole transcriptome sequencing and sqRT-PCR. The T cell stimulatory function of monocytic-derived dendritic cells (moDC) differentiated in the presence of EVs was analyzed by cytokine multiplex assay and flow cytometry. Endogenous retroelements (RE) and satellite repeats were quantified by sqRT-PCR in $CD14^+$ myeloid cells and assessed by PrimeFlow RNA assay in peripheral blood mononuclear cells (PBMCs) of EwS patients and healthy donors.

Results: EV preparations exhibited characteristics of small EVs, including size (100–170 nm) and protein markers CD63, CD81 and TSG101. Treatment of $CD33^+$ and $CD14^+$ myeloid cells with EwS EVs, but not with MRC5 or healthy donor plasma EVs induced pro-inflammatory cytokine release, including IL-6, IL-8 and tumor-necrosis factor (TNF). Moreover, EwS EVs impaired their differentiation towards moDCs, as evidenced by reduced expression of co-stimulatory molecules CD80, CD86 and human leukocyte antigen (HLA)-DR. Whole transcriptome analysis demonstrated activation of expression programs consistent with a pro-inflammatory response, semi-mature phenotype and interferon (IFN)-stimulated genes (ISGs). EwS EV-treated moDCs significantly inhibited the proliferation of $CD4^+$ and $CD8^+$ T cells and reduced the IFNγ-release, while inducing secretion of IL-10 and IL-6. EwS EV-treated $CD14^+$ monocytes upregulated cGAS and RIG-I, released type I IFNs and accumulated RE, including HERV-K and LINE-1, and satellite repeats, including HSAT2 and ACRO1. Finally, expansion of $CD33^+$ myeloid cells with a myeloid-derived suppressor cell (MDSC)-like phenotype expressing HERV-K and HSAT2 was observed in EwS patients compared to healthy donors.

Conclusion: EwS EVs elicit a pro-inflammatory response and impair the maturation and stimulatory function of moDCs. EwS EVs may induce expression of RE and satellite repeats in myeloid cells rather than transferring them, warranting further mechanistic and functional studies. Therefore, EwS EVs may pathologically activate myeloid cells in the blood and the TME promoting tumor-infiltrating immunosuppressive myeloid cells in EwS patients.

1.2 German abstract

Hintergrund und Ziele: Das Ewing Sarkom (EwS) ist ein aggressiver, nicht-immunogener Knochen- und Weichteiltumor des Kindes- und jungen Erwachsenenalters. Während das EwS nur gering von T-Zellen infiltriert ist, zeigt sich eine deutliche Infiltration mit immunsuppressiven M2 Makrophagen. Jedoch sind die Mechanismen der Entstehung dieses immunsuppressiven *tumor microenvironment* (TME) nur teilweise verstanden. Extrazelluläre Vesikel (EVs) sind ein wesentlicher Bestandteil in der Kommunikation eines Tumors mit seiner Umgebung. Daher war die Hypothese dieser Arbeit, dass EVs des EwS myeloische Zellen pathologisch aktivieren und ihre Reifung und Funktionalität beeinträchtigen.

Methoden: EVs wurden mittels differentieller Zentrifugation oder Größenausschluss-Chromatographie aus dem Zellkulturüberstand von EwS und MRC5 Fibroblasten Zelllinien oder dem Plasma von EwS Patienten und gesunden Spendern isoliert. EV Präparationen wurden anhand von *nanoparticle tracking analysis*, Western Blot und Durchflusszytometrie quantifiziert und charakterisiert. Untersucht wurde der *in vitro*-Effekt von 0.075–4.0 x 10^{10} EV Partikeln auf $CD33^+$ and $CD14^+$ myeloische Zellen von gesunden Spendern mittels Zytokin Multiplex-ELISA, Durchflusszytometrie, Ganztranskriptom-RNA-Sequenzierung und sqRT-PCR. Die T-Zell-stimulatorische Funktion von Monozyten, die während der Differenzierung zu dendritischen Zellen (moDCs) mit EVs behandelt wurden, wurde mit Zytokin Multiplex-ELISA und Durchflusszytometrie bestimmt. Die Expression von endogenen Retroelementen (RE) und Satelliten-DNA wurde in $CD14^+$ myeloischen Zellen mittels sqRT-PCR quantifiziert und in mononukleären Zellen des peripheren Blutes (PBMCs) von EwS Patienten und gesunden Spendern anhand des *PrimeFlow RNA assay* gemessen.

Ergebnisse: EV Präparationen wiesen die Eigenschaften von *small EVs* auf, einschließlich der Größe (100–170 nm) und der Proteinmarker CD63, CD81 und TSG101. Im Gegensatz zu MRC5 EVs oder EVs aus dem Plasma von gesunden Spendern induzierte die Behandlung von $CD33^+$ und $CD14^+$ myeloischen Zellen mit EwS EVs die Freisetzung entzündlicher Zytokine, einschließlich IL-6, IL-8 und Tumornekrosefaktor (TNF). Darüber hinaus blockierten EwS EVs

die Differenzierung zu moDCs, was sich an einer geringeren Expression der kostimulatorischen Moleküle CD80, CD86 und des Humanen Leukozytenantigens (HLA)-DR zeigte. Die Ganztranskriptom-RNA-Sequenzierung ergab die Aktivierung von Expressionsprogrammen einer entzündlichen Reaktion, eines unreifen Phänotypen und von Interferon (IFN)-stimulierten Genen (ISGs). MoDCs, die in der Anwesenheit von EwS EVs differenziert wurden, hemmten signifikant die Proliferation von $CD4^+$ und $CD8^+$ T-Zellen und verminderten die Freisetzung von IFNγ, während die Ausschüttung von IL-10 und IL-6 stimuliert wurde. Die Behandlung von $CD14^+$ Monozyten mit EwS EVs induzierte cGAS und RIG-I, führte zur Freisetzung von Typ I IFN, sowie zur Akkumulation von RE (HERV-K und LINE-1) und der Satelliten-RNAs HSAT2 und ACRO1. Im Vergleich zu gesunden Spendern, waren die $CD33^+$ myeloische Zellen im Blut von EwS Patienten erhöht, zeigten den Phänotyp von *myeloid-derived suppressor cells* (MDSC) und wiesen eine höhere Expression von HERV-K und HSAT2 auf.

Schlussfolgerung: EVs von EwS Zelllinien rufen eine entzündliche Reaktion in myeloischen Zellen hervor und blockieren deren Reifung und Funktionalität. EwS EVs scheinen hierbei die Expression von RE und Satelliten-DNA in myeloischen Zellen eher zu induzieren als diese zu transferieren. EwS EVs könnten daher myeloischen Zellen im peripheren Blut sowie im TME pathologisch aktivieren, was möglicherweise zur Entstehung von Tumor-infiltrierenden immunsuppressiven myeloischen Zellen in Patienten mit EwS führt.

2 Introduction

2.1 Ewing sarcoma (EwS)

2.1.1 Molecular characteristics, epidemiology and therapy of EwS

Pediatric sarcomas account for roughly 10–12 % of childhood cancers [1]. Together, osteosarcoma and Ewing Sarcoma (EwS) comprise the two most frequent bone tumors. EwS is a non-immunogenic tumor of bones and soft tissues with poor survival in case of metastasis or relapse within 2 years [2].

EwS features small, round, blue tumor cells of mesenchymal or neuroectodermal origin immunohistochemically staining for cluster of differentiation (CD)99 [3-5]. EwS harbor a chromosomal translocation generating a gene fusion between the FET gene family[1] (Ewing's sarcoma breakpoint region 1 (EWSR1), fused in sarcoma (FUS) and TATA-binding protein-associated factor 15 (TAF15)) and the E-twenty-six (ETS) family of transcription factors [6]. In 85 % of the cases, the chromosomal translocation occurs between EWSR1 and Friend leukemia virus integration 1 (FLI1), t(11;22)(q24;q12) [7]. The resulting FET-ETS fusion proteins interfere with gene expression and redirect the epigenome by recruiting the chromatin remodelling complexes BAF, CBP/p300 and MLL methyltransferase [8]. Further mutations are rare with mutations in the cohesin subunit SA-2 (STAG2) and tumor suppressor p53 (TP53) genes arising in 22 % and 6 % of total cases [9,10].

EwS develops at a median age of 15 years with an incidence of 1.5/1,000,000 [8,11]. 80 % of EwS localize in the bone mostly affecting the lower and upper extremities, pelvis, thoracic wall and the spine. Extraosseous manifestations occur mainly at the trunk, extremity, head and neck as well as retroperitoneum [12]. In localized EwS, the 5-year survival is 75 %. However, 25 % of patients present with metastasis at diagnosis, which decreases the 5-year survival to ≤ 30 % [13-15]. The most common metastatic sides include lung, bone and bone marrow. Patients with advanced EwS, defined as ≥ 2 bone metastases, bone marrow involvement or relapse ≤ 24 months, carry a poor prognosis with 5-year survival rates ≤ 15 % [15-17].

Standard therapy in Germany is based on the Ewing 2012 protocol comprising induction multi-agent chemotherapy, surgery and/or radiation therapy for local tumor control and consolidation chemotherapy [6]. Induction chemotherapy contains vincristine, ifosfamide, doxorubicin and etoposide (VIDE) and is administered in 6 cycles of 3–4 week-intervals [18]. Consolidation chemotherapy includes either vincristine and actinomycin D with

[1] The FET gene family is also known as the TET family (Translocated in liposarcoma, Ewing's sarcoma and TATA-binding protein-associated factor 15), which differs from the ten-eleven translocation (TET) family of methylcytosine dioxygenases.

cyclophosphamide or ifosfamide [19], or high-dose busulfan and melphalane chemotherapy followed with autologous stem cell rescue for high risk patients (poor histological response to induction chemotherapy, tumor volume > 200 ml) [20].

In disseminated multifocal EwS and advanced EwS, allogeneic stem cell transplantation (SCT) has been utilized [21], intending a graft-versus-tumor effect. Long-term survival after allogeneic transplantation was reported in 3/11 patients with metastasized EwS not exceeding results from standard treatment [22,23]. A retrospective data analysis compared reduced- with high-intensity-conditioning regimes prior to allogeneic SCT and found no difference in overall survival [24]. Furthermore, haploidentical transplantation showed no improved survival compared with human leukocyte antigen (HLA)-matched allogeneic grafts suggesting the absence of a graft-versus-EwS effect [25]. Prospective randomized trials are required to further evaluate the effect of allogeneic SCT in patients with advanced EwS. For patients with metastasis or bone marrow involvement, novel therapy strategies are highly needed [26].

2.1.2 Immunotherapy in EwS

Harnessing the immune system for cancer treatment dates back to the 19th century, where Sir William Coley inoculated patients with inoperable sarcomas with heat inactivated bacteria achieving clinical remissions [27]. Since than the field of immunotherapy has grown and technology has advanced. Currently, cancer immunotherapy is categorized in immune modulatory approaches as well as active and passive immunization.

To enhance an anti-tumor immune response, the negative regulators of T cell activation, called immune checkpoint molecules, can be blocked. Immune checkpoint molecules are cell surface receptors and include the programmed cell death protein 1 (PD-1), programmed death ligand 1 (PD-L1) and cytotoxic T lymphocyte antigen-4 (CTLA-4). However, PD-L1 and PD-1 expression are infrequent on EwS (0–19 % [28-32] and 19–26 % [30,32], respectively) and checkpoint inhibitors (CPI) failed to demonstrate clinical responses in patients with EwS [31,33,34].

Anti-tumor immune responses can also be mounted by adoptively transferring tumor-infiltrating or genetically engineered T cells [35-37]. Genetically engineered chimeric antigen receptor (CAR) T cells express antibody binding domains with antigen specificity on the cell surface combined with the intracellular domain of the CD3ζ chain. Thus, CAR T cells can target surface proteins on tumor cells independent of major histocompatibility complexes (MHCs). Anti-CD19 CAR T cells achieved complete remissions in adult hematological malignancies [38,39] and 70–90 % response rates in pediatric lymphoblastic leukemia [40,41]. In preclinical

sarcoma models, CAR T cells showed encouraging results targeting B7-H3 (CD276) [42], type I insulin-like growth factor receptor (IGF1R), receptor tyrosine kinase-like orphan receptor 1 (ROR1) [43] or vascular endothelial growth factor receptor 2 (VEGFR2) [44]. Human epidermal growth factor receptor-2 (HER2)-CAR T cells achieved stable disease in 4/17 osteosarcoma patients for 3 to 14 months, while the solitary EwS patient enrolled in the trial showed progressive disease [45]. CAR T cells targeting the ganglioside antigen GD2, HER2 and B7H3 are currently evaluated in clinical trials for osteosarcoma and EwS (NCT03356782, NCT04433221). In contrast to CAR T cells, T cell receptor (TCR) transgenic T cells are directed against antigens in the context of MHCs, thus able to selectively target peptides derived from intracellular proteins, which are mutated or overexpressed in tumor cells. In EwS preclinical models, T cells retrovirally transduced with HLA-A*02:01 allorestricted TCRs recognizing peptides derived from chondromodulin-1 (CHM1), pregnancy-associated plasma protein-A (PAPPA) and six-transmembrane epithelial antigen of the prostate 1 (STEAP1) showed specific tumor recognition and lysis [46-49]. Promisingly, partial response in one of three refractory EwS patients was observed after administration of $CD8^+$ T cells with transgenic HLA-A*02:01/CHM1-specific allorestricted T cell receptor [50], suggesting assessment in phase I/II clinical trials.

Oncolytic virotherapy represents a further approach to lyse tumor cells and stimulate the immune system. Oncolytic viruses selectively infect and replicate in tumor cells sparing normal tissues [51]. The lysis of tumor cells by oncolytic viruses induces immunogenic cell death releasing tumor antigens and pro-inflammatory danger- and pathogen-associated molecular patterns (DAMPs, PAMPs), which activate the innate and adaptive immune system. In pediatric sarcomas, the oncolytic adenovirus XVir-N-31 increased the immunogenicity of tumor cells, promoted phagocytosis and antigen presentation by myeloid cells as well as T cell activity *in vitro* and in preclinical models, providing the rationale for further evaluation in a phase I/II clinical trial [52,53].

Despite promising results in pediatric hematological malignancies and preclinical sarcoma models, immunotherapy bares limitations in patients with pediatric bone and soft tissue tumors due to their low immunogenicity and immunosuppressive microenvironment [54].

2.1.3 Local and systemic tumor microenvironment in EwS

The tumor microenvironment (TME) in solid tumors comprises a three dimensional structure containing tumor cells, vessels, stromal cells and immune cells. Signaling in the TME is facilitated by cell-cell contacts or in para- and autocrine manner by soluble molecules, including

cytokines and chemokines, and vesicles [55]. The immunogenicity of solid tumors depends on their mutational load, the antigen presentation and the tumor-infiltrating immune cells [56].

Most pediatric solid tumors like EwS are non-immunogenic tumors with low mutation rate and T cell infiltration [57]. In contrast to the immunogenic melanoma, which carries a high mutational load, EwS harbors a low mutational burden forming few neoantigens [10,58,59] and shows low to absent MHC class I and II expression [60,61]. Low MHC class I expression correlates with reduced $CD8^+$ T cell infiltration in EwS [61]. Additionally, 30 % of EwS express non-classical MHC class I molecules with immunosupressive properties, like HLA-G [62,63].

The TME of EwS is scarcely infiltrated by cytotoxic $CD8^+$ T cells (12–38 %) [30,32,63], which correlates with worse survival rates [61,64,65]. However, EwS show heterogeneity in T cell infiltration, as one study reported T cell infiltration in 92 % of EwS samples [28]. Reasons for this heterogeneity might include the variable expression of MHC class I or of the C-X-C Motif Chemokine Ligand 9/10 - C-X-C Motif Chemokine Receptor 3 (CXCL9/10 - CXCR3) axis within the TME of EwS [61,64]. Of note, increased levels of $CD4^+CD25^{hi}FoxP3^+$ regulatory T cells in the bone marrow may contribute to metastasis in EwS [66].

EwS is also barely infiltrated by dendritic cells (DCs) [67], which are required for priming the adaptive T cell-mediated anti-tumor immunity. DCs are antigen-presenting cells, which sample tissues and present foreign or self peptides on MHC class I and II molecules (like HLA-DR) to T cells. Together with the presented antigen, DCs provide co-stimulatory signals, including surface molecules (e.g. CD80 and CD86) and cytokines for the activation of antigen-specific T cells. Thereby, DCs prime specific T cell responses against respective tumor-derived peptides and promote anti-tumor immunity [68].

In contrast to poor infiltration of $CD8^+$ T cells and DCs into the TME of EwS, the most frequent tumor-infiltrating immune cell type are tumor-associated macrophages (TAMs) with an immunosuppressive M2 transcriptome signature [65,69,70]. TAMs are mainly recruited as monocytes from the bone marrow by chemotactic signaling, for example by chemokine (C-C motif) ligand 2 (CCL2) and its receptor the C-C chemokine receptor type 2 (CCR2) [71]. Cytokines and other signals from the TME polarize the tumor-infiltrating monocytes into pro-tumorigenic TAMs and M2 macrophages, which in turn promote tumor growth by angiogenesis and tissue remodeling [72], as well as invasion and extravasation of EwS [73]. TAMs and M2 macrophages inhibit immune effector cells by interleukin (IL)-10 secretion, exclude T cells from entering the tumor core [74] or deprive L-arginine required for CD3ζ chain re-expression on T cells [75]. Myeloid cells in the TME of EwS can also express the inhibitory HLA-G, which was shown to impede degranulation of GD2-specific

CAR T cells *in vitro* [62]. In EwS, increased levels of $CD68^+$ macrophages [70] and the M2 macrophage transcriptome signature correlate with poor survival [65], while infiltration of $CD163^+$ TAMs was associated with localized disease [76]. Depleting macrophages using trabectidin enhanced the effect of the oncolytic herpes simplex virus rRp450 in an EwS A673 xenograft model [77].

Beside tumor-infiltrating immune cells, stromal cells may also influence the survival rates of EwS patients [78]. Fibroblasts in the TME of EwS were immunohistochemically shown to express IL-6 and *in vitro* treatment of EwS cell lines with IL-6 lead to signaling via IL-6R and phosphorylation of Signal Transducer And Activator Of Transcription 3 (STAT3), which protected the EwS cells from apoptosis and promoted migration [79].

In the blood circulation of EwS patients, the expansion of fibrocytes with properties of myeloid-derived suppressor cells (MDSCs) was reported [80]. These fibrocytes exhibited a phenotype different from myeloid cells ($CD45^+CD34^+CD33^{low}CD14^-CD163^-HLA\text{-}DR^+$) and produced indoleamine 2,3-dioxygenase (IDO) suppressing T cell proliferation *in vitro* [80]. MDSCs are immature myeloid cells able to inhibit T cell functions [81]. Expansion and chronic pathological activation of immature myeloid cells lead to accumulation of monocytic MDSCs (M-MDSCs; $CD11b^+CD33^+CD14^+HLA\text{-}DR^{low/-}CD15^-$) [82]. In particular, TME- or bone marrow-derived granulocyte colony-stimulating factor (G-CSF) or granulocyte-macrophage colony-stimulating factor (GM-CSF) promote the myelopoesis and expand immature myeloid cells, which in turn are recruited by chemokines like CCL2 to the TME. Within the TME, myeloid cells get pathologically activated by persistent pro-inflammatory signals like IL-1β, IL-6 and tumor-necrosis factor (TNF) [83]. Key transcription factors in the development of MDSCs include CCAAT-Enhancer Binding Protein (C/EBP), STAT1, STAT3 and nuclear factor kappa B (NF-κB) [84,85]. MDSCs impede T cells using several mechanisms: for example, MDSCs deplete L-arginine through secretion of arginase 1 (ARG1) [86], produce oxidative stress by generation of reactive oxygen species or release IL-10 and TGFβ promoting regulatory T cells [84]. Depleting MDSCs by all-trans retinoic acid improved the efficacy of GD2-CAR T cells in osteosarcoma xenografts [87]. In contrast to osteosarcoma, expansion of M-MDSCs in the blood circulation of EwS patients has not been reported before [80,88].

In summary, the local TME of EwS is characterized by scarce T cell infiltrates and is mainly populated by immunosuppressive myeloid cells. However, the mechanisms leading to the immunosuppressive TME in EwS are currently poorly understood.

2.2 Extracellular vesicles (EVs)

Extracellular vesicles (EVs) play key roles in the crosstalk of tumor cells and the immune system [89]. EVs comprise a heterogeneous population of vesicles enclosed by a lipid bilayer, are produced by nearly every cell and can transmit biomolecules to recipient cells [90].

2.2.1 Biogenesis and function of EVs

EVs either bud off from the plasma membrane as ectosomes (size 50–10,000 nm) or derive from the multivesicular endosome (MVE) in the cytoplasm as exosomes (30–160 nm) [91,92]. Exosomes are produced in the MVE by inward budding of the endosomal membrane forming intraluminal vesicles (ILVs) [93]. ILVs are loaded by the endosomal sorting complex required for transport (ESCRT) with biomolecules like proteins, lipids and nucleic acids [90]. ESCERT-independent mechanisms involved in the biogenesis of exosomes include the syntenin-Alix pathway [94], tumor susceptibility gene 101 (TSG101) and tetraspanins (CD63, CD81) [95]. Upon fusion of the MVE with the plasma membrane, the ILVs are released as exosomes into the extracellular space.

After release from the cell, ectosomes and exosomes interact with proteins in the interstitial fluid and blood plasma covering EVs with a protein corona [96]. EVs share biochemical and physical properties with lipoproteins and enveloped viruses complicating the attribution of functional effects to a certain subpopulation of EVs [97]. Furthermore, additional subtypes of EVs have been identified called exomers [98,99] and supermers [100]. Currently, the separation of small EV subtypes is under investigation, therefore the heterogeneous group of vesicles are here referred to as EVs [101].

Circulating EVs target and enter the recipient cell on several routes including surface binding, endocytosis and phagocytosis [102]. After internalization, EVs deliver their heterogeneous content mostly into the endosome from where 10–30 % of EVs reach the cytosol [103,104]. Depending on the cargo, EVs modulate gene expression, differentiation, proliferation, apoptosis and signaling in the recipient cell. Importantly, EVs can shuttle functional RNA molecules from the parental to the recipient cell, in which the RNA is translated [105]. An example for functional RNA transport by EVs are EBV-infected lymphoblastoid B cells, which can transfer EBV-encoded miRNAs via exosomes into monocytic-derived dendritic cells (moDCs) repressing EBV target genes [106].

In cancer, EVs orchestrate and remodel the TME, alter the cellular metabolism, prepare the metastatic niche, convey therapy resistance and educate immune cells [90]. Myeloid cells appear as a major recipient of tumor-derived EVs [107-113], likely because of their phagocytic activity.

Tumor-derived EVs contribute to chronic inflammation and promote the development of myeloid cells with immunosuppressive properties [114]. In particular, glioblastoma-derived EVs polarize monocytes into pro-tumorigenic M2 macrophages [115] and EVs derived from chronic lymphatic leukemia transfer the non-coding Y RNA hY4 to circulating monocytes, which is recognized intracellularly by toll-like receptor 7 (TLR7) inducing PD-L1 expression [116]. Melanoma EVs carrying heat shock protein (Hsp) 86 signal via TLR4 and upregulate PD-L1 on monocytes [117]. Thus, EVs exert pleiotropic functions in various cancers, yet the role of EVs in the TME of EwS has not been determined before.

2.2.2 EwS EVs

EVs from EwS cell lines and patient plasma range in size from 50–300 nm and carry the exosomal proteins Alix, Annexin A1, CD63 and CD81 as well as the chaperone proteins Hsp70 and Hsp90 [118-120]. The protein cargo in EwS EV functions mainly as binder for proteins and nucleic acids or mediates catalytic and structural molecule activity [120]. The majority of transcripts in EwS EVs are derived from intergenic or non-coding genomic regions [121] and the transcriptional signature is associated with G-protein-coupled signaling, neurotransmitter signaling and stemness [119].

The content of EwS EVs is affected by cell culture conditions and regulated by CD99. Culturing the EwS cell line SK-N-MC in 3D scaffolds increases the RNA amount of exosomal enhancer of Zeste, *Drosophila*, Homolog 2 (EZH2) [118], a downstream target of EWS-FLI1 [122]. EwS cell lines A4573, TC32 and TC71 exposed to oxidative stress produce EVs enriched for transcripts from intergenic and non-coding genomic regions [121]. Hypoxic EwS cell lines A673 and SK-ES-1 secret exosomes containing HIF-1α-induced miR-210, which targets CASP8AP2 in recipient EwS cells promoting cell survival and sphere formation [123]. CD99-silenced EwS cell lines TC71 and IOR/CAR release EVs enriched for miR-34a and miR-199a-3p. These miRNAs inhibited growth, proliferation and migration as well as induced neural differentiation in the recipient EwS cell lines via inhibition of Notch-NF-κB signaling and c-Fos downregulation [124,125].

EwS EVs disseminate via the blood circulation, as EWS-FLI1 mRNA was detected in plasma EVs isolated by 0.45 µm filtration from 3/7 and 4/10 mice xenografted with EwS cell lines A673 and TC135, respectively [126]. Moreover, in 7/10 EwS patients, EWS-FLI1 mRNA was detectable in plasma EVs isolated by immunoaffinity using antibodies against CD99 and nerve growth factor receptor (NGFR) [120]. Additionally, plasma particle counts were elevated in EwS patients compared to healthy donors [120]. Reminiscent of a chronic viral infection,

plasma EVs of EwS patients were significantly enriched for transcripts derived from non-coding genomic regions, in particular endogenous retroelements and satellite DNA, which were also detectable in EVs from EwS cell lines [121]. The role of increased levels of transcripts derived from endogenous retroelements and satellite DNA in the blood plasma and their effect on the immune system are currently unknown.

2.3 Role of repetitive non-coding genomic regions in cancer immunity

Over the past decade, the human genome and ENCODE projects as well as emerging research evidence demonstrated that three quarters of the human genome is transcribed [127], including endogenous retroelements (RE) and satellite DNA[2], which account for up to 43 % and 3 % of the genome, respectively (Figure 1) [128]. Being located in the constitutive heterochromatin regions, these non-coding repetitive DNA sequences were initially considered as "junk" in the genome. Recent studies showed that non-coding repetitive DNA sequences broadly impact the genome, cellular functions and immunity [129-133]. Aberrant activity of RE and satellite DNA is linked to aging, autoimmunity and cancer [130,134,135].

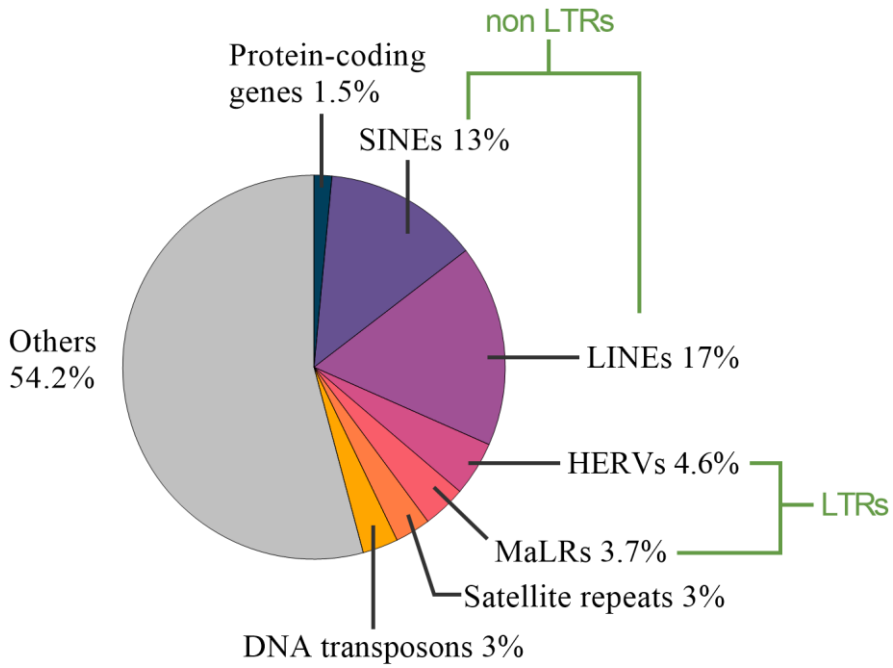

Figure 1 Repetitive sequences comprise large parts of the human genome.

The human genome contains the non-long-terminal repeat elements (LTR), in particular 17 % long interspersed nuclear elements (LINEs) [128] and 13.1 % short interspersed nuclear elements (SINEs) [136]; the LTR elements,

[2] The term satellite DNA derives from the lower buoyant density of satellite DNA in density gradient centrifugation due to the high AT base pair content in comparison to the main DNA.

in particular 4.6 % human endogenous retroviruses (HERVs) [137] and 3.65 % mammalian apparent LTR retrotransposons (MaLR) [128]; 3 % satellite DNA / satellite repeats [138] and 3 % DNA transposons [130].

2.3.1 Endogenous retroelements (RE)

RE are repetitive DNA sequences dispersed across the human genome. RE integrated into the human genome as exogenous retroviruses and throughout evolution most RE became replication-defective and immobile, due to accumulating mutations and truncations [139]. Epigenetic silencing restricts RE transcription, whereby epigenetic mechanisms include DNA methylation, interacting small RNAs, binding of Krüppel-associated box domain zinc-finger (KRAB-ZNF) proteins and chromatin remodeling [140,141].

Despite the lack of retrotransposition activity and epigenetic silencing, REs retained multiple regulatory functions in the genome, providing chromatin architecture, transcriptional control, and non-coding RNAs [142,143]. In particular, RE sequences were co-opted as promoters and enhancers, to modulate the expression of neighboring coding genes and regulatory networks, which operate during embryonic development, stem cell pluripotency [144,145], cancer [146] and immune responses [147,148]. For instance, MHC genes contain high RE density in their promoter regions and introns, contributing to genetic variations of MHC genes [149]. REs also play a pivotal role in shaping innate and adaptive immune responses, by functioning as interferon (IFN)-stimulated response elements (ISREs) to activate IFN networks [147].

Depending on the absence or presence of long terminal repeats (LTRs), REs can be divided into two subclasses. The non-LTR class includes long and short interspersed nuclear elements (LINEs and SINEs), which together constitute ~ 70–80 % of the genome-encoded REs. The remaining 20 % are LTR-containing elements, such as human endogenous retroviruses (HERVs) and mammalian apparent LTR retrotransposons (MaLR), which are spread in 700,000 different loci across the genome [139,150]. The canonical HERV structure shares genomic properties of exogenous retroviruses, with two LTRs flanking the *gag*, *env*, *pro* and *pol* genes encoding structural proteins (gag), the envelope protein (env) and viral enzymes, protease (pro) and polymerase (pol)/reverse transcriptase (RT), respectively [151]. The LTR regions contribute to transcription initiation and termination, while non-LTR REs utilize their 5'-untranslated regions (UTR) and 3'UTR as promoters and poly(A) sequence, respectively [152].

Although most of the HERV elements are represented by solitary LTRs, around 4,000 HERVs may possess partially intact open reading frames (ORFs) for HERV proteins, most notably, env, gag, RT and endonuclease, and some are still capable of autonomous retrotransposition [153]. This particularly concerns the most recently acquired and thus

biologically active HERV-K (HML-2) group[3], with multiple members retaining the capacity to form viral-like particles and to reinsert into the genome [151]. Among the non-LTR elements, only a small subset of LINE-1 elements (~ 100 of 500,000 copies) is retrotransposition-active and encodes functional RT and endonuclease [152]. Importantly, the HERV- and LINE-1-encoded enzymes may also reverse transcribe other RNAs, including SINEs, defective HERVs and various mRNAs, giving rise to pseudogenes, gene rearrangements, R-loops and RNA-DNA intermediates. In turn, accumulation of RNA-DNA hybrids as well as uncapped single-stranded (ss) and double-stranded (ds) RNAs in the affected cells induces innate immune responses, as described below in section 2.3.3 in more detail.

2.3.2 Pericentromeric and centromeric satellite DNA

Contrary to REs whose activities are largely neutral or deleterious for the genome [130,154], pericentromeric and centromeric satellite regions are critical for chromatin architecture, genome integrity and accurate chromosome segregation during mitosis [155-157]. In the human genome, satellite DNA is composed of highly variable tandemly repeated nucleotide sequences, mostly from alpha satellite and human satellite 2 and 3 (HSAT2, 3) families, which constitute ~ 2.6 % and 1.5 % of the human genome, respectively [138]. Centromeric chromatin is exclusively made up of alpha satellite, which is arranged into long arrays (3–5 Mb) of 171-base pair (bp) AT-rich tandemly repeated units [155]. It is distinguished by formation of the unique CENP-A-containing nucleosomes, and is important for centromere identity and kinetochore assembly. Conversely, pericentromeric heterochromatin is additionally populated by HSAT2, 3, ACRO1, LINEs and LTR/HERVs [158]. The large blocks of HSAT2 are defined by tandemly repeated ~23- to 26-bp ATTCC-enriched consensus motifs, and are found on chromosomes 1, 2, 7, 10, 16 and 22 [138,159]. Likewise, HSAT3 also consists of pentameric ATTCC/GGAAT repeats, albeit they are highly divergent and dispersed throughout pericentromeric regions of many chromosomes, often adjacent to HSAT2 and ACRO1. The latter is a moderately frequent 147-bp satellite repeat, mostly located on short arms of acrocentric chromosomes within the higher-order pericentromeric repeats [160]. Heterochromatin at centromeric and pericentromeric regions is formed through epigenetic mechanisms including histone lysin methylation, histone variants, DNA methylation and chromatin-remodeling complexes [155].

[3] HERVs are categorized in three classes (I, γ-retroviruses; II, β-retroviruses; III, spumaviruses) according to the sequence similarity in their *pol*-gene. HERV classes are further subgrouped based on the tRNA that binds the primer-binding site between the 5'LTR and *gag*-gene, e.g. lysine-tRNA for HERV-K (see reference 153). The term HML abbreviates human endogenous mouse mammary tumor virus-like.

Although satellite repeats are located in constitutively silent heterochromatin, low-level transcription from these regions is required for maintaining heterochromatin silencing and structural organization [157]. Pericentromeric regions are responsible for epigenetic regulation and reprogramming during early embryonic development, aging, cancer and stress response [156]. For instance, HSAT3 expression is activated from the 9q12 locus in HeLa cells in response to heat shock, oxidative stress and other stress conditions, with the respective HSAT3 RNAs acting as scaffolds for nuclear stress body assembly [161]. These bodies sequester RNA pol II, transcription and splicing factors, suggesting their role in regulating transcription and splicing during stress and recovery. Likewise, the mega-blocks of HSAT2 on 1q12 are frequently demethylated in cancer cells and are involved in sequestering Polycomb group repressive complexes and other chromatin-remodeling enzymes into the prominent Cancer-Associated Polycomb bodies, which may play a role in switching gene expression programs [162]. Hypomethylation of pericentromeric regions was also observed during physiological and premature aging and senescence, and was accompanied by elevated levels of HSAT2 and LINE-1 RNAs [163,164]. However, hypomethylation alone may not be sufficient for HSAT2 activation [165]. As described in the next sections, RE and HSAT2 are expressed in cancer and activate innate immune mechanisms by their immunogenic motifs.

2.3.3 Expression and immune response to RE and pericentromeric satellites in cancer

RE and satellite repeats are normally epigenetically silenced by DNA methylation and histone modifications [155]. However, cancer-associated epigenetic changes and cellular stress result in a wide-spread expression of RE and satellite repeats in various types of human malignancies [134,166-168], including pediatric solid tumors like osteosarcoma [169], EwS [121] and rhabdoid tumors [170]. In particular, compared to normal tissues, HSAT2 is one of the most abundant non-coding RNAs in epithelial cancers [134] and osteosarcomas [171]. HSAT2 RNAs are expressed in sense and antisense orientations and thus are prone to form dsRNAs [172,173]. In addition, HSAT2 RNAs are enriched in motifs containing CpG dinucleotides in AU-rich contexts, which are typically found in exogenous viral RNA [174]. Liposomal transfection of HSAT2 RNA into moDCs induced the release of the pro-inflammatory cytokines IL-6, IL-12 and TNF [174]. Due to these and further virus-like features, such as uncapped 5’ ends with exposed di- and triphosphate groups and the ability to generate RNA-DNA intermediates, HSAT2 and ERV/RE-encoded RNAs are recognized as “non-self” by the intracellular pattern recognition receptors (PRRs), thereby eliciting antiviral and pro-inflammatory responses in immune and non-immune cells [139,175-177].

Due to their ability to recognize PAMPs, PRRs play critical roles in restricting expression of RE and satellite repeats [139,175,176]. Deficiency of PRRs caused retroviral viremia and T cell lymphoblastic leukemia in murine models [178,179]. Intracellular PRRs reside within two compartments: (i) the endosomal TLRs (TLR3, TLR7, TLR8 and TLR9) and (ii) cytosolic receptors, including sensors of dsDNA and RNA-DNA hybrids (cyclic GMP-AMP synthase (cGAS)) or dsRNAs (the retinoic acid-inducible gene I (RIG-I) and melanoma differentiation associated gene 5 (MDA5)) [135,180]. Similar to TLR3, closely related RIG-I and MDA5 proteins recognize short (10–100 bp) and long (>300 bp) dsRNAs, respectively, including those of LTR/HERVs [176,181]. In addition, RIG-I can also be activated by uncapped ssRNAs with 5'-di- or tri-phosphate moieties [180,182].

While endosomal and cytosolic PRRs are activated by different PAMPs and proceed through distinct signaling cascades, they both converge upon activating NF-κB-driven pro-inflammatory responses and production of type I interferons (IFNs). Specifically, TLRs signal through myeloid differentiation primary response 88 protein (MYD88) or TIR-domain-containing adapter-inducing interferon-β (TRIF), while RIG-I and MDA5 engage the mitochondrial antiviral signaling protein (MAVS). Oligomerization of MAVS in turn activates TANK-binding kinase 1 (TBK1) and IκB kinase-ε (IKKε), and their downstream targets, the transcription factors IFN-regulatory factor 3 (IRF3) and IRF7 [180]. Upon activation, IRF3 and/or IRF7 translocate to the nucleus and together with NF-κB induce the expression of pro-inflammatory genes, including IL-6, IL-8 and TNF as well as IFNs. Likewise, sensing of cytosolic dsDNA or RNA-DNA hybrids by cGAS also induces type I IFNs, by converting GTP and ATP into cyclic GMP-AMP and activating the stimulator of IFN genes (STING) [176,183]. These mechanisms were shown to be activated by LTR/HERV-derived RNAs in cells treated with demethylating drugs [184], or by LINE-1 in autoimmune disorders and senescent cells [164,185].

Once secreted, type I IFNs signal in an autocrine and paracrine manner, by binding to the IFNα/β receptors (IFNARs) and activating the JAK-STAT pathway, including STAT1, STAT2 and IRF9. This heterodimeric complex binds to the promoters of ISREs and thereby enables the transcription of hundreds of IFN-stimulated genes (ISGs) [186]. The ISGs-encoded proteins inhibit cellular proliferation and potentiate antiviral defense [187]. For example, interferon-induced transmembrane proteins (IFITMs) impair the entry of enveloped viruses by trafficking viral particles into the lysosomes for degradation [188,189]. Together, the innate immune mechanisms of PRRs with downstream activation of type I IFNs and ISGs efficiently prevent

the accumulation of RE and satellite repeats, which otherwise could lead to neurodegenerative disorders, autoimmunity and cancer [135,190].

2.3.4 Role of RE and HSAT2 RNAs in cancer immunogenicity

Although RE and satellite repeats contribute to cancer development and progression [167,191,192], their role in cancer immunogenicity and immune evasion is controversial.

From one standpoint, the expression of RE and satellite repeats in cancer cells induces antiviral responses, thereby imposing a cellular state called viral mimicry [193]. In particular, elevated RE RNA levels in multiple cancer are associated with immunogenic signatures [166,194], immune infiltration [170,194-196], cytolytic activity [197] and responsiveness to anti-PD-1 immunotherapy [196,198]. Consequently, de-repression of RE/HERVs using the DNA methyltransferase inhibitors (DNMTi) decitabine and azacytidine (Aza) was proposed as a therapeutic strategy to activate viral mimicry and induce immunogenicity in non-immunogenic tumors [193]. Treatment with Aza improved survival in patients with myelodysplastic syndrome and acute myeloid leukemia [199], and enhanced anti-CTLA4 immune checkpoint blockade in a melanoma mouse model [184]. Monotherapy with Aza, however, failed to show antitumor activity in 7 advanced EwS patients [200]. In addition to demethylating agents, several other combinational treatments directed at inducing viral mimicry to enable checkpoint blockade are currently considered. This comprises pharmacologic activation of p53 [201], inhibition of cyclin-dependent kinases (CDKs, CDK4/6) [202] or blockade of epigenetic regulators, including histone deacetylases, methylases, demethylases (LSD1) and Polycomb proteins (EZH2) [203]. Targeting EZH2 may be especially relevant in EwS, given its role in EWS-FLI1-driven tumor growth and metastasis [122]. Indeed, EZH2 inhibitors were shown to induce RE expression together with interferon responses in EwS cell lines and in a variety of other cancer cells, while sparing non-transformed cells [204,205].

In contrast, several studies associated an elevated expression of RE and satellite repeats with worse survival and less immune infiltration. In gastrointestinal cancers, hypomethylation of LINE-1 as well as increased LINE-1 transcription and insertions were associated with reduced immune infiltration and advanced tumor stage [206,207]. In soft tissue sarcomas, increased HERV-K mRNA correlated with reduced relapse-free survival [208]. A recent study has identified a subclass of IFN-inducible HERV RNAs capable of activating TBK1-IRF3 and STAT1 signaling by engaging the RIG-I/MDA5-MAVS and cGAS-STING pathways [209]. The respective tumors expressing this subclass of HERVs exhibited features of an immunosuppressed TME with infiltration of MDSCs and macrophages, despite of MHC class I

upregulation on tumor cells and T cell infiltration [209]. Likewise, high expression of LINE-1 and HERVs was associated with downregulation of immune response signature genes and worse survival in colon and rectal adenocarcinomas [195]. The same study also demonstrated low cytotoxic $CD8^+$ T cell infiltration in 75 colon tumors with high HSAT2 expression [195]. A similar phenomenon was reported in a subset of $methylation^{low}$ pancreatic ductal adenocarcinomas (PDAC), where elevated expression of HERV transcripts was associated with MAVS-dependent upregulation of ISGs, a pro-inflammatory and pro-tumorigenic TME and poor patient outcome [210].

In summary, multiple whole transcriptome studies revealed co-expression of more than thousand different HERVs, LINEs and satellite transcripts in various types of cancer, likely due to broad dysregulation of epigenetic and innate immune regulatory mechanisms. Recently, it becomes apparent that RE are not restricted to cells, but can be released from parental cells in EVs [121,211-216]. Transcripts from RE and satellite repeats are upregulated in EwS cell line EVs and increased in plasma EVs of EwS patients compared to healthy donors [121].

In this study, we examined the possibility that EwS tumors may use EVs to release RE and satellite RNAs as a part of their immune evasion strategy. How tumor-derived EVs associated or loaded with viral-like transcripts derived from RE and satellites affect the immune system is currently unknown. The hypothesis of this study was that EwS EVs associated with RE transcripts may pathologically activate myeloid cells and skew their functionality, thereby promoting immune escape of EwS.

3 Research objectives and scientific aims

3.1 Research objectives

EwS is a non-immunogenic tumor with prominent immunosuppressive M2 macrophage infiltration, however, the underlying mechanisms are not well understood. As EVs mediate key roles in cancer-host communication, the hypothesis of present study was that EVs from EwS induce immunosuppressive properties in myeloid cells. The effect of EwS EVs on healthy donor-derived myeloid cells was assessed in an established *in vitro* model for the generation of moDCs [46]. Findings from the *in vitro* model were further evaluated in the plasma and peripheral blood mononuclear cells (PBMCs) from EwS patients and healthy donors.

3.2 Scientific aims

1. Isolation and characterization of EVs from EwS and MRC5 fibroblast cell lines as well as EVs from plasma of EwS patients and healthy donors.
2. Exploration of the effect of EwS EVs in comparison to control EVs from MRC5 and healthy donor plasma on the
    a. cytokine release,
    b. differentiation and maturation,
    c. gene expression and
    d. functionality

    of $CD14^+$ and $CD33^+$ myeloid cells and moDCs *in vitro*.
3. Investigation of the RE and satellite repeat expression in myeloid cells treated with EVs from EwS and MRC5 cells *in vitro.*
4. Analysis of RE and satellite expression in EwS patient PBMCs.

4 Materials and methods

4.1 Materials

4.1.1 List of manufacturers

Table 1: List of manufacturers

Manufacturer	Location
Abcam	Cambridge, UK
Adobe Inc	San José, California, USA
Agilent Technologies	Santa Clara, California, USA
Amcor	Zurich, Switzerland
Analytik Jena	Jena, Germany
Applied Biosystems	Darmstadt, Germany
ATCC	Rockyville, Maryland, USA
B. Braun Biotech	Melsungen, Germany
Biosciences Europe	Heidelberg, Germany
BioLegend	San Diego, California, USA
Bio-Rad Laboratories	Richmond, California, USA
Bio-Techne	Minneapolis, Minnesota, USA
Brand	Wertheim, Germany
Branson	Connecticut, USA
Carestream Health	Rochester, New York, USA
Carl Roth	Karlsruhe, Germany
Cayman Chemical Company	Ann Arbor, Michigan, USA
Cell Signaling Technology	Frankfurt a. M., Germany
Clarivate Analytics	Philadelphia, Pennsylvania, USA
Clinigen, Inc.	Yardley, Pennsylvania, USA
Childhood Cancer Repository (CCR)	Texas Tech University, USA
Corning	Corning, New York, USA
Cytiva	Marlborough, Massachusetts, USA
DRK-Blutspendedienst	Ulm, Germany
DSMZ	Braunschweig, Germany
Elma	Singen, Germany
Eppendorf	Hamburg, Germany
GE Healthcare	Little Chalfont, UK
Genzyme	Neu-Isenburg, Germany
GFL	Burgwedel, Germany
GLW	Würzburg, Germany
GraphPad Software	San Diego, California, USA
Greiner Bio-One	Frickenhausen, Germany
Heidolph Instruments	Schwabach, Germany
Heraeus	Hanau, Germany
Hettich	Tuttlingen, Germany
IKA-Werke	Staufen, Germany
Implen	München, Germany
Izon Science LTD	Lyon, France
Kern & Sohn	Balingen, Germany
Kisker Biotech	Steinfurt, Germany
Kodak	Rochester, New York, USA
Leica	Wetzlar, Germany
Lonza	Basel, Switzerland
Merck Millipore	Darmstadt, Germany
Metabion	Planegg, Germany
Mettler Toledo	Greifensee, Switzerland
Microsoft	Albuquerque, New Mexico, USA
Miltenyi Biotec	Bergisch Gladbach, Germany

Nalgene	Rochester, New York, USA
neoLab Migge	Heidelberg, Germany
Nobamed	Wetter, Germany
Particle Metrix	Inning am Ammersee, Germany
Paul Marienfeld	Lauda-Königshofen, Germany
Promega	Madison, Wisconsin, USA
Ratiopharm	Ulm, Germany
R&D Systems	Minneapolis, Minnesota, USA
Roche	Penzberg, Germany; Basel, Switzerland
Roth	Karlsruhe, Germany
Sanofi	Bridgewater, New Jersey, USA
Santa Cruz Biotechnology (Biotech)	Heidelberg, Germany
Sarstedt	Nümbrecht, Germany
Sartorius	Göttingen, Germany
Scientific Industries	Bohemia, New York, USA
Siemens	Munich, Germany
Sigma-Aldrich	St. Louis, Missouri, USA
Starlab	Hamburg, Germany
Systec	Wettenberg, Germany
Tanon Science & Technology	Shanghai, China
Taylor-Wharton (Auguste Cryogenics Germany)	Husum, Germany
Tecan	Männedorf, Switzerland
Thermo Fisher Scientific	Waltham, Massachusetts, USA
TKA	Niederelbert, Germany
TKD	Fraunberg-Tittenkofen, Germany
UniEquip	Planegg, Germany
VWR	Radnor, Pennsylvania, USA
Wessamat	Kaiserslautern, Germany
Zeiss	Jena, Germany

4.1.2 General materials

Table 2: General materials

Material	Manufacturer
50ml Reagent Reservoir, polysterene	Corning
Alufoil	neoLab
Amicon®Ultra-15 Centrifugal Filters	Merck Milipore
Cell culture flasks, 250 ml, 75 cm^2; 550 ml, 175 cm^2, PS, sterile	Greiner Bio-One
Cell scraper (16 cm)	Sarstedt
Columns (MACS, LS, MS)	Miltenyi Biotec
CryoPure Tube 1.6 ml	Sarstedt
Dry ice	TKD
Ethylenediaminetetraacetic acid (EDTA)-tubes, S-Monovotte 1.2ml K3E	Sarstedt
Gloves (latex), size S-L	Nobamed
HTS Transwell-96® well Permeable Support with 3.0 µm pore polycarbonate membrane, TC-treated	Corning
Hybond-P PVDF membrane	GE Healthcare
Invitrogen™ Exosome Spin Columns (MW 3000)	Thermo Fisher Scientific
MicroAmp™ Fast Optical 96-Well Reaction Plate	Applied Biosystems
Oak Ridge Centrifuge Tube, PPCP Size 50 ml	Thermo Scientific
Omnifix Luer Lock Solo 5 ml or 20 ml syringe	B. Braun Biotech
Parafilm® M All-Purpose Laboratory Film	Amcor
Pipette tips (10, 20, 100, 200 or 1000 µL) with or without filter	Starlab
qEV10 / 70 nm columns	Izon Science SAS
qEV2 / 70 nm columns	Izon Science SAS
Safe-lock microcentrifuge tubes (0.2, 1.5, 2 ml) DNA-/ DNase-/ RNase-/PCR inhibitor-free	Eppendorf
Safe-lock microcentrufuge tubes (1.5, 2 mL)	Eppendorf

Sensoplate Microplate, 96 well, PS, F-Bottom, Glass bottom, black	Greiner Bio-One
Syringe filter 0.22 µm, sterile	Sartorius
Thermo Scientific TUBE PC THICKWALL 4ML	Thermo Scientific
Tissue culture dish 150, Cell+	Sarstedt
Tissue culture plate, 6 well	Falcon
Tissue culture testplate 96U, conical, growth enhanced treated	Sartorius
Tissue culture testplate 96U, flat bottom, growth enhanced treated	Sartorius
Tubes 15 ml/50 ml, PP, graduated, conical bottom, sterile	Greiner Bio-One
Whatman gel blot paper	GE Healthcare

4.1.3 Equipment and instruments

Table 3: Equipment and instruments

Device	Specification	Manufacturer
Analytical balances	770-14, EW3000-2M	Kern & Sohn
Autoclaves	V95, 2540 EL	Systec
Biological Safety Cabinets	HERAsafe KS 18, Class II	Thermo Fisher Scientific
Cell count chamber	Neubauer	Paul Marienfeld
Centrifuges	Microcentrifuge 220R	Hettich
	Microcentrifuge 5415 R	Eppendorf
	F-45-30-11 Rotor	Eppendorf
	Multifuge 1 S-R (Heraeus)	Thermo Fisher Scientific
	Multifuge 3 S-R (Heraeus)	Thermo Fisher Scientific
	Sorvall® RC6 centrifuge	Thermo Fisher Scientific
	Sorvall® SS34 rotor	Thermo Fisher Scientific
CO_2 Incubators	BioSpa 8 Automated Incubator	BioTek/Agilent Technologies
	HERA cell 150	Thermo Fisher Scientific
Cryotank	Liquid nitrogen reservoir L-240k Series	Whortington / Tec-lab
Electrophoresis cell (gel electrophoresis)	Electrophoresis chamber Easy cast PowerPac™ Basic Power Supply	Thermo Fisher Scientific Bio-Rad Laboratories
Electrophoresis cell (immunoblotting)	VE-180 Mini Verticel Gel	Tanon Science & Technology
Electrophoresis Blotting System (semi-dry)	Biometra Fastblot B43	Analytik Jena
Electrophoresis tool	2100 Bioanalyzer Instrument	Agilent Technologies
Freezing containers	Mr. Frosty, Nalgene	Sigma-Aldrich
Flow cytometers	BD Fortessa X-20 SORP	BD Biosciences
	FACSCalibur	BD Biosciences
	MACSQuant Analyzer 10	Miltenyi Biotec
Freezer (-80 °C)	HERAfreeze, HLE Series	Thermo Fisher Scientific
Fridge / freezer (4 °C / -20 °C)	Siemens coolVario	Siemens
	-20 °C Freezer	AEG Electrolux
Gel documentation	Benchtop UV Transilluminotor, BioDoc-It Imaging System	UVP LLC
	Hybrid Graphic Printer UP-X898MD	Sony
Heating block	ThermoMixer comfort 5355	Eppendorf
Ice machine	Flake Line, MOD. F75W, KF85	Wessamat
Immunoblotting imaging	Gel Logic 1500 Imaging System	Kodak
Magnetic separators	BD IMag™ Cell Separation Magnet	BD Biosciences
	Bio-Plex® Handheld Magnetic Washer	Bio-Rad Laboratories
	MidiMACS	Miltenyi Biotec
	QuadroMACS	Miltenyi Biotec
Magnetic stirrer	IKAMAG REO	IKA-Werke
Micropipettes (adjustable)	10, 20, 100, 200, 1000 μL	Eppendorf
	Multichannel 100 μL	Eppendorf
Microscopes	Axiovert 100	Zeiss
	Camera AxioCam Mrm	Zeiss

	Cytation 5 Cell Imaging Multimode Reader	BioTek/Agilent Technologies
	Leica DM IL LED	Leica
Microwave	HF23024 Microwave 900 W	Siemens
Multiplex immunoassay reader	Bio-Plex 200 System (Luminex 200)	Bio-Rad Laboratories
Nanoparticle tracking device	ZetaView PMX110	Particle Metrix GmbH
Nanophotometer	NanoPhotomete Pearl	Implen
PCR cycler	iCycler	Bio-Rad Laboratories
pH meter	FiveEasy	Mettler Toledo
Photometer	Infinite M Nano	Tecan
Pipette controllers	accu-jet pro	Brand
	Stripettor Ultra	Corning
Power supply	Biometra Standard Power Pack P25	Analytik Jena
Real-Time PCR System	StepOnePlus	Applied Biosystems
RNA analysis	Bioanalyzer 2100	Agilent Technologies
Rotating wheel	Test-Tube-Rotator 220V/50 Hz	Kisker Biotech
Shakers	Duomax 2030	Heidolph Instruments
	Orbital Shaker UniTwist 3D	UniEquip
	IKA Rocker 3D digital	IKA-Werke
Sonicater	Digital Sonifier 250	Branson
Vortexers	Genie 2 G560-E	Scientific Industries
	Microplate Genie	Scientific Industries
	MS2 Minishaker	IKA-Werke
	Relax Top	Heidolph Instruments
Water bath	Water bath 1002	GFL

4.1.4 Software

Table 4: Software

Computer program	Manufacturer
Adobe Illustrator 24.2.1	Adobe Inc
Adobe Photoshop 21.2.1	Adobe Inc
BD FACSDiva 8.0.2	BD Biosciences
Bio-Plex® Manager Version 6.2	Bio-Rad Laboratories
Capture Molecular Imaging 5.0.7.24	Carestream Health
Endnote X7.7.1	Clarivate Analytics
Excel 2013	Microsoft
FlowJo V10.7.2.	BD Biosciences
Gen 5 V3.08 software	BioTek/Agilent Technologies
GrapPad Prism 9	GraphPad Software
i-control for Infinite 200 Pro 2.0	Tecan
MACSQuantify 2.13.1	Miltenyi Biotec
PowerPoint 2013	Microsoft
Word 2013	Microsoft
ZetaView software version 8.05.12.SP1	Particle Metrix GmbH

4.1.5 Chemicals and reagents

Table 5: Chemicals and reagents

Chemical/reagent	Manufacturer
100 bp-DNA-Ladder equimolar	Carl Roth
10x RIPA buffer	Abcam
4’,6-diamidino-2-phenylindole (DAPI) staining solution	Miltenyi Biotec
Acetic acid ≥ 99.7 %	Sigma-Aldrich
ACK Lysis Buffer (Red blood cell lysis)	Thermo Fisher Scientific
Acrylamide/Bis-acrylamide solution 30 %	Sigma-Aldrich
Agarose	Sigma-Aldrich

Aldehyde/Sulfat Latexbeads, 4 % w/v, 4 µm	Thermo Fisher Scientific
Amersham ECL Western Blotting Reagent Pack	GE Healthcare
Ammonium persulfate (APS)	Sigma-Aldrich
anti-CD3 (clone OKT3)	BioLegend
autoMACS Rinse Solution	Miltenyi Biotec
BD IMag™ Buffer (10x)	BD Biosciences
Bovine serum albumin (BSA) ≥ 96 %	Sigma-Aldrich
Bromophenol blue	Merck Millipore
CD28 antibody anti-human, pure-functional grade, clone 15E8	Miltenyi Biotec
DAPI Staining Solution	Miltenyi Biotec
DEPC-treated Water	ThermoFisher Scientific
Dimethylsulfoxide (DMSO)	Merck Millipore
Dithiothreitol (DTT)	VWR
DNA Gel Loading Dye (6x)	Thermo Fisher Scientific
Dulbecco's Phosphate Buffered Saline 10x (PBS), diluted 1:10 with double distilled (dd)H_2O	Thermo Fisher Scientific
Dulbecco's Modified Eagle Medium (DMEM/F12)	ThermoFisher Scientific
eBioscience™ Cell Proliferation Dye eFluor™ 450	Thermo Fisher Scientific
EDTA 99.4-100.6%, powder	Sigma-Aldrich
Ethanol ≥ 99.8 %	Carl Roth
Ethidium bromide solution, 10 mg/ml	Sigma-Aldrich
Exosome-depleted fetal bovine serum (FBS)	Thermo Fisher Scientific
FACS Clean	BD Biosciences
FACS Flow	BD Biosciences
FACS Rinse	BD Biosciences
FBS	Thermo Fisher Scientific
Ficoll-Paque™ Plus	Cytiva
Glycerine ≥ 99 %	Sigma-Aldrich
Glycine ≥ 99 %	Sigma-Aldrich
GM-CSF, recombinant human (rh)	Sanofi
Heparin-Natrium-5000	Ratiopharm
Human AB serum	Lonza
IL-1, rh	R&D Systems
IL-4, rh	R&D Systems
IL-6, rh	R&D Systems
Isopropanol	Merck Millipore
L-Glutamine 200mM	Thermo Fisher Scientific
Linear Acrylamide (5 mg/ml) (1 ml Tube)	ThermoFisher Scientific
Lipopolysaccharides (LPS) from Escherichia coli O127:B8	Sigma-Aldrich
MACS Comp Bead Kit anti-REA	Miltenyi Biotec
MACSQuant Calibration Beads	Miltenyi Biotec
MACSQuant Running Buffer	Miltenyi Biotec
MACSQuant Washing Solution	Miltenyi Biotec
MACSQuant/MACSima Storage Solution	Miltenyi Biotec
Methanol ≥ 99.8 %	Merck Millipore
milliQ water	Merck Millipore
Minimum Essential Medium (MEM) α, nucleosides	Thermo Fisher Scientific
PageRule Prestained Protein Ladder	Thermo Fisher Scientific
Penicillin- Streptomycin, 10,000 U/ml	Thermo Fisher Scientific
PharmingenStain Buffer (BSA)	BD Biosciences
Phenylmethylsulfonyl fluoride (PMSF) protease inhibitor	ThermoFisher Scientific
Polyinosinic–polycytidylic acid (poly(I:C)), P1530	Sigma-Aldrich
Proleukin (rh IL-2)	Clinigen, Inc.
Propidium Iodide (PI) Solution, 2 mL	Miltenyi Biotec
Prostaglandin E2 (PGE_2)	Cayman Chemical Company
RNase A, DNase and protease-free (10 mg/mL)	ThermoFisher Scientific
Roswell Park Memorial Institute Medium (RPMI-)1640	ThermoFisher Scientific
Skim milk powder	Sigma-Aldrich
Sodium dodecyl sulfate (SDS) ≥ 98.5 %	Sigma-Aldrich

Tetramethylethylenediamine (TMED)	Sigma-Aldrich
TNF, rh	R&D Systems
Tris(hydroxymethyl)aminomethane (Tris)	Merck Millipore
Trypan blue stain (0.4 %)	Thermo Fisher Scientific
Trypsin/EDTA	Thermo Fisher Scientific
UltraComp eBeads™ Compensation Beads	ThermoFisher Scientific
X-VIVO 15, Serum-free Hematopoietic Cell Medium	Lonza

4.1.6 Commercial kits

Table 6: Commercial kits

Kit	Manufacturer
Agilent High Sensitivity DNA assay	Agilent Technologies
Anti-Human CD14 Magnetic Particles – DM, Clone MφP9	BD Biosciences
ArC™ Amine Reactive Compensation Bead Kit	ThermoFisher Scientific
BD IMag™ Anti-Human CD14 Magnetic Particles - DM	BD Biosciences
Bio-Plex Human Cytokine Screening Panel, 48-plex panel	Bio-Rad Laboratories
Bio-Plex Pro HuCSP, Standards	Bio-Rad Laboratories
Bio-Plex Pro Human Chemokine TNF-α Set (171BK55MR2)	Bio-Rad Laboratories
Bio-Plex Pro Reagent Kit 3 Flat Plate	Bio-Rad Laboratories
BP Pro Hu INF PNL1 Std, 1PK	Bio-Rad Laboratories
CD33 MicroBeads, human 2ml	Miltenyi Biotec
GoTaq® qPCR Master Mix	Promega
High Capacity cDNA Reverse Transcription Kit	ThermoFisher Scientific
Hu INF PNL1 IFN-beta Set	Bio-Rad Laboratories
KAPA RNA HyperPrep Kit with RiboErase (HMR)	Roche
mirVana™ miRNA Isolation Kit	ThermoFisher Scientific
MycoAlert™ Mycoplasma Detection Kit	Lonza
Pierce™ BCA Protein Assay Kit	ThermoFisher Scientific
PrimeFlow™ RNA Assay Kit	ThermoFisher Scientific
RNA 6000 Pico chip	Agilent Technologies
SYTO™ RNASelect™ Green Fluorescent cell Stain	ThermoFisher Scientific
TURBO DNA-free™ Kit	ThermoFisher Scientific

4.1.7 Antibodies and dyes for flow cytometry and immunoblotting

4.1.7.1 Antibodies and dyes for flow cytometry on FACS Calibur and MACSQuant Analyzer 10

Table 7: Anti-human fluorochrome-conjugated antibodies for flow cytometry on FACS Calibur and MACSQuant Analyzer 10

Epitope	Clone	Fluorochrome	Concentration	Manufacturer
CD14	REA599	VioGreen	1:50	Miltenyi Biotec
CD25	REA579	APC	1:50	Miltenyi Biotec
CD3	REA613	PE-Vio770	1:100	Miltenyi Biotec
CD4	REA623	APC-Vio770	1:100	Miltenyi Biotec
CD63	REA1055	FITC	1:50	Miltenyi Biotec
CD69	FN50	PE	1:50	BD Biosciences
CD8	REA734	FITC	1:100	Miltenyi Biotec
CD80	REA661	PE	1:50	Miltenyi Biotec
CD81	REA513	PE	1:50	Miltenyi Biotec
CD83	REA714	APC-Vio770	1:50	Miltenyi Biotec
CD86	REA968	VioBlue	1:50	Miltenyi Biotec
HLA-DR	REA805	PE-Vio770, APC	1:50	Miltenyi Biotec
Isotype Mouse IgG1	X40	PE	1:100	BD Biosciences

REA isotype	REA293	VioBlue, FITC, PE. PE-Vio770, APC-Vio770	1:50	Miltenyi Biotec

Table 8: Dyes and solutions used for flow cytometry on FACS Calibur and MACSQuant Analyzer 10

Application	Dye/Name	Reference	Concentration	Manufacturer
Cell proliferation	eFluor450	65-0842-85	10 µM	Thermo Fisher Scientific
Dead cell exclusion	DAPI staining solution	130-111-570	1:100	Miltenyi Biotec
	PI solution	130-093-233	1:100	Miltenyi Biotec

4.1.7.2 Antibodies and dyes for flow cytometry on BD Fortessa X-20 SORP

Table 9: Anti-human fluorochrome-conjugated antibodies for flow cytometry on BD Fortessa X-20 SORP

Epitope	Clone	Fluorochrome	Concentration	Manufacturer
CD19	HIB19	PE-eFluor 610	1:20	Thermo Fisher Scientific
CD3	UCHT1	Super Bright 600	1:20	Thermo Fisher Scientific
CD33	WM-53	PE-Cyanine7	1:20	Thermo Fisher Scientific
CD4	RPA-T4	PE	1:20	Thermo Fisher Scientific
CD45	2D1	eFluor 450	1:20	Thermo Fisher Scientific
CD8A	RPA-T8	FITC	1:20	Thermo Fisher Scientific
HERV-K pol (Type 1)	RNA probe VF1-18759-210	Alexa Fluor (AF) 647	1:20	Thermo Fisher Scientific
HLA-DR	LN3	Super Bright 436	1:20	Thermo Fisher Scientific
HSAT2 (Type 6)	RNA probe VA6-19493-210	AF750	1:20	Thermo Fisher Scientific
RPL13a	RNA probe VA1-13100-PF-204	AF647	1:20	Thermo Fisher Scientific

Table 10: Dyes and solutions used for flow cytometry on BD Fortessa X-20 SORP

Application	Dye/Name	Order-Nr.	Concentration	Manufacturer
Dead cell exclusion	Fixable Viability Dye eFluor™ 506	65-0866-14	1:1000	Thermo Fisher Scientific

4.1.7.3 Antibodies for immunoblotting

Table 11: Antibodies for immunoblotting

Epitope	Reference	Concentration	Manufacturer
Annexin A1	ab214486	1:2000	Abcam
Anti-mouse IgGκ-HRP	sc-516102	1:1000	Santa Cruz Biotechnology
Calnexin	sc-23954	1:200	Santa Cruz Biotechnology
CD63	sc-5275	1:200	Santa Cruz Biotechnology
CD81	sc-7637	1:200 - 1:500	Santa Cruz Biotechnology
cGAS	#79978	1:1000	Cell Signaling Technology
Hsp70	sc-32239	1:1000	Santa Cruz Biotechnology
Hsp90	sc-69703	1:1000	Santa Cruz Biotechnology
Mouse anti-rabbit IgG-HRP	sc-2357	1:1000	Santa Cruz Biotechnology
Phospho-TBK1	#5483	1:1000	Cell Signaling Technology
RIG-I	#3743	1:1000	Cell Signaling Technology
Syntenin-1	ab133267	1:1000	Abcam
TBK1	#3504	1:1000	Cell Signaling Technology
TSG101	sc-7964	1:200 - 1:500	Santa Cruz Biotechnology
β-actin	sc-47778	1:2000	Santa Cruz Biotechnology
β-tubulin	sc-5274	1:1000	Santa Cruz Biotechnology

4.1.8 Primer sequences for semi-quantitative real-time polymerase chain reaction (sqRT-PCR)

Primer sequences were obtained from the indicated publications, the PrimerBank (https://pga.mgh.harvard.edu/primerbank/index.html), or the USCS Genome Browser (https://genome.ucsc.edu/cgi-bin/hgPcr). ACRO1 and HSAT2 primers were designed by Valentina Evdokimova, PhD and Syed Hassan Zaidi, PhD, both Ontario Institute for Cancer Research, Toronto, Canda, and confirmed by Sanger sequencing. Primers were purchased from Metabion.

Table 12: List of primers for sqRT-PCR

Name	Species	Forward 5'-3'	Reverse 5'-3'	Source
ACRO-1	human	TCATTGTGTTCTCCCGTGTCC	GCTGCTGGATGATGGCAGTAAG	Syed Hassan Zaidi
DDX58/RIG-I	human	CCATGTAAGACTTGCCTGCTT	AAGAGGCTTAATAGATTCACAGTTCC	
GAPDH	human	CTCTGCTCCTCCTGTTCGAC	ACGACCAAATCCGTTGACTC	USCS genome browser ENST00000229239.10
HERV-K env	human	GCTGCCCTGCCAAACCTGAG	CCTGAGTGACATCCCGCTTACC	[133]
HERV-K pro	human	GCCGATGAAAAAGCCCGTAAGG	TTGACACTCAGGATTGGCGTTTTC	[133]
HSAT2	human	TTGAATCGTCATCGAATGAACTG	TCGCTAATTCCGTTTGATTCCG	Syed Hassan Zaidi,
IFI16	human	CCGTTCATGACCAGCATAGG	TCAGTCTTGGTTTCAACGTGGT	[217]
IFI30	human	CCCCTCTGCAAGCGTTAGAC	CCCGCAGGTATAGATTGCCT	PrimerBank ID 29826337c1
IFI35	human	AACAAAAGGAGCACACGATCA	CTCCGTTCCTAGTCTTGCCAA	[218]
IFI6	human	GGTCTGCGATCCTGAATGGG	TCACTATCGAGATACTTGTGGGT	[219]
IFITM1	human	CTTGAACTGGTGCTGTCTGG	AATCAGGGCCCAGATGTTCA	[220]
IFITM2	human	GAACCACATTGTGCAAACCTTCTCTC	TTCCTGCTCCTCCTTGAGCATC	[221]
IFITM3	human	ATCGTCATCCCAGTGCTGAT	ACGTGGGATACAGGTCATGG	[221]
IFNAR1	human	ATTTACACCATTTCGCAAAGCTC	TCCAAAGCCCACATAACACTATC	PrimerBank ID 46488931c2
IFNα	human	GACTCCATCTTGGCTGTGA	TGATTTCTGCTCTGACAACC	
IFNβ	human	CTTTCGAAGCCTTTGCTCTG	CAGGAGAGCAATTTGGAGGA	USCS genome browser ENST00000380232.4
IL-6	human	ATGAACTCCTTCTCCACAAGC	GTTTTCTGCCAGTGCCTCTTTG	[222]
IL-10	human	TCAAGGCGCATGTGAACTCC	GATGTCAAACTCACTCATGGCT	PrimerBank ID 24430216c2
IRF3	human	AGAGGCTCGTGATGGTCAAG	AGGTCCACAGTATTCTCCAGG	PrimerBank ID 308199457c1
IRF7	human	CCCACGCTATACCATCTACCT	GATGTCGTCATAGAGGCTGTTG	PrimerBank ID 98985817c3
LINE-1	human	TTGAACAATGAGATCACATG	GTGCCATGCTGGTGCGCTGC	[223]
IFIH1/MDA5	human	AGGCACCATGGGAAGTGAT	ATTTGGTAAGGCCTGAGCTG	
MX1	human	GTTTCCGAAGTGGACATCGCA	CTGCACAGGTTGTTCTCAGC	PrimerBank ID 222136618c1

OASL	human	TGTGTCAGAAAACAGCTCAAAAA	GCAACGATGTCCCATCTGTA
U1	human	CAGGGGAGATACCATGATCACGAAG	GGTCAGCACATCCGGAGTGCAATGG

4.1.9 Buffers, cell culture media and solutions

4.1.9.1 Buffers for flow cytometry

Table 13: Buffers for flow cytometry

Buffer	Components
Blocking buffer	1 M glycine (in ddH_2O)
Staining buffer	PBS for CD14-depleted PBMCs, $CD14^+$ and $CD33^+$ cells PBS/0.5 % BSA for EVs PharmingenStain Buffer (BSA) for PrimeFlow RNA assay

4.1.9.2 Buffer and gel for DNA gel electrophoresis

Table 14: Buffer and gel for DNA gel electrophoresis

Buffer/gel	Components
Electrophoresis gel	150 ml 1x Tris-acetate-EDTA (TAE), 1 % agarose, 40 µg ethidium bromide
50x TAE running buffer	2 M Tris, 10 % EDTA (0.5 M), 5.71 % acetic acid

4.1.9.3 Buffers and gels for immunoblotting

Table 15: Buffers and gels for immunoblotting

Buffer/gel	Components
Antibody dilution buffer	5 % BSA in TBS-T, 0.02 % NaN_3
Lysis buffer	10x RIPA buffer, 1 mM PMSF
Protein loading buffer	0.25 M Tris-HCl (pH 6.8), 8 % SDS, 40 % glycerine, 0.04 % bromophenol blue
Running buffer (1x)	25 nM Tris, 192 mM glycine, 0.1 % SDS
Separating gel (10 %), 10 ml	4.0 mL ddH_2O 3.3 mL Acrylamide/Bis-acrylamide 30 % 2.5 mL 1.5 M Tris (pH 8.8) 0.1 mL 10 % SDS (in ddH_2O) 0.1 mL 10 % APS (in ddH_2O) 0.004 mL TMED
Stacking gel, 4mL	2.7 mL ddH_2O 0.67 mL Acrylamide/Bis-acrylamide 30 % 0.5 mL 1M Tris (pH 6.8) 0.04 mL 10 % SDS (in ddH_2O) 0.04 mL 10 % APS (in ddH_2O) 0.004 mL TMED
TBS (10x)	0.5 M Tris-HCl (pH 7.6), 1.5 M NaCl
TBST	0.1 % Tween-20 in TBS (1x)
Transfer buffer (1x)	48 mM Tris, 39 mM glycine, 10 % methanol

4.1.10 Human cell lines

Table 16: Human cell lines

Cell line	Source	Age/ Sex	Primary site of established cell line	EWS-FLI1 status	P53 status	Growth conditions*
A4573	ATCC	17/F	Clavicle, pleural effusion	FLI1, type 3	Unknown	RPMI 1640, 10 % FBS
A673	ATCC	15/F	Muscle, peripheral neuroepithelioma, primary	FLI1, type1	Non-functional	RPMI 1640, 10 % FBS
MRC5	ATCC	Fetal/M	Lung	-	-	DMEM/F12, 10 % FBS
MUTZ-3	DSMZ	29/M	Peripheral blood, acute myelomonocytic leukemia	-	Non-functional	MEM α, nucleosides, 20 % FBS, 40 ng/ml GM-CSF
TC32	CCR repository	17/F	Illeum and adjacent soft tissue, primary	FLI1, type1	Non-functional	RPMI 1640, 10 % FBS
TC71	DSMZ	22/M	Humerus, primary	FLI1, type1	Non-functional	RPMI 1640, 10 % FBS

*each cell culture medium was supplemented with 2 mM L-glutamine, 100 U/mL penicillin and 100 µg/mL streptomycin.

4.2 Methods

4.2.1 Cell culture

EwS cell lines A4573, A673, TC32 and TC71 were cultured in RPMI 1640 medium and MRC5 fibroblasts were cultured in DMEM/F12 medium, both supplemented with 10 % FBS, 100 U/mL penicillin and 100 µg/mL streptomycin at 37 °C and 5 % CO_2. For passage, cells were detached with trypsin for 5 min at 37 °C and 5 % CO_2, resuspended in 10 ml of respective medium and seeded in 175 mm^2 flasks or 150 mm dishes. For cryopreservation, 1 x 10^7 cells were centrifuged at 300 g for 5 min, resuspended in FBS supplemented with 10 % DMSO and transferred to cryovials. After 48 h of storage in Mr. Frosties at -80 °C, cells were stored in liquid nitrogen at -190 °C. In order to thaw cells, cryovials were warmed in a water bath at 37 °C for 3 min, the cells transferred to 10 ml pre-warmed cell culture medium and centrifuged at 300 g for 5 min. Cell pellets were carefully resuspended in cell culture medium and seeded at 4 x 10^6 cells in 20 ml and 15ml within 175 mm^2 flasks and 150 mm dishes, respectively. Cell counts and viability was assessed using a Neubauer cell counting chamber and Trypan blue staining. Cells were regularly tested for mycoplasma contamination using the MycoAlert assay.

4.2.2 Isolation of EVs

EVs encompass a heterogeneous population of vesicles, in which subpopulations vary in size, content and markers [224]. Methods for EV isolation utilize various biochemical and physical approaches differing in yield, purity and feasibility [225]. In this study, 0.22 µm ultrafiltration

and ultracentrifugation (UC) were combined as main method for EV isolation, in order to enrich small EV subpopulations independent of markers and yield sufficient amount of EVs [226]. As UC co-pellets proteins not associated with EVs leading to contamination or formation of aggregates, EV isolation was also performed by size-exclusion chromatography (SEC). SEC purifies small EVs in columns with porous of polysaccharide resins while removing contaminating proteins or aggregates. However, SEC yields lower EV particle counts than UC [224,227].

EVs were isolated from cell culture supernatant of EwS and fibroblast cell lines by differential centrifugation and 0.22 µm ultrafiltration followed by either UC or SEC. EVs were isolated from plasma of EwS patients and healthy donors by 0.22 µm ultrafiltration and UC.

4.2.2.1 EV isolation from cell culture supernatant and plasma by UC

Cell lines were seeded at 4 x 10^6 cells/15 ml in ten 150 mm dishes. At 70–80 % confluency, cells were washed once with pre-warmed PBS and fresh cell culture medium supplemented with 2 % exosome-depleted FBS was added. After overnight incubation for 12–18 h, the conditioned medium was collected and subjected to differential centrifugation and ultrafiltration [228]. EV isolation was performed from cells with viability > 90 %. For differential centrifugation, conditioned medium was cleared from cellular contaminants at 2,000 g for 10 min, followed by removal of cell debris at 10,000 g for 30 min. Cleared supernatant was concentrated at 4,200 g for 7 min using Amicon Ultra-15mL-30K tubes and subsequently filtered through 0.22 µm filters. For UC, the filtered medium was diluted 1:1 with ice-cold PBS and centrifuged at 100,000 g for 2 h (S110-AT rotor, fixed-angle, *k*-factor 78.4). Afterwards the supernatant was discarded, the pellet was resuspended in ice-cold PBS and centrifuged again at 100,000 g for 2 h. The cleared EV pellets were resuspended in 200 µl ice-cold PBS, aliquoted in five separate 1.5 ml Eppendorf tubes (to avoid freeze-thaw cycles), snap frozen on dry ice and stored at -80 °C until further use. Each step of EV isolation was performed at 4 °C.

For isolation of EVs from EDTA blood of healthy donors and EwS, 1 ml plasma of stored at -80 °C (s. 4.2.10) was thawed on ice, centrifuged at 10,000 g for 10 min to remove aggregates, diluted 1:1 with ice-cold PBS, passed through 0.22 µm filters, and subjected to UC as described above.

4.2.2.2 EV isolation from cell culture supernatant by SEC

The steps for the purification of EVs from cell culture supernatant by SEC comply with those of UC until after the step of 0.22 µm filtration. For SEC, filtered medium was loaded on

qEV2 / 70 nm or qEV10 / 70 nm columns (both IZON) and the isolation was performed according to the manufacturer's instructions. The collected EV and protein fractions were concentrated at 4,200 for 7 min using Amicon Ultra-15mL-30K tubes. EV preparations were aliquoted in five separate 1.5 ml Eppendorf tubes (to avoid freeze-thaw cycles), snap frozen on dry ice and stored at -80 °C. EV isolation by SEC was performed at room temperature.

4.2.3 Nanoparticle Tracking Analysis

EV size distribution and particle number were quantified by Nanoparticle Tracking Analysis (NTA) using the ZetaView PMX110. After initialization of the ZetaView, the cell was rinsed with milliQ water and 'AutoAlignment' was performed. After running the 'Daily Performance', the sample cell was equilibrated with PBS. The EV probes were diluted 1:500–1:2000 with PBS and manually injected. The ten positions of the sample cell were checked for bubbles, steady particle number and absence of particle drift. EV probes were analyzed at 80 % sensitivity, shutter set at 70 and 24 °C. At least 500 traces/probe were detected. Between EV probes, the sample cell was rinsed with 30 ml PBS. For shutdown, the sample cell was cleaned with 100 ml milliQ water and air-dried. ZetaView software (version 8.05.12.SP1) was used for data analysis.

4.2.4 Protein isolation

Total protein was isolated from 2–4 x 10^6 EwS and MRC5 cells by cell lysis and sonication. In particular, cells were trypsinized, counted, washed twice with PBS and pelleted in 1.5 ml Eppendorf tubes by centrifugation at 400 g for 5 min at 4 °C. Supernatant was discarded and 300 µl 1x RIPA buffer containing 1 mM PMSF (protease inhibitor) were added to the cell pellets. Cell pellets were sonicated three times for 1 s at 10 % amplitude with a digital sonicater on ice. After quick spin at 400 g for 3–5 s at 4 °C, sonication was repeated until the pellets were completely dissolved. Debris was pelleted at 15,000 g for 30 min at 4 °C, while the protein-containing supernatant was collected and stored at -80 °C until further use.

4.2.5 Protein quantification of cell lysates and EV preparations

Total protein amount in cell lysates and EV preparations was quantified using the Pierce™ BCA Protein Assay Kit according to the manufacturer´s instructions. In brief, Pierce™ protein staining solutions A and B were mixed at a ratio of 50:1 and vortexed. Samples were diluted 1:1 with lysis buffer (cell lysates) or PBS (EV preparations). 12.5 µl of diluted sample, BCA standard dilution or lysis buffer/PBS for background correction were added per well in duplicates on a 96-well flat-bottom plate. Then 112.5 µl of mixed Pierce™ staining solution

were added to each well. The 96-well plate was covered with parafilm and wells were mixed on a shaker for several seconds. After incubation at 37 °C for 30 min, the samples were measured at 560 nm wavelength using the Tecan absorbance plate reader and referenced to the BSA standards.

4.2.6 Immunoblotting

Protein concentrations were equalized between cell lysates or EV preparations in protein loading buffer (supplemented 1:5 with 100 µl 1M DTT before use) and boiled at 99 °C for 3 min. Afterwards samples were stored at -80 °C or put on ice until loading. Samples (0.1–30 µg protein) and the protein ladders were loaded onto the SDS gel. Gel electrophoresis was performed in running buffer at 60 V for 30–60 min. Afterwards, the separated proteins were blotted onto PVDF membranes, which were activated before with methanol, in transfer buffer at 200 mA / 4 V for 60 min. After transfer, PVDF Membranes were blocked with 5 % nonfat dry milk in TBST buffer and incubated with specific primary and secondary antibodies. Protein bands were visualized using a commercial ECL solution and the Gel Logic 1500 luminometer.

4.2.7 Flow cytometry of EVs and cells

To detect EV markers, EVs were bound to 4.0 µm latex beads, stained with antibodies and analyzed by flow cytometry [119]. In brief, 50 µl of EV preparation in PBS were added to 100 µl PBS and incubated at room temperature with 1.5 µl of aldehyde/sulfate latex beads (4 % w/v, 4 µm) in a 1.5 ml microcentrifuge tube for 15 min. Afterwards, the volume was filled up with PBS to 300 µl and incubated on a wheel at 4 °C overnight. On the next day, latex beads were blocked with 1 M glycin/ddH_20 at room temperature for 30 min, pelleted at 15,000 g at room temperature for 3 min and washed once with PBS/0.5 % BSA. The latex beads were pelleted again at 15,000 g at room temperature for 3 min, resuspended in 200 µl PBS/0.5 % BSA and split equally for the four stainings: (1) beads only, (2) beads + isotype controls for FITC and PE, (3) beads + CD63 FITC antibody and (4) beads + CD81 PE antibody. Antibodies were used at 1:50 dilution. After 15 min incubation protected from light at 4 °C, latex beads were pelleted at 4,000 g at room temperature for 3 min, resuspended in 200 µl PBS/0.5 % BSA and analyzed on the MACSQuant Analyzer 10 flow cytometer.

To analyze protein surface expression on cells, 2 x 10^5 myeloid cells were washed once with PBS and stained with respective fluorochrome-conjugated antibodies at a 1:50 dilution in a total volume of 50 µl PBS protected from light at 4° C for 15 min. Afterwards, cells were washed with 200 µl PBS, centrifuged at 300 g for 5 min and resuspended in 200 µl PBS for acquisition on the FACS Calibur or MACSQuant Analyzer 10 flow cytometer. For compensation of the

multicolor-panels, single stainings or auto compensation with REA-compensation beads were used according to the protocol provided by Miltenyi. For acquisition and data analysis, the following gating strategy was applied: (1) exclusion of doublets in FSC-H vs. FSC-A, (2) gating on cells in SSC-A vs. FSC-A, (3) exclusion of dead cells using PI in B3-A vs B2-A and (4) gating on lineage marker CD14 for monocytes or CD3 for T cells (Supplementary Figure 9). Data were analyzed and dot plots generated using MACSQuantify, FlowJo V10.7.2 and GraphPad Prism 9.

4.2.8 PrimeFlow RNA assay

The PrimeFlow RNA Assay is an in situ hybridization method combining a branched DNA assay with single-cell resolution of flow cytometry. The assay simultaneously detects RNA targets and cell surface proteins using pairs of RNA transcript-specific probes and fluorochrome-conjugated antibodies. The experiments were performed in cooperation with Valentina Evdokimova, PhD (Ontario Institute for Cancer Research, Toronto, Canada) and Christopher Spring (Core Facilities, St. Michael's Hospital, Toronto, Canada) according to the manufacturer's instructions. Shortly, PBMCs of EwS patients and healthy donors were thawed as described in 4.2.1 and stained with the fixable viability dye eFluor506 and fluorescently-labeled antibodies against the respective cell surface markers. For target probe hybridization, cells were fixed, permeabilized and incubated with the target RNA probes for HERV-K pol AF647 (Type 1) and HSAT2 AF750 (Type 6). The probe RPL13a AF647 (Type 1) was used as positive control. For acquisition on the flow cytometer BD Fortessa X-20 SORP, cells were re-suspended in 200 µl of PharmingenStaining Buffer. Compensation was performed using UltraComp eBeads and the ArC™ Amine Reactive Compensation Bead Kit according to instructions of the manufacturer. Non-viable cells and doublets were excluded. Fluorescence minus one (FMO) controls were used to determine positive events. Data were analyzed using the BD FACSDiva 8.0.2 software.

4.2.9 Sonication and RNAse A treatment of EVs

EVs were sonicated and treated with RNAse A as described before [119]. In particular, freshly isolated TC32 UC EVs were resuspended in 200 µl PBS, equally split on four 1.5 ml Eppendorf tubes and treated either with sonication, 0.1 µg/µl RNAse A, sonication and 0.1 µg/µl RNAse A or left untreated. Sonication was performed before addition of RNAse A. Respective samples were sonicated on ice three times at 10 % amplitude for 10 s on a digital sonicator. Then 0.1 µg/µl RNAse A was added to respective samples and all four samples were incubated at 37 °C for 10 min.

4.2.10 Isolation of plasma and PBMCs from blood of EwS patients and healthy donors

The study was approved by the Ethics Commission of the Medical Faculty of the Technical University of Munich (2562/09, 649/20 S-KH). After informed consent, venous blood was collected from healthy donors and EwS patients in EDTA tubes and centrifuged at 400 g for 10 min to pellet cellular blood components. The supernatant was centrifuged at 10,000 g for 15 min to remove remaining cellular components. Plasma was stored at -80 °C until further analysis. PBMCs were isolated by density-gradient centrifugation (FICOL plaque) from healthy donors or commercial buffy coats (DRK Blutspendedienst Ulm, Germany, after informed consent and approval of local government regulatory authorities), as described before [46,229]. Contaminating erythrocytes were removed using the ACK Lysis Buffer.

4.2.11 Isolation of $CD14^+$ monocytes and $CD33^+$ myeloid cells from PBMCs

$CD14^+$ monocytes and $CD33^+$ myeloid cells were purified from healthy donor PBMCs using anti-human CD14 magnetic particles or anti-human CD33 MicroBeads as described previously and according to the instructions of the suppliers [46,230]. CD14-depleted PBMCs were frozen and stored at -80 °C until further use.

4.2.12 Differentiation and maturation of myeloid cells towards moDCs

An established *in vitro* model was used for the differentiation and maturation of monocytes to moDCs [46]. For differentiation, 1 x 10^6 $CD14^+$ monocytes or $CD33^+$ myeloid cells were seeded per 1 ml X-VIVO 15 medium supplemented with 1 % human AB serum, 800 U/mL rhGM-CSF and 30 ng/mL rhIL-4 in 75 cm^2 and 175 cm^2 cell culture flasks or 12-well plates (final volumes 20 ml and 1 ml, respectively). The medium was renewed on day 3. Maturation was induced on day 5 by replacing the medium with fresh X-VIVO 15 medium containing 10 ng/mL rhIL-1β, 1000 U/mL, rhIL-6, 1 mg/mL PGE_2 and 10 ng/mL rhTNF. The phenotype and functionality of moDCs was analyzed at day 7.

4.2.13 Treatment of myeloid cells with EVs

0.2 or 1 x 10^6 $CD14^+$ and $CD33^+$ myeloid cells were treated with 5 x 10^8 to 4 x 10^{10} EV particles in a final volume of 200 µl or 1 ml medium for 6 h to 72 h. Treatment was performed in 6-, 12- and 96-well plates as well as in 75 cm^2 and 175 cm^2 cell culture flasks.

4.2.14 Cytokine single- and multiplex assays

Concentration of cytokines and chemokines in cell culture supernatants and plasma were quantified using cytokine single- and multiplex assays. To this end, conditioned medium was

centrifuged at 2,000 g for 10 min at 4 °C and stored at -80 °C until further analysis. Plasma was processed as described in 4.2.10. For analysis, frozen conditioned medium or plasma were thawed on ice and centrifuged at 2,000 g for 10 min at 4 °C to pellet aggregates. Single- and multiplex assays were performed according to the instruction of the manufacturer and samples were acquired using the Bio-Plex 200 system. The concentrations of the analytes were calculated using the Bio-Plex Manager Version 6.2. At least two biological replicates were analyzed.

4.2.15 T cell proliferation assay

T cell proliferation was assessed using flow cytometry by adapting a published protocol [231]. In detail, CD14-depleted PBMCs, obtained as CD14-negative fraction during the $CD14^+$ cell isolation described in 4.2.11, were thawed and seeded in RPMI 1640 medium supplemented with 5 U/mL rhIL-2 in 48-well plates. At the next day, 1×10^7 CD14-depleted PBMCs were stained with 10 µM eFluor 450 Dye following the protocol of the manufacturer. CD14-depleted PBMCs were seeded in quadruplicates at 50,000 cells/well in 96-well tissue culture plates and stimulated with 1 µg/mL coated anti-CD3 (clone OKT3), 2 µg/mL soluble anti-CD28 and 5 U/mL rhIL-2. moDCs were added to allogeneic CD14-depleted PBMCs in a ratio of 1:8. After co-culture at 37 °C and 5 % CO_2 for 4 days, the conditioned medium was collected and analyzed by cytokine multiplex assay, as described in 4.2.14. eFluor 450 intensity of $CD3^+CD4^+$ and $CD3^+CD8^+$ T cells was quantified by flow cytometry.

4.2.16 Total RNA isolation and removal of contaminating DNA

Total RNA from $CD14^+$ cells or EVs was isolated and contaminating DNA removed using the mirVana miRNA Isolation Kit and the TURBO DNA-free Kit, respectively. In brief, 0.5–2 x 10^6 cells were harvested from cell cultures and washed with PBS at 2,500 g for 4 min at 4 °C. The dry cell pellets were snap frozen on dry ice and stored at -80 °C until RNA isolation. 50 µl of TC32 EVs (corresponding to 25 % of total EVs isolated from 60 ml conditioned medium of 4 x 10^7 TC32 cells after 19.5 h incubation) were used for RNAse A treatment and subsequent RNA isolation. Isolation of total RNA and removal of contaminating DNA was performed according to the manufactures instructions. Then, 1 ml 80 % ethanol and 5 µl linear acrylamide were added to RNA dissolved in 100 µl DEPC-treated H_20. After overnight incubation at -20 °C, RNA was pelleted at 10,000 g for 20 min at 4 °C and dissolved in 15 µl DEPC-treated H_20. RNA concentration and quality was determined by a NanoPhotometer at 260 nm.

4.2.17 Reverse transcription

To investigate gene expression, RNA was reversely transcribed into complementary DNA (cDNA) using the High Capacity cDNA Reverse Transcription Kit. In brief, 250–1000 ng RNA were adjusted to 14.2 µl and added to 5.8 µl reverse transcription master mix containing 2 µl buffer (10x), 2 µl random primers (10x), 0.8 µl dNTPS (100 mM) and 1 µl MultiScribe Reverse Transcriptase (50 U/µl). The final reaction volume was 20 µl. The Thermo Cycler settings were as follows:

Step	Temperature [°C]	Duration [min]
1	**25**	**10**
2	**37**	**60**
3	**37**	**60**
4	**85**	**5**
5	**4**	**∞**

cDNA was quantified and checked for quality photometrically and afterwards subjected to gene expression analysis using sqRT-PCR.

4.2.18 sqRT-PCR

For analysis of differential gene expression, cDNA was subjected to sqRT PCR. A sqRT-PCR reaction contained 50 ng cDNA diluted in 5 µl DEPC-treated H_20, 7.5 µl GoTaq qPCR Master Mix, 0.75 µl 10 µM forward primer, 0.75 µl 10 µM reverse primer and 1 µl DEPC-treated H_20. The final reaction volume was 15 µl. sqRT-PCR was performed in MicroAmp Fast Optical 96-Well Reaction Plates. Gene expression was assessed in technical triplicates. The primer sequenced are listed in 4.1.8. DEPC-treated H_20 was used as controls for contamination with nucleic acids. On the StepOnePlus Real-Time PCR System the steps of PCR reaction were as follows: initiation at 94 °C for 90 sec, denaturation at 94 °C for 15 sec, annealing at 60 °C for 30 sec and polymerase activity at 72 °C for 30 sec. Denaturation, annealing and polymerase activity were repeated 44x times. A melting curve analysis was performed in each experiment. Gene expression was calculated using the 2^{-ddCt} method. Glyceraldehyde 3-phosphate dehydrogenase (GAPDH) was used as housekeeping gene in EV-treated $CD14^+$ cells.

4.2.19 Agarose gel electrophoresis

PCR products were separated and visualized using gel electrophoresis and a UV light imaging system. In particular, 1 % agarose gel was prepared by dissolving 1.5 g agarose in 150 ml 1x TAE, boiling in a microwave at 900 Watt for 1–3 min and afterwards adding 4 µl ethidium bromide solution (10 mg/ml). After casting and cooling the gel for 60 min, 6 µl containing 1 µl DNA gel loading dye (6x), 2 µl PCR products and 3 µl ddH_20 were added per lane. The 100 bp

DNA ladder was added at a concentration of 0.8 µg/lane. PCR products and the DNA ladder were separated at 90 V for 30–60 min and visualized using the BioDoc-It Imaging System.

4.2.20 Whole transcriptome sequencing

The preparation of RNA for whole transcriptome sequencing was performed by Valentina Evdokimova, PhD. RNA was isolated as described in 4.2.16. RNA integrity was evaluated using the RNA 6000 Pico chip and 2100 Bioanalyzer. Strand-specific RNA-seq libraries were prepared and quality of libraries confirmed using the KAPA RNA HyperPrep Kit with RiboErase (HMR) and Agilent High Sensitivity DNA assay, respectively. Sequencing of samples was performed to about 100 M reads per sample with at least 2 × 100 bp on an Illumina NovaSeq at the Ontario Institute for Cancer Research, Toronto, Canada.

4.2.21 Bioinformatical analysis

The bioinformatical analysis was performed by Peter Ruzanov, PhD at the Ontario Institute for Cancer Research, Toronto, Canada. Raw paired-end strand-specific 100-bp reads were aligned to the reference human genome build 38 (hg38/GRCh38) using the Bowtie2 aligner v.2.3.5.1. Reads of rRNA and tRNA were filtered, and secondary alignments and reads with mapping scores less than 30 were excluded. Transcript expression was quantified as the number of fragments per kilobase of transcript per million mapped reads (FPKM) with cufflinks suite (http://cole-trapnell-lab.github.io/cufflinks/; accessed on 15.12.2020). Statistical analysis and plotting of the graphs was performed in R statistical environment with the ggplot2 package (https://www.R-project.org/; accessed on 01.12.2020). Immune cell populations were deconvoluted based on the transcriptome signature using CIBERSORT [35]. Hallmark gene sets of the Molecular Signature Database (MSigDB, http://www.gsea-msigdb.org/gsea/msigdb/collections.jsp; accessed on 01.03.2020) and published gene data sets [36,37] were used to assemble the gene lists for DC, M1 and M2 macrophages, and the ISG signature.

4.2.22 Statistical analysis

Statistical analysis was performed using R statistical environment and GraphPad Prism 9. Statistical tests are indicated in the result section and respective figure legends. For parametric data, p values were calculated using the un(paired) two-tailed t-tests and ordinary one-way or two-way analysis of variance (ANOVA) in combination with Tukey's multiple comparison tests. For nonparametric values, the Mann-Whitney U test was applied. p values ≤ 0.05 were considered statistically significant (* $p \leq 0.05$, ** $p \leq 0.01$,*** $p \leq 0.001$, **** $p \leq 0.0001$), or

not significant (ns) when $p > 0.05$. Illustrations for the experimental layouts were obtained from BioRender.com (accessed on 8 October 2020) and figures were generated using PowerPoint. The graphical abstract of the proposed model was created in Adobe Illustrator and Adobe Photoshop with the help of Dr. Dr. med. Sebastian Schober.

5 Results

5.1 Isolation and characterization of EVs from cell culture supernatant and human plasma

In order to investigate the effect of EwS EVs on myeloid cells, EVs were isolated from conditioned medium of EwS A4573, A673, TC32 or TC71 and MRC5 fibroblast cell lines using ultrafiltration followed by UC or SEC. EVs from MRC5 fibroblasts were chosen as non-cancer EV control, because fibroblasts are present in the TME of EwS and MRC5 cells merely express HERV-K(HML2) and HSAT3 [79,232,233]. To examine the effect of blood circulating EVs on myeloid cells, EVs were isolated from the plasma of EwS patients and healthy donors using ultrafiltration and UC (Table 17: Characteristics of EwS patients and healthy donors in this study).

Modal particle size of EVs isolated by UC from the conditioned medium of A4573, A673, TC32, TC71 and MRC5 ranged between 100–170 nm as determined by NTA (Figure 2A). Immunoblotting and flow cytometry of three independent EV preparations confirmed the presence of EV markers including CD63, CD81 and TSG101, the chaperone proteins Hsp70 and Hsp90 as well as the cytoskeletal proteins actin and tubulin (Figure 2B, C, Supplementary Figure 1A–C). Calnexin, a frequent cellular contaminant, was not detectable (Supplementary Figure 1C).

Since UC can co-pellet proteins and aggregates, which may false positively activate myeloid cells, SEC was used as additional method for EV isolation. NTA showed that the median particle size was comparable between EVs isolated in parellel by UC and SEC from the conditioned medium of A673, TC32 or MRC5 (Supplementary Figure 2A, $p > 0.05$, two-way ANOVA with multiple comparison Tukey test). BCA protein assay confirmed that SEC separated proteins from EV fractions (Supplementary Figure 2B). However, the particle count was one order of magnitude lower in EV preparations isolated by SEC compared to UC (Supplementary Figure 2C). Therefore, EVs isolated by UC were used for the majority of functional EV experiments (hereinafter referred to as EVs unless otherwise indicated). Immunoblotting confirmed that UC and SEC showed comparable presence of EV markers, including Annexin A1, CD81, Syntenin-1 and TSG101 (Supplementary Figure 2D). Calnexin was not detectable. Hsp90, and tubulin were also not detectable in these EV preparations in contrast to Figure 2 and Supplementary Figure 1, which might indicate exosomes with less cytoplasmic contamination from the parental cells [234].

Table 17: Characteristics of EwS patients and healthy donors in this study

Donor	Age/ Gender	Primary site/ Status	Sample/ Treatment	NTA	Immuno blotting	PrimeFlow RNAassay: EVs/Frequency/Phenotype		
EwS 1	11/M	Thigh, multifocal, osseous/localized	Diagnosis/before	x			x	
EwS 2	14/F	Clavicle, osseous/ bone metastasis	Diagnosis/before	x			x	
EwS 3	16/F	Kidney, extraosseous/lung metastasis	Diagnosis/before	x	x	x	x	
EwS 4	11/F	Mandible, osseous/ lung metastasis	Relapse/after	x				
EwS 5	16/M	Clavicle, osseous/ localized	Diagnosis/before	x				
EwS 6	17/M	Femur, osseous/ localized	Diagnosis/before	x		x	x	
EwS 7	3/M	Femur, osseous/ localized	Diagnosis/before	x	x		x	
EwS 8	16/F	Pelvis, osseous/lung metastasis	Diagnosis/before	x	x		x	
EwS 9	13/M	Multifocal, osseous/multiple metastasis	Relapse/after	x	x		x	
EwS 10	4/F	Multifocal, osseous/multiple metastasis	Relapse/after	x		x	x	
EwS 11	8/F	Os sacrum, osseous/bone marrow metastasis	Diagnosis/before	x		x	x	
EwS 12	13/F	Femur, osseous/localized	Diagnosis/before	x			x	
EwS 13	12/F	Femur, osseous/localized	Diagnosis/before	x			x	x
EwS 14	10/M	Clavicle, osseous/localized	Diagnosis/before					x
EwS 15	9/M	Clavicle, osseous/localized	Diagnosis/before					x
EwS 16	8/M	Radius, osseous/localized	Diagnosis/before					x
Healthy 1	54/F	-	-	x	x	x	x	x
Healthy 2	58/F	-	-	x	x	x	x	x
Healthy 3	58/M	-	-	x	x	x	x	x
Healthy 4	58/M	-	-		x	x		
Healthy 5	46/F	-	-				x	x
Healthy 6	28/M	-	-				x	x
Healthy 7	48/M	-	-				x	

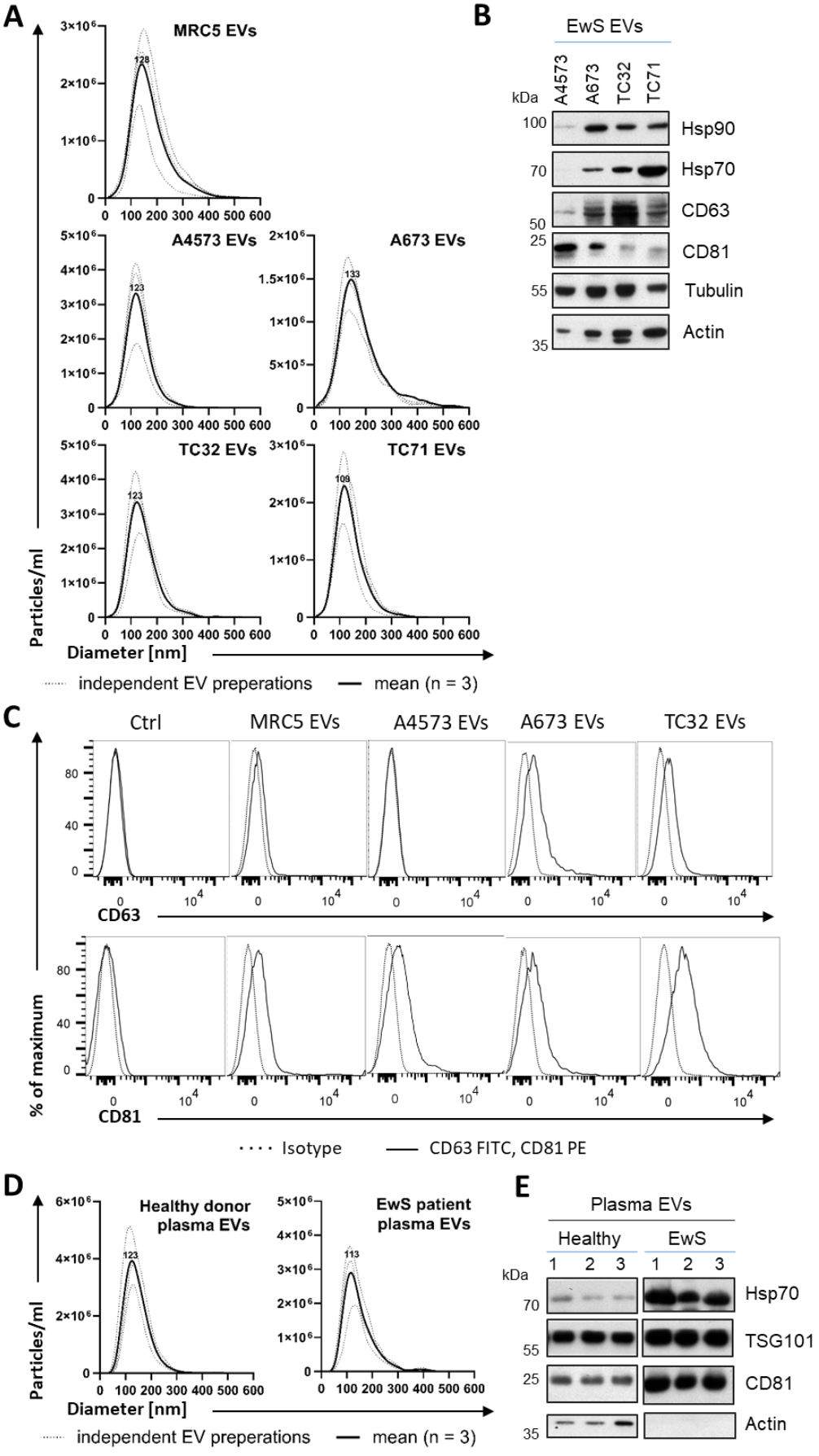

Figure 2 Isolation and characterization of EVs from cell culture supernatant and human plasma.

(**A**) Size distribution of EV preparations isolated by ultrafiltration and UC from conditioned medium of EwS cell lines A4573, A673, TC32 and TC71 and MRC5 fibroblasts. NTA results of three independent EV preparations (dotted line) and the respective mean (solid line) is displayed. (**B**) Immunoblotting of EwS cell line EVs for EV markers CD63 and CD81, chaperone proteins Hsp70 and Hsp90, and cytoskeleton proteins actin and tubulin. (**C**) Flow cytometry of EwS and MRC5 EV preparations coupled with 4.0 µm latex beads detecting EV markers CD63 or CD81 (solid lines) and respective isotype controls (dashed lines). Representative results of three independent EV preparations is displayed. (**D**) Size distribution of EV preparations isolated by UC from plasma of EwS patients and healthy donors. NTA results of three independent EV preparations (dotted line) and the respective mean (solid line) is presented. (**E**) Immunoblotting of plasma EVs from three independent healthy donors and EwS patients for EV markers CD81 and TSG101, Hsp70 and actin.

Comparable to cell line EVs, NTA of EVs isolated from 1 ml plasma of EwS patients and healthy donors exhibited similar modal size of 110 nm and 123 nm (Figure 2D). Immunoblotting of plasma EV preparations confirmed the presence of EV markers CD81 and TSG101 as well as Hsp70 (Figure 2E). In contrast to healthy donor plasma EVs, actin was undetectable in EwS patient plasma EVs, which might indicate exosomes with less cytoplasmic contamination, as mentioned above.

EVs from EwS patient plasma and EwS cell lines were shown to be associated with RE and satellite transcripts [121]. To test whether RE and satellite repeats are carried within or outside of EwS EVs, TC32 EVs isolated by UC were sonicated, treated with RNAse A or exposed to both conditions. Sonication alone did not affect RE and satellite transcripts, while the addition of RNAse A to EV preparations degraded HERV-K env, HERV-K pro, HSAT2, LINE-1, ACRO1 and GAPDH (Supplementary Figure 3A,B). This result might either indicate that RNAs including RE and satellites are exposed on the outside of EwS EVs or degraded by remaining traces of RNAse A during RNA isolation. The latter possibility is supported by the finding that the addition of RNAse A to MUTZ-3 cells before RNA isolation degraded total RNAs during the subsequent RNA isolation (Supplementary Figure 3C). Hence, RNAse A-treatment with complete inactivation or removal of RNAse A is needed to analyze whether REs are exposed at the outside or localized within EVs. Further studies are required to examine the mechanisms by which RE are released from EwS cells and how they are transported.

5.2 EwS cell line EVs induce a pro-inflammatory response in myeloid cells

To evaluate the functional effect of EwS EVs on blood-circulating myeloid cells, $CD33^+$ myeloid cells and $CD14^+$ monocytes were purified from the blood of healthy donors and treated in dose- and time-dependent manners with EwS cell line EVs *in vitro*.

First, the effect of EV preparations on the release of TNF, a major pro-inflammatory cytokine [235], from myeloid cells was tested. Cytokine singleplex assay showed that TNF was strongly elevated in the supernatant of $CD14^+$ monocytes after 6-h treatment with three independent EV preparations from the EwS cell lines A4573, A673, TC32 and TC71. In contrast, PBS-, MRC5 EV- and healthy donor plasma EV-treated $CD14^+$ monocytes did not release TNF (Figure 3).

Next, conditioned medium of CD33$^+$ myeloid cells and CD14$^+$ monocytes treated with EwS A4573, A673 and TC32 EVs for 24 h was analyzed by cytokine multiplex assay. In addition to TNF, the pro-inflammatory cytokines IL-1β, IL-6 and IL-8 as well as the chemokines CCL2, CCL3 and CCL4 were increased by 10–1,000-fold compared to PBS-treated cells (Figure 4A, B). CD33$^+$ and CD14$^+$ cells exhibited a similar cytokine response, with A4573 EVs inducing the strongest cytokine release (Figure 4A,B). In contrast to healthy donor plasma EVs, the release of IL-6, IL-8 and TNF from CD33$^+$ cells was dose-dependently induced by A4573 EVs (Figure 4C). These cytokines were not detected in conditioned medium spiked in with A4573 EVs, therefore ruling out a cytokine transfer by EVs. Despite medium change after 6-h treatment with A673 EVs, CD33$^+$ cells released IL-6 and IL-8 in a sustained and concentration-dependent manner at 24 h, whereas MRC5 EVs did not induce IL-6, IL-8 or TNF secretion (Figure 4D). Similarly, TC32 and TC71 EVs stimulated persistent TNF release from CD14$^+$ cells (Figure 4E). To test if EwS EVs prompt a pro-inflammatory response during differentiation of myeloid cells, CD33$^+$ cells were differentiated towards immature moDCs with GM-CSF and IL-4 in the presence of EVs. In comparison to PBS, TC32 EVs induced 16- and 480-fold increases of TNF ($p > 0.05$) and IL-6 ($p \leq 0.05$), which despite medium change persisted after 120 h (Figure 4F, unpaired two-tailed t-test). MRC5 EVs showed a slight induction of TNF and IL-6. In summary, EwS cell line EVs induced sustained pro-inflammatory responses in CD14$^+$ and CD33$^+$ myeloid cells.

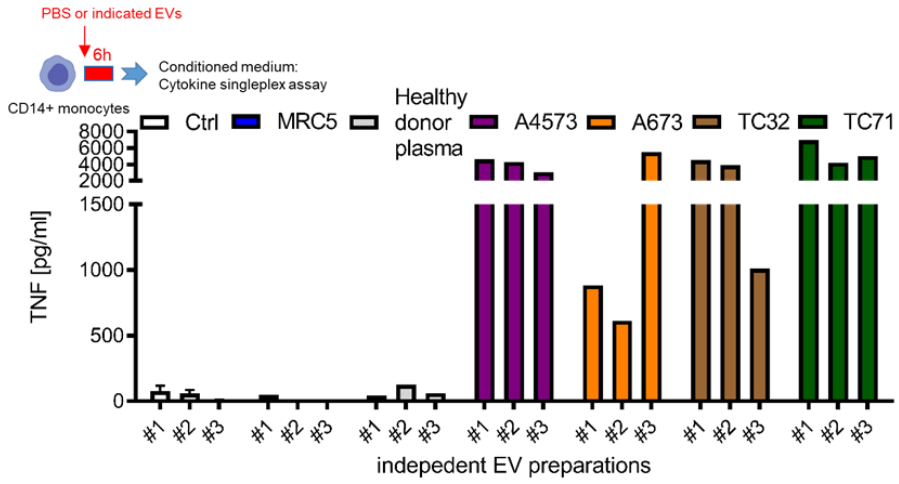

Figure 3 EwS EVs induce TNF release from CD14$^+$ monocytes.

TNF singleplex assay of cell culture supernatant from healthy donor-derived CD14$^+$ monocytes treated for 6 h with three independent EV preparations (3 x 10^9 EV particles/ml) of EwS cell lines A4573, A673, TC32 and TC71, healthy donor plasma, MRC5 fibroblasts or PBS as control (Ctrl).

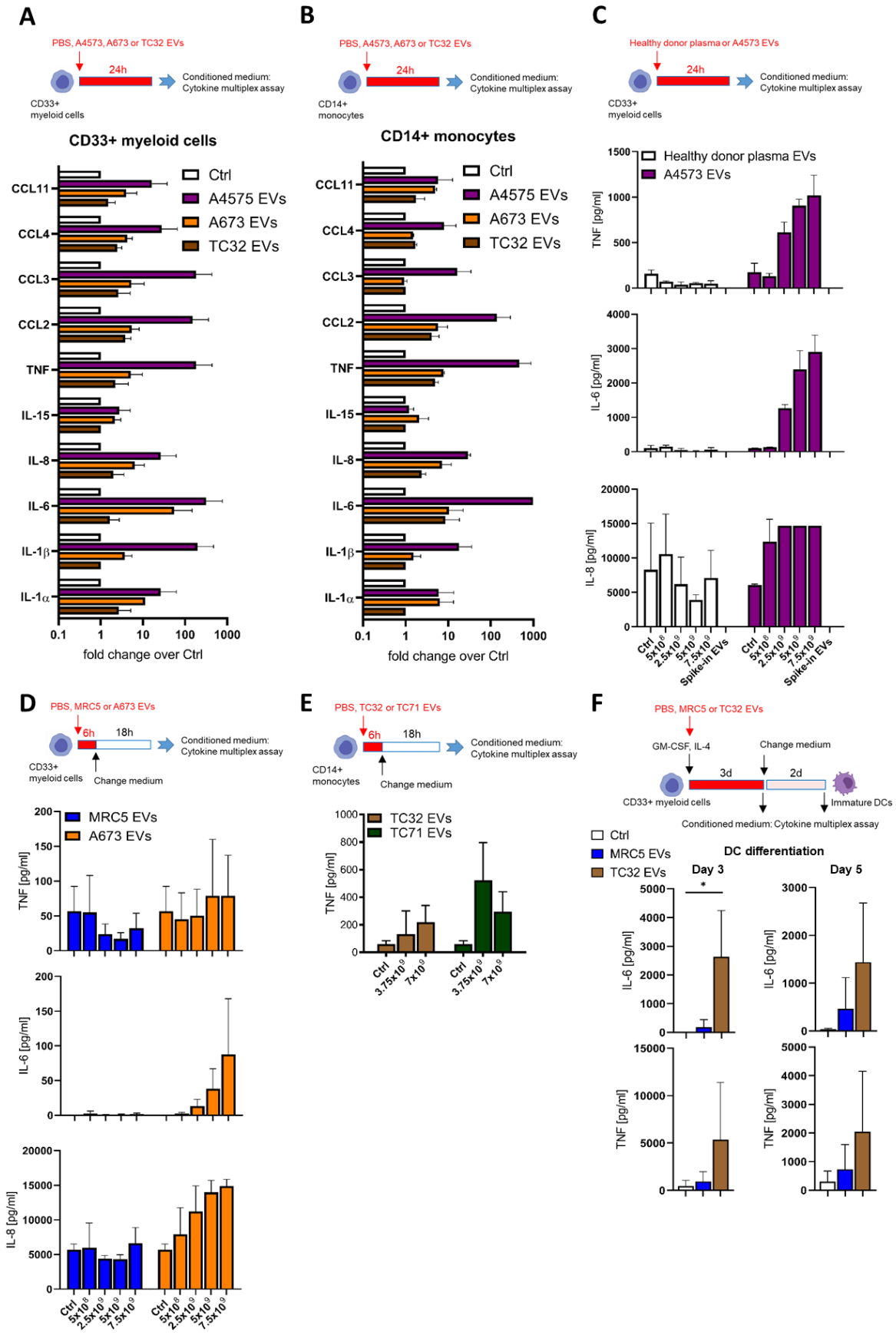

Figure 4 EwS EVs induce persistent pro-inflammatory cytokine release from CD33$^+$ and CD14$^+$ myeloid cells.

(**A**–**F**) Results of cytokine multiplex assays of conditioned medium are shown. (**A**) $CD33^+$ and (**B**) $CD14^+$ myeloid cells were treated with 3 x 10^9 EV particles/ml from EwS cell lines A4573, A673 and TC32 for 24 h. (**C**) $CD33^+$ myeloid cells were treated for 24 h with indicated amount of EVs from A4573 or healthy donor plasma. (**D**) $CD33^+$ and (**E**) $CD14^+$ monocytes were treated for 6 h with indicated amount of EVs from TC32 and TC71 or PBS as control (Ctrl) before medium was renewed and incubated for another 18 h. (**F**) $CD33^+$ myeloid cells were differentiated with GM-CSF and IL-4 in the presence of 3 x 10^9 EV particles/ml from TC32 or MRC5 or PBS as Ctrl. Medium was renewed after 72 h and incubated for another 48 h. Results were obtained from one (E), two (C), or three (A,B,D,F) independent donors with one (D), two (C), or three (A,B,E,F) independent EV preparations. Data are presented as mean ± SD. Unpaired two-tailed t-test was used to calculate p values (E). * $p \leq 0.05$.

5.3 EwS cell line EVs impair the differentiation and maturation of myeloid cells towards moDCs

Because EwS EVs induced persistent pro-inflammatory responses in $CD33^+$ and $CD14^+$ myeloid cells, we hypothesized that EwS EVs interfere with the maturation of myeloid cells towards DCs. To this end, an established *in vitro* model was used for the differentiation and maturation of $CD14^+$ and $CD33^+$ myeloid cells towards moDCs by the addition of cytokine cocktails containing GM-CSF and IL-4 followed by IL-1β, IL-6, PGE_2 and TNF [46]. EwS EVs and MRC5 EVs were added on day 0 and 3 of differentiation as well as on day 5 during maturation. At day 7, the phenotype of moDCs was assessed by flow cytometry (Figure 5A,E).

EwS A673, TC32 and TC71 EVs added to $CD14^+$ cells on day 0 of differentiation significantly impaired the upregulation of the co-stimulatory molecules CD80 and CD86 as well as the antigen-presenting molecule HLA-DR compared to PBS- or MRC5 EV-treated cells (Figure 5B, $p \leq 0.05$, one-way ANOVA with multiple comparison Tukey test). This effect was consistently induced by three independent TC32 EV preparations (Figure 5C, $p \leq 0.05$, unpaired two-tailed t-test). In $CD33^+$ cells differentiated and maturated to moDCs, TC32 EVs added on day 0 significantly inhibited the upregulation of HLA-DR, while changes in CD80 and CD86 were not statistically significant (Figure 5D, $p \leq 0.05$, paired two-tailed t-test). The addition of TC32 EVs to $CD33^+$ or $CD14^+$ cells on day 0, but not on days 3 or 5, significantly reduced the viability and upregulation of CD80, CD86 and HLA-DR (Figure 5E, Supplementary Figure 4A–D, $p \leq 0.05$ unpaired and paired two-tailed t-test). Taken together, EwS EVs impaired the differentiation and maturation of myeloid cells at an early stage resulting in semi-mature moDCs.

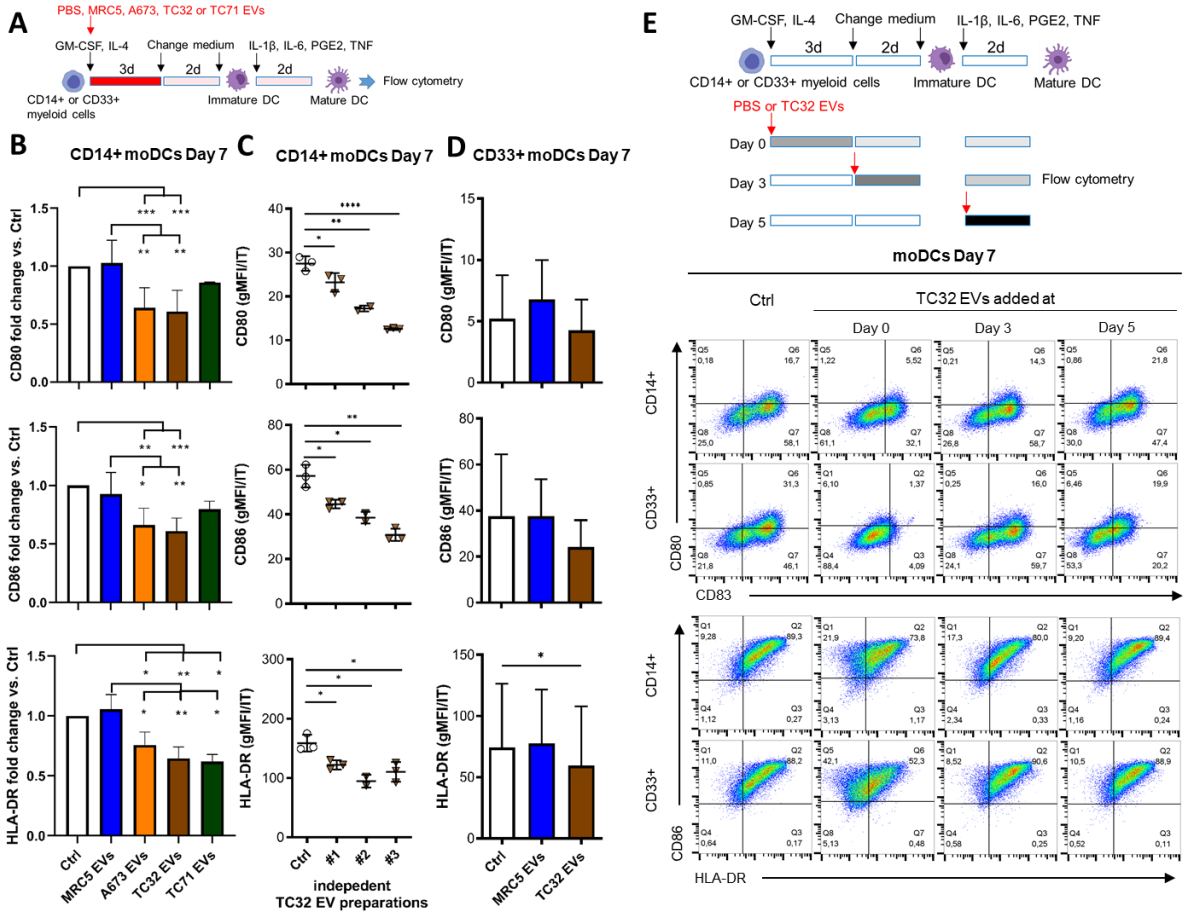

Figure 5 EwS EVs impair the differentiation and maturation of myeloid cells to moDCs at an early stage.

(**A**) Experimental layout (B–D). Healthy donor-derived $CD14^+$ or $CD33^+$ myeloid cells were differentiated by GM-CSF and IL-4 for 5 days and matured to moDCs by IL-1β, IL-6, PGE_2 and TNF for 2 additional days. 3 x 10^9 EV particles/ml from A673, TC32 or TC71 or MRC5 cells or PBS as control (Ctrl) were added on day 0. At day 7, surface expression of CD80, CD86 and HLA-DR was assessed by flow cytometry. (**B**) Geometric mean fluorescence intensity (gMFI) normalized to the respective isotype (IT) control of CD80, CD86 and HLA-DR on $CD14^+$ myeloid cells treated with EVs from MRC5, A673, TC32 and TC71 cells or PBS as Ctrl. Fold change to Ctrl is shown. (**C**) gMFI normalized to IT of CD80, CD86 and HLA-DR on $CD14^+$ myeloid cells treated with three independent TC32 EV preparations. (**D**) gMFI normalized to IT of CD80, CD86 and HLA-DR on $CD33^+$ myeloid cells treated with EVs from MRC5 or A673 cells or PBS as Ctrl. (**E**) Representative pseudocolor plots of CD80, CD83, CD86, HLA-DR and respective IT antibodies on $CD14^+$ or $CD33^+$ myeloid cells treated with TC32 EVs added on day 0 or 3 of differentiation or day 5 during maturation, or PBS as Ctrl. Results were derived from one (C) or three (B,D,E) independent donors with three independent EV preparations (B–E). Data are presented as mean ± SD. P values were calculated using one-way ANOVA with multiple comparison Tukey test (B), unpaired (C) and paired (D) two-tailed t-tests. * $p \leq 0.05$, ** $p \leq 0.01$, *** $p \leq 0.001$ and **** $p \leq 0.001$.

5.4 EwS cell line EVs modulate gene expression of myeloid cells associated with inflammatory responses and semi-mature phenotype

As exposure to EwS EVs resulted in a semi-mature phenotype of moDCs, it was tested whether EwS EVs disturb the transcriptome in myeloid cells, inducing pro-inflammatory as well as immunosuppressive gene expression.

$CD14^+$ cells were differentiated to immature moDCs with GM-CSF and IL-4 in the presence of PBS or EVs from TC32 or TC71 and harvested after four days (Figure 6A). Whole

transcriptome sequencing showed that 8254/10519 (81 %) genes were commonly regulated between the PBS control and EV-treated cells (Figure 6B). EVs from TC32 and TC71 commonly regulated 412 genes in $CD14^+$ cells, whereby 331 and 196 genes were specifically regulated by TC32 EVs and TC71 EVs, respectively. CIBERSORT analysis identified that $CD14^+$ cells differentiated in the presence of EwS EVs displayed decreased fractions of "Dendritic cells activated" and increased signatures of monocytes and macrophages (Figure 6C), suggesting a relation between EwS EVs and the prevalence of these immune cell types in the TME of EwS [67,69]. Subsequently, hallmark genes for M1 and M2 macrophages as well as DCs were analyzed, where TC32 EVs and TC71 EVs shared effects compared to the control cells (Figure 6D). For M1, EwS EVs upregulated genes encoding pro-inflammatory cytokines *IL1B*, *IL6*, *IL8/CXCL8*, *TNF* and *CCL4*, in line with cytokine multiplex data in Figure 4, as well as the receptors *IL7R* and *CCR7*, a marker for DC maturation. Regarding M2 genes, EwS EVs induced the anti-inflammatory cytokines *IL10*, *TGFβ* and *CCL18*, the receptors *IL21R [236]*, *IL27RA [237]*, *CXCR4* [238], *HLA-G* [239] as well as the immune checkpoint ligand *CD274/PDL1*. Hallmark transcription factors *STAT3* for MDSCs and *TRIB1* for M2 macrophages were also upregulated [240,241]. In the DC signature, genes associated with maturation showed opposing expression patterns: *CD80*, *CD209* and *LAMP3* were induced, whereas *CD86*, *HLA-DRA* and *HLA-DRB* were downregulated in line with flow cytometry data shown in Figure 5, indicating semi-mature phenotypes. Opposing expression patterns induced by TC71 vs TC32 EVs may reflect the biological heterogeneity of the parental cell lines and their respective EVs, which requires further investigations.

Because EwS EVs were reported to be associated with RE and satellite repeats [121], the expression of ISGs including cytosolic and endosomal RNA sensing and type I IFN response was analyzed. EwS EVs activated a distinct pattern of ISGs in $CD14^+$ cells compared to the PBS control (Figure 6E). The presence of EwS EVs upregulated the dsRNA sensors *IFIH1/MDA5* and *DDX58/RIG-I*, the viral restriction factors *OASL*, *MX1*, *IFITM1-3* and *IFI6* as well as the IFN receptors *IFNAR1/2*. These findings may suggest sensing of nucleic acids and type I IFN signaling in EV-treated $CD14^+$ cells. In summary, EwS EVs strongly altered gene expression during differentiation of $CD14^+$ cells, in line with induction of pro-inflammatory and antiviral signaling as well as a semi-mature DC phenotype.

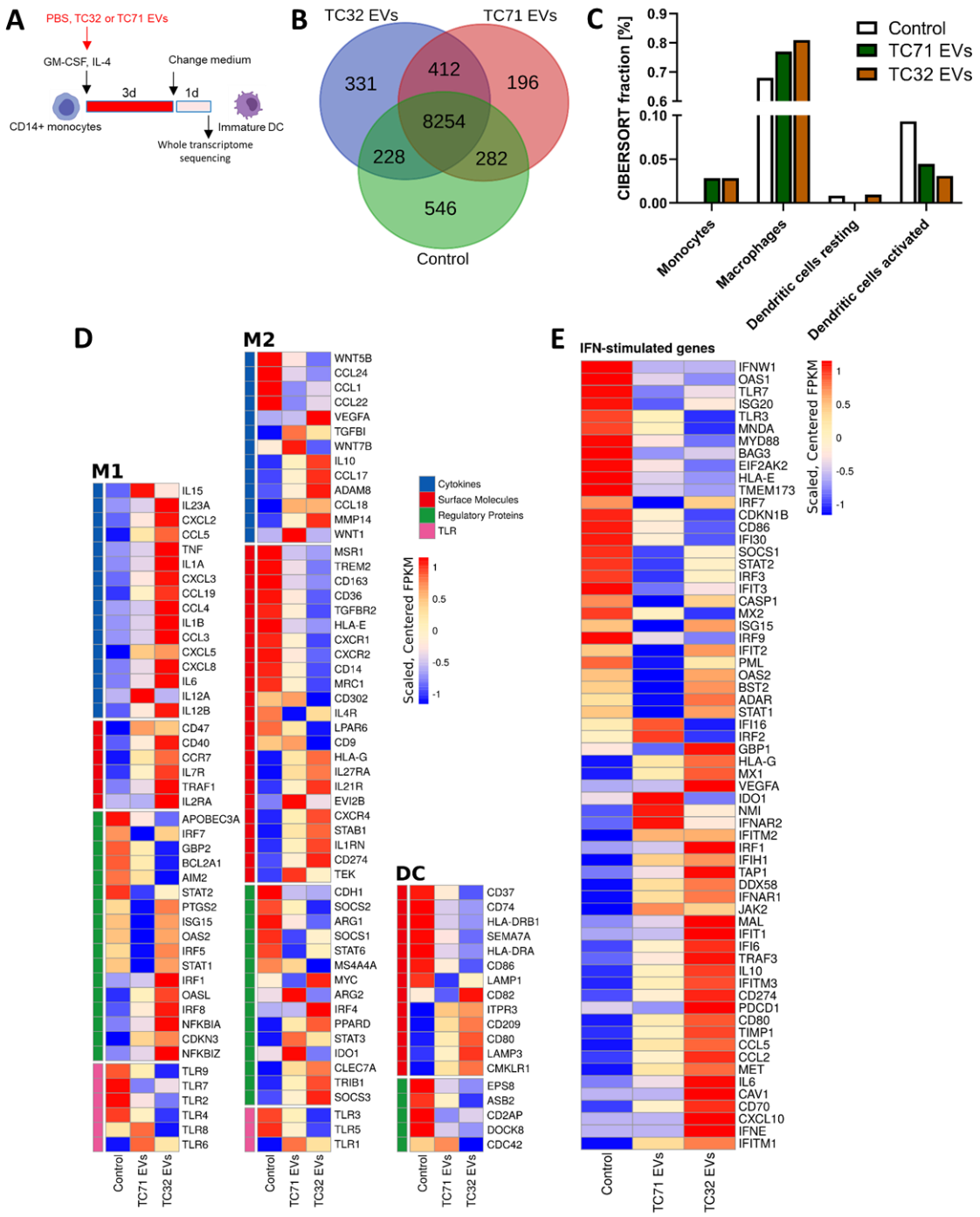

Figure 6 EwS EVs promote pro- and anti-inflammatory gene expression in CD14⁺ monocytes differentiated to immature moDCs.

(**A**) Experimental layout (B–E). Healthy donor-derived CD14⁺ monocytes cells were differentiated by GM-CSF and IL-4 in the presence of 3 x 10^9 EV particles/ml from TC32 or TC71 cells or PBS as Control. Medium was renewed at day 3 and cells were harvested at day 4 for whole transcriptome analysis. (**B**) Venn diagram displaying the overlap between expressed genes (≥ 10 FPKM) in CD14⁺ cells treated with EwS EVs or PBS. (**C**) CIBERSORT analysis quantifying the fractions of four myeloid cell sub-populations in CD14⁺ monocytes differentiated in the presence of EwS EVs or PBS. (**D**, **E**) Heatmaps of signature genes for M1 and M2 macrophages, DC (**D**) or ISGs (**E**) using gene list adapted from the MSigDB Hallmark database or publicly available gene sets. Genes displayed are assembled in the categories cytokines (blue), surface molecules (red), regulatory proteins (green), and toll-like receptors (TLR, pink). Data represent expression values sorted according to fold change in TC32 and TC71 EV-treated CD14⁺ cells compared to Control. Visualizations were created using FPKM values computed with cufflinks, scaled, and centered prior to plotting.

5.5 EwS cell line EVs reduce the T cell stimulatory capacity of moDCs

To evaluate their functionality, moDCs differentiated and matured in the presence of EwS or MRC5 EVs were co-cultured with allogeneic CD14-depleted PBMCs for 96 h. T cell activation and proliferation were quantified by cytokine multiplex assay and flow cytometry (Figure 7A).

After 96-h co-culture, the release of the T cell effector molecule IFNγ was significantly reduced when $CD14^+$ cells were differentiated in the presence of TC32 EVs compared to MRC5 EVs and the PBS control, while IL-10 and IL-6 were significantly upregulated (Figure 7B, $p \leq 0.05$, Mann-Whitney U test). TNF was unselectively released when $CD14^+$ cells were differentiated in the presence of both TC32 EVs and MRC5 EVs, in line with slight TNF secretion from $CD33^+$ cells differentiated in the presence of MRC5 EVs (Figure 4F).

In addition to the reduced IFNγ release, the proliferation of $CD8^+$ T cells and particularly $CD4^+$ T cells was significantly decreased when CD14-depleted PBMCs were co-cultured with moDCs differentiated in the presence of A673 and TC32 EVs, but not MRC5 EVs or the PBS control (Figure 7C, $p \leq 0.01$ and $p \leq 0.001$, one-way ANOVA with multiple comparison Tukey test). Consistent with decreased proliferation, the early T cell activation marker CD69 was significantly less upregulated on allogeneic $CD8^+$ T cells when co-cultured for 24 h with EwS EV-pretreated moDCs compared to MRC5 EVs and the PBS control (Supplementary Figure 5A,B, $p \leq 0.05$, one-way ANOVA with multiple comparison Tukey test). The surface expression of CD25 was unchanged (Supplementary Figure 5A,B). Even though the detailed mechanisms need to be investigated, these data suggest that the differentiation of $CD14^+$ monocytes in the presence of EwS cell line EVs leads to semi-mature DCs with reduced T cell stimulatory capacity.

5.6 EwS EVs induce cGAS signaling and type I IFN secretion in myeloid cells

To explore a potential mechanism of the pro-inflammatory response induced by EwS EVs in myeloid cells, MUTZ-3, an acute myelomonocytic leukemia cell line capable of differentiation to DCs [242], and $CD14^+$ monocytes were treated with EwS EVs.

Protein content of tumor-derived EVs was reported to induce a pro-inflammatory response in myeloid cells by transferring heat shock proteins, which signal via TLR4 on myeloid cells inducing pro-inflammatory cytokine release [117,243]. As Hsp70 and Hsp90 were detected in EwS EV preparations (Figure 2, Supplementary Figure 1), EwS EVs were used for the treatment of MUTZ-3 myeloid cells, shown to be deficient in TLR4 signaling [244].

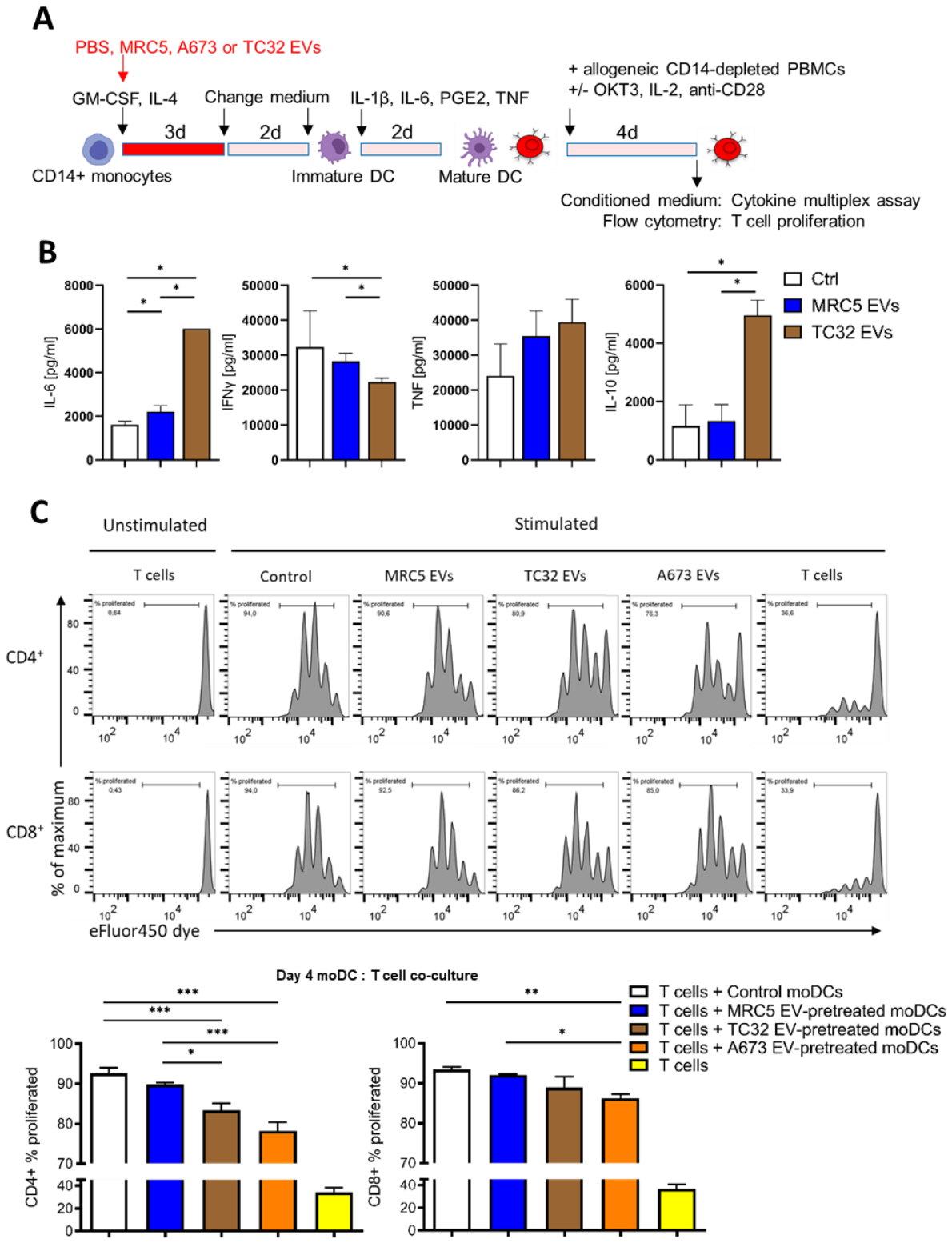

Figure 7 EwS EVs impair the T cell stimulatory capacity of moDCs.

(**A**) Experimental layout (B, C). Healthy donor-derived $CD14^+$ monocytes were differentiated by GM-CSF and IL-4 for 5 days and matured to moDCs by IL-1β, IL-6, PGE_2 and TNF for 2 additional days. 3 x 10^9 EV particles/ml from A673, TC32 or MRC5 cells or PBS as control (Ctrl) were added on day 0. At day 7, allogeneic CD14-depleted PBMCs were labeled with eFluor450 dye, stimulated with IL-2, soluble antiCD28 and coated antiCD3 (OKT3) antibodies, and co-cultured with EV-pretreated $CD14^+$ moDCs for 96 h. (**B**) IFNγ, IL-6, IL-10 and TNF

were quantified in the conditioned medium by cytokine multiplex after 96-h co-culture. (**C**) Proliferation of $CD3^+CD4^+$ and $CD3^+CD8^+$ T cells was assessed by e450 fluorescence intensity detected by flow cytometry. Representative histograms (top) and bar charts (bottom) are shown. Results were obtained from two (B) or three (C) independent donors with two (B) or three (C) independent EV preparations. Data are presented as mean ± SD. Mann-Whitney U test (B) and one-way ANOVA with multiple comparison Tukey test (C) were used to calculate p values. * $p \leq 0.05$, ** $p \leq 0.01$ and *** $p \leq 0.001$.

In contrast to the TLR4-agonist LPS, EwS EVs induced TNF secretion from MUTZ-3 cells (Figure 8A, $p \leq 0.05$, one-way ANOVA with multiple comparison Tukey test), indicating that EwS EVs can activate pro-inflammatory signaling in MUTZ-3 cells independent of TLR4 signaling. Furthermore, $CD14^+$ cells differentiated to immature moDCs in the presence of TC32 and TC 71 EVs did not upregulate *TLR2*, *TLR4* and *MYD88* (Figure 6D,E), suggesting signaling independent or in addition to the Hsp-TLR axis in myeloid cells.

In line with TNF secretion from MUTZ-3 cells in a TLR4 independent manner, 24-h treatment of $CD14^+$ cells with TC32 SEC EVs induced cGAS, a RNA-DNA hybrid sensor, and the phosphorylation of the downstream kinase TBK1 as shown by immunoblotting (Figure 8B). TC32 EVs isolated by UC had weak effects on cGAS and pTBK1. RIG-I was only induced by the positive controls LPS and poly(I:C), a dsRNA mimic binding to MDA5, RIG-I and TLR3 (Figure 8B). As cGAS activation promotes type I IFN production, it was tested by cytokine multiplex assay if EV-treated myeloid cells release type I IFNs. Indeed, healthy donor PBMCs treated with TC32 EV for 24 h secreted more IFNα compared to the PBS control (Figure 8C). A4573 EVs, but not healthy donor plasma EVs, stimulated a dose-dependent IFNα-release from $CD33^+$ cells after 24 h (Figure 8D). Lastly, IFNβ was significantly elevated in the supernatant from the 96-h co-culture of allogeneic CD14-depleted PBMCs and moDCs differentiated in the presence of TC32 EVs compared to MRC5 EVs and PBS controls (Figure 8E, $p \leq 0.01$ and $p \leq 0.001$, one-way ANOVA with multiple comparison Tukey test). Although further investigations are needed to study the mechanisms, EwS EVs might promote pro-inflammatory signaling and type I IFN secretion in myeloid cells via cGAS and potentially other nucleic acid sensors.

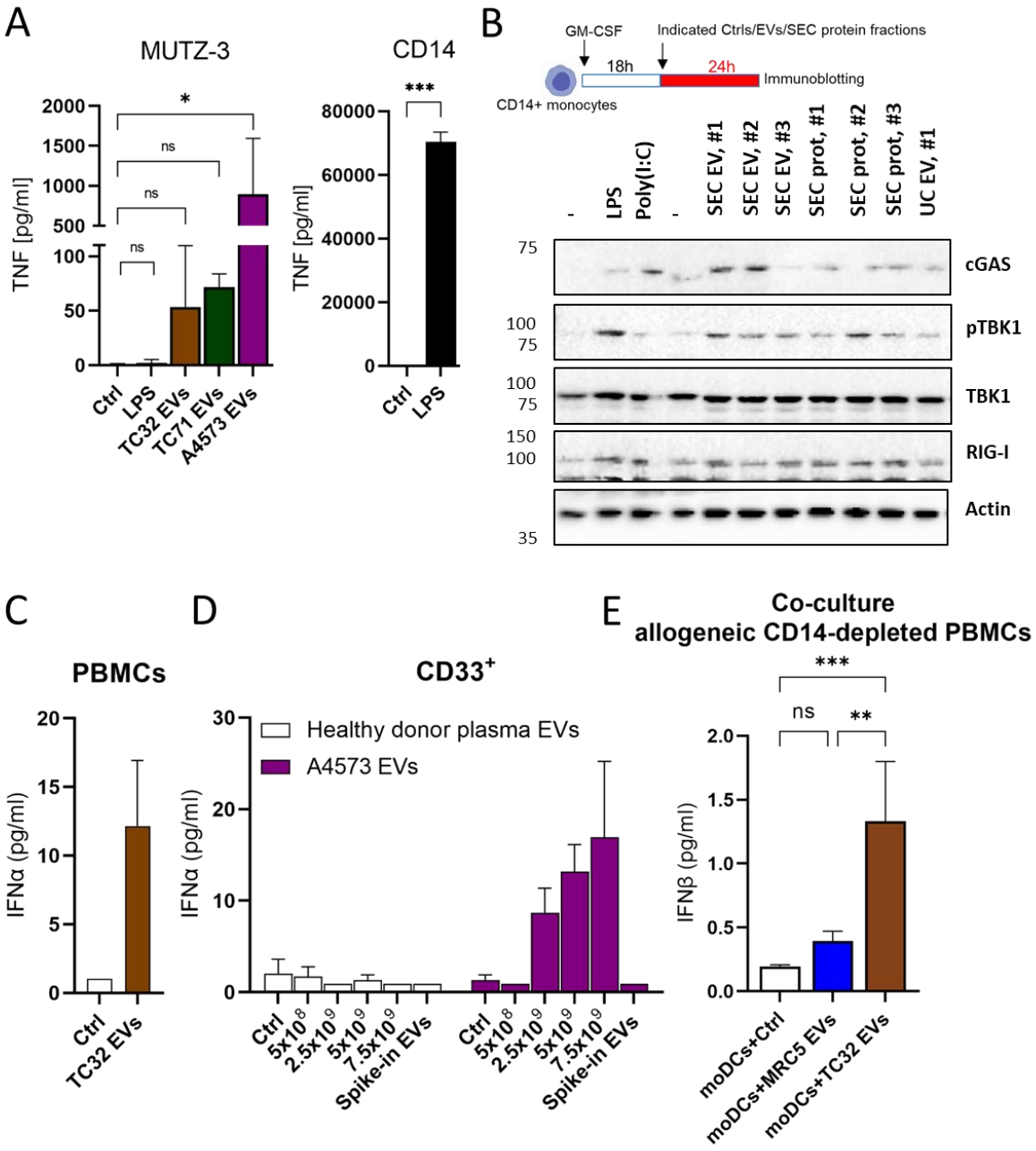

Figure 8 EwS EVs induce cGAS signaling and type I IFN secretion in myeloid cells.

(**A**) MUTZ-3 were treated with PBS as control (Ctrl), LPS (1 mg/ml) and indicated EVs ($3x10^9$/ml) for 6 h. $CD14^+$ myeloid cells were treated in parallel with PBS or LPS (1 mg/ml) as positive control. Cell culture supernatant was analyzed by TNF singleplex assay. (**B**) Immunoblotting for cGAS, pTBK1, TBK1, RIG-I and actin of $CD14^+$ monocytes treated for 24 h with 5 x 10^9 EV particles/ml from TC32 isolated by UC and SEC as well as the protein fraction of SEC. SEC EV and protein flow through were collected in three equal consecutive fractions. PBS was used as negative control, LPS (1 ng/ml) and poly(I:C) (2 µg/ml) as positive controls. (**C–E)** Cytokine multiplex assay quantifying IFNα (C, D) and IFNβ (E) in the cell culture supernatant. (**C**) Healthy donor PBMCs were treated with 4 x 10^{10} TC32 EVs/ml or PBS as Ctrl for 24 h. (**D**) Healthy donor $CD33^+$ myeloid cells were treated with indicated amount of EVs derived from A4573 or healthy donor plasma or PBS as Ctrl. (**E**) 96 h-co-culture of EV-pretreated $CD14^+$ moDCs and allogeneic CD14-depleted PBMCs, stimulated with soluble antiCD28 antibodies, coated antiCD3 antibodies (OKT3) and IL-2. The results from two (A, C, D, E) biological and three (B) technical replicates are shown. Data are presented as mean ± SD. One-way ANOVA with multiple comparison Tukey test (A, E) was used to calculate p values. * $p \leq 0.05$, ** $p \leq 0.01$ and *** $p \leq 0.001$.

5.7 EwS EVs lead to accumulation of RE and satellite repeats in $CD33^+$ and $CD14^+$ myeloid cells

Because of the induction of cGAS and type I IFNs, we hypothesized that EwS EVs transfer RE and satellites into recipient myeloid cells.

Healthy donor PBMCs were treated for 48 h with EVs derived from plasma of healthy donors and EwS patients as well as with EVs from EwS cell lines. The expression of HERV-K pol and HSAT2 was quantified using PrimeFlow RNA assay. The strongest effect for EwS EV-induced HERV-K pol and HSAT2 accumulation was observed in the $CD33^+$ myeloid cells (19.2–47.3 %) compared to $CD4^+$ (1.1–10.5 %), $CD8^+$ (2.7–11.4 %) and $CD19^+$ (4.4–9.1 %) lymphocytes (Figure 9A), suggesting that EwS EVs might primarily affect myeloid cells. In contrast to healthy donor plasma EVs, EVs from EwS cell lines and EwS patient plasma lead to a significantly accumulation of HERV-K pol- (4.8 % vs. 30.6 % vs. 47.3 %, $p \leq 0.01$ and $p \leq 0.0001$, one-way ANOVA with multiple comparison Tukey test) and HSAT2- (1.3 % vs. 28.0 % vs. 42.8 %, $p \leq 0.001$ and $p \leq 0.0001$, one-way ANOVA with multiple comparison Tukey test) positive $CD33^+$ myeloid cells (Figure 9A).

To verify the EwS EV-mediated accumulation of RE and satellite repeats, $CD14^+$ monocytes were treated with EVs isolated by UC and SEC from A673, TC32 or MRC5, and gene expression was quantified by sqRT-PCR. HERV-K pro and HSAT2 dose-dependently accumulated in $CD14^+$ monocytes after 48-h treatment with increasing doses of TC32 UC EVs (Figure 9B). Moreover, HERV-K pro and HSAT2 were both upregulated in $CD14^+$ monocytes treated with A673 and TC32 UC EVs, but not when exposed to MRC5 UC EVs or PBS (Figure 9C, $p \leq 0.05$ and p 0.066, unpaired two-tailed t-test). EVs isolated from A673 by UC as well as SEC significantly and dose-dependently upregulated HERV-K pro ($p \leq 0.001$ and $p \leq 0.0001$) and HSAT2 ($p \leq 0.001$ and $p \leq 0.01$, unpaired two-tailed t-test) in $CD14^+$ cells (Figure 9D), indicating that EwS EVs upregulate RE and satellites independent of the EV isolation method. Notably, the SEC protein fraction (adjusted to 52.8 µg equivalent to $1x10^{10}$ A673 UC EV particles containing 52.8 µg protein) also upregulated HERV-K pro and HSAT2 (Figure 9D, $p \leq 0.001$, unpaired two-tailed t-test). This suggests that the SEC protein fractions either contained HERV-K pro and HSAT2 transcripts and transferred them into $CD14^+$ cells or induced the endogenous expression of RE and satellite repeats.

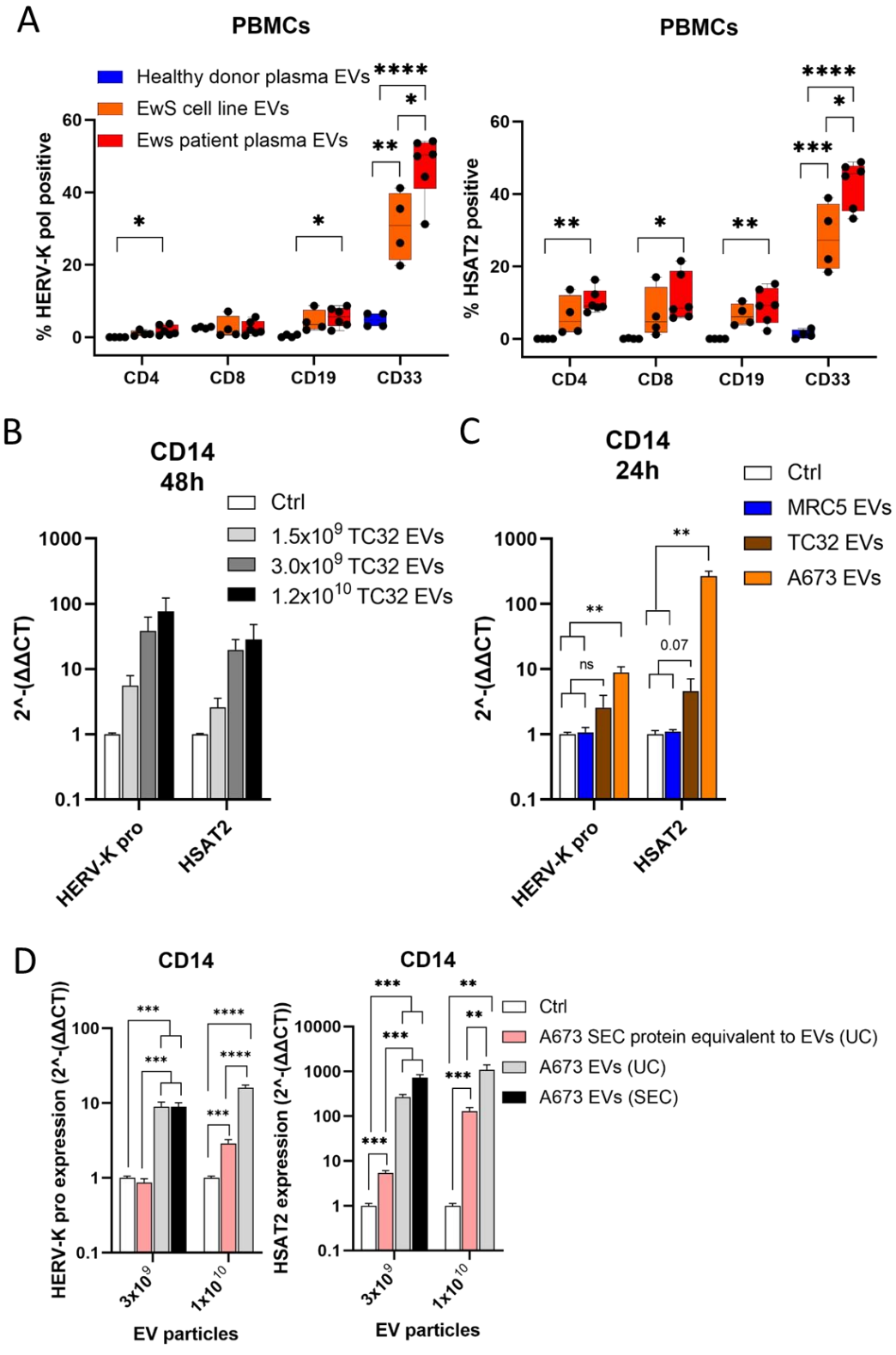

Figure 9 EwS EVs upregulate HERV-K pol, HERV-K pro and HSAT2 in myeloid cells.

(**A**) PrimeFlow RNA assay simultaneously detecting HERV-K pol (left panel) and HSAT2 (right panel) RNA probes and surface expression of leukocyte lineage markers. Healthy donor PBMCs were treated with indicated EVs (2 x 10^9/ml) for 48 h. (**B**) HERV-K pro and HSAT2 expression was quantified by sqRT-PCR in $CD14^+$ monocytes treated with indicated amount of TC32 EVs or PBS as control (Ctrl) for 48 h. (**C**) HERV-K pro and HSAT2 expression were quantified by sqRT-PCR in $CD14^+$ monocytes treated for 24 h with 3 x 10^9 EVs/ml from MRC5, A673 or TC32 cells or PBS as Ctrl. (**D**) HERV-K pro and HSAT2 expression were quantified by sqRT-

PCR. $CD14^+$ monocytes were treated for 24 h either with indicated amount of A673 EVs isolated by UC or SEC, or by the SEC protein fraction equivalent in protein amount to A673 UC EVs. The results were obtained from two independent experiments (A) and one (A, D), two (C) or three (B) independent donors. Data are presented as mean ± SD. One-way ANOVA with multiple comparison Tukey test (A) and unpaired two-tailed t-test (C, D) were used to calculate p values. * $p \leq 0.05$, ** $p \leq 0.01$, *** $p \leq 0.001$ and **** $p \leq 0.0001$.

Next, the effect of EwS EVs, MRC5 EVs, PBS, LPS and poly(I:C) on further repeat elements, cytosolic RNA sensors and ISGs was analyzed by sqRT-PCR. In contrast to EVs isolated by UC or SEC from MRC5 (Figure 10A), TC32 UC EVs (Figure 10B) as well as A673 UC and SEC EVs (Figure 10C) dose-dependently upregulated RE including HERV-K pro, HERV-K env and LINE-1 as well as the satellites HSAT2 and ACRO1. A673 EVs also induced DDX58/RIG-I and IFITM3. Further ISGs, in particular IFI6, IFI16, IFI30, IFI35, IFNAR1, IFTITM1, IFITM2 and MX1, were unchanged by TC32 or A673 EVs (Supplementary Figure 6A,B). This could be due to shorter treatment duration in comparison to Figure 6E. MRC5 EVs did not upregulate REs, satellites, cytosolic RNA sensors or ISGs, but dose-dependently induced IL-10. Poly(I:C) induced HERV-K pro, HSAT2, ACRO1, LINE-1, MDA5, DDX58, OASL and IFNα, implying that the activation of nucleic acid sensors induces expression of RE and satellite repeats. LPS did not upregulated RE or satellites (Figure 10D), suggesting that these elements are not responsive to TLR4 signaling or donor-dependently regulated [245,246].

In $CD14^+$ cells of one healthy donor, RE and satellites were downregulated by EwS EVs, MRC5 EVs and poly(I:C) (Supplementary Figure 7A–D), while IL-6 and IL-10 were again dose-dependently induced by EwS EVs as observed before (Figure 4, Figure 6 and Figure 10). Therefore, RE and satellites might be expressed at basal levels in myeloid cells of healthy donors and are modulated in response to pro-inflammatory stimuli.

In summary, EV-induced RE accumulation was assessed in $CD33^+$ or $CD14^+$ myeloid cells of five independent donors. RE transcripts and ISGs were upregulated in three (Figure 9), unchanged in one (data not shown) and downregulated in one donor (Supplementary Figure 7). Additional studies are needed to investigate the expression of RE and satellite repeats in response to EwS EVs and pro-inflammatory stimuli, and to investigate, if RE and satellite repeats are transferred into myeloid cells by EwS EVs. Taken together, EwS EVs lead to the accumulation of RE and satellite transcripts in myeloid cells, which might be due to endogenous re-expression rather than EV-mediated transfer.

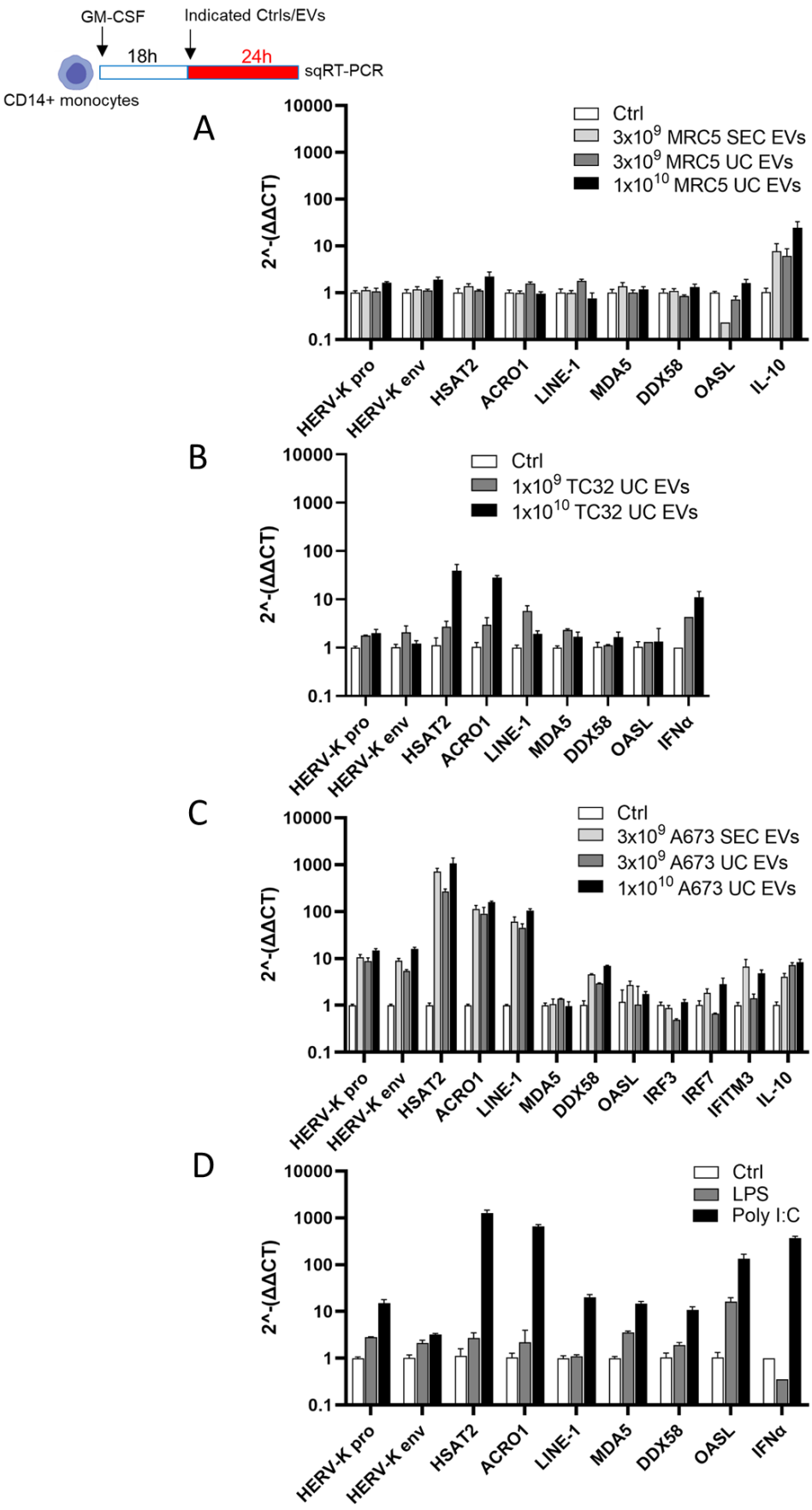

Figure 10 EwS EVs upregulate RE, satellite repeats and ISGs in CD14$^+$ monocytes.

(**A**–**D**) CD14$^+$ monocytes were seeded for 18 h in X-VIVO medium containing 1 % human AB serum and GM-CSF (80 U/ml), and treated for 24 h with indicated amount of EVs isolated by UC and SEC from MRC5 (**A**), TC32 (**B**) and A673 (**C**) cells or PBS as control (Ctrl). LPS (1 ng/ml) and poly(I:C) (2 µg/ml) were used as positive controls (**D**). Gene expression was quantified by sqRT-PCR. Results were obtained from one independent donor. Data are presented as mean ± SD.

5.8 EwS patients harbor increased frequency of blood circulating CD33$^+$ myeloid cells expressing HERV-K pol and HSAT2

To investigate the phenotype and expression of repeat elements in blood circulating myeloid cells, PBMCs of EwS patients and healthy donors (Table 17) were compared by PrimeFlow RNA assay. EwS patients showed an increased frequency of circulating CD33$^+$ myeloid cells positive for HERV-K pol (Figure 11A, top panel 22.7 % vs. 1.7 %, $p \leq 0.0001$, Mann-Whitney U test) and HSAT2 (Figure 11B, bottom panel 22.5 % vs. 2.9 %, $p \leq 0.001$, Mann-Whitney U test) compared to healthy donors. Additionally, HERV-K pol expressing CD8$^+$ T cells were significantly elevated in EwS patients (Figure 11A, top panel 15.1 % vs. 0.4 %, $p \leq 0.0001$, Mann-Whitney U test). The frequency of CD33$^+$ HERV-K pol$^+$ or HSAT2$^+$ myeloid cells did not correlate with plasma cytokines or plasma EV particle count (data not shown). In EwS patients, CD33$^+$ myeloid cells were significantly expanded in CD45$^+$ PBMCs (Figure 11B, 10.6 % vs. 4.8 %, $p \leq 0.05$, Mann-Whitney U test) and displayed significantly higher number of CD33$^+$HLA-DR$^-$ myeloid cells compared to healthy donors (Figure 11C, 45.1 % vs. 16.0 %, $p \leq 0.05$, Mann-Whitney U test). While HERV-K pol and HSAT2 were almost undetectable in CD33$^+$HLA-DR$^{+/positive}$ myeloid cells, significantly more CD33$^+$HLA-DR$^{-/negative}$ myeloid cells of EwS patients expressed HERV-K pol (Figure 11D, left panel, 12.9 % vs. 2.1 %, $p \leq 0.05$, Mann-Whitney U test), and showed increase of HSAT2 (Figure 11D, right panel, 18.7 % vs. 3.2 %, $p = 0.11$, ns, Mann-Whitney U test) in comparison to healthy donors. As the expression of RE and satellites varies with age [247], the age difference between EwS patients and healthy donors is a limitation in this study and needs further investigations.

Of note, in this EwS patient cohort the relative frequencies of CD4$^+$ T cells (Supplementary Figure 8A, 64.4 % vs. 28.8 %, $p \leq 0.001$, Mann-Whitney U test) and CD19$^+$ B cells (Supplementary Figure 8B, 5.6 % vs. 3.8 %, $p \leq 0.05$, Mann-Whitney U test) were significantly reduced compared to the healthy donors, which needs further investigation. The frequency of CD8$^+$ T cells did not differ (Supplementary Figure 8A).

In summary, the blood circulating CD33$^+$ myeloid cells of EwS patients are expanded, display a MDSC-like phenotype and express more frequently HERV-K pol and HSAT2.

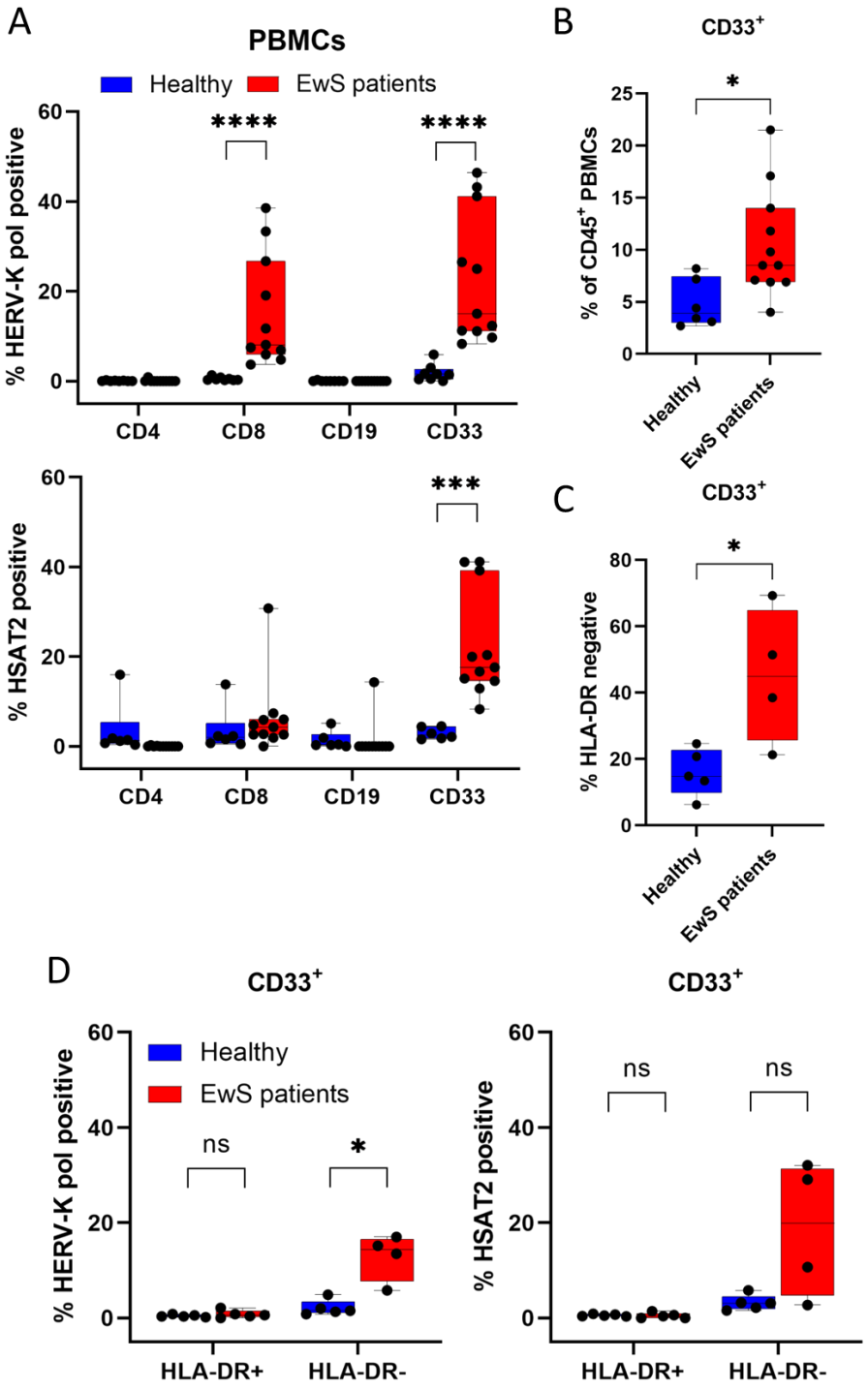

Figure 11 CD33$^+$ myeloid cells expressing HERV-K and HSAT2 are expanded and show MDSC-like phenotype in the blood of EwS patients.

(**A**–**D**) PrimeFlow RNA assay of PBMCs from healthy donors and EwS patients. (**A**) Expression of HERV-K pol (top panel) and HSAT2 (bottom panel) in CD4$^+$ or CD8$^+$ T cells, CD19$^+$ B cells or CD33$^+$ myeloid cells of CD45$^+$ PBMCs from healthy donors (n = 6) or EwS patients (n = 11). (**B**) Frequency of CD33$^+$ myeloid cells among CD45$^+$ PBMCs of healthy donors (n = 6) or EwS patients (n = 11). (**C**) Frequency of CD33$^+$HLA-DR$^-$ myeloid cells among CD45$^+$CD33$^+$PBMCs of healthy donors (n = 5) and EwS patients (n = 4). (**D**) HERV-K pol and HSAT2 expression in CD33$^+$ cells positive or negative for HLA-DR of healthy donors (n = 5) and EwS patients (n = 4). Data are presented as box plots with min, median and max. (A–D) Mann-Whitney U test was used to calculate p values. * $p \leq 0.05$, *** $p \leq 0.001$ and **** $p \leq 0.0001$.

6 Discussion

Because EwS are often infiltrated by macrophages with an immunosuppressive M2 transcriptome signature and EVs mediate cell-cell communication, the hypothesis of this study was that EwS EVs induce immunosuppressive myeloid cells. In this study, EwS EVs stimulated pro- and anti-inflammatory cytokine release from healthy donor-derived $CD33^+$ and $CD14^+$ myeloid cells and impaired their maturation promoting semi-mature DCs with reduced T cell stimulatory capacity. In parallel, EwS EVs lead to the accumulation of RE and satellite repeat transcripts accompanied by antiviral signaling in these myeloid cells. In EwS patients, $CD33^+$ myeloid cells expressing HERV-K pol and HSAT2 were expanded and displayed a MDSC-like phenotype ($CD33^+HLA\text{-}DR^-$). Therefore, EwS EVs may pathologically activate circulating and tumor-infiltrating myeloid cells skewing transcription, maturation and functionality (Figure 12).

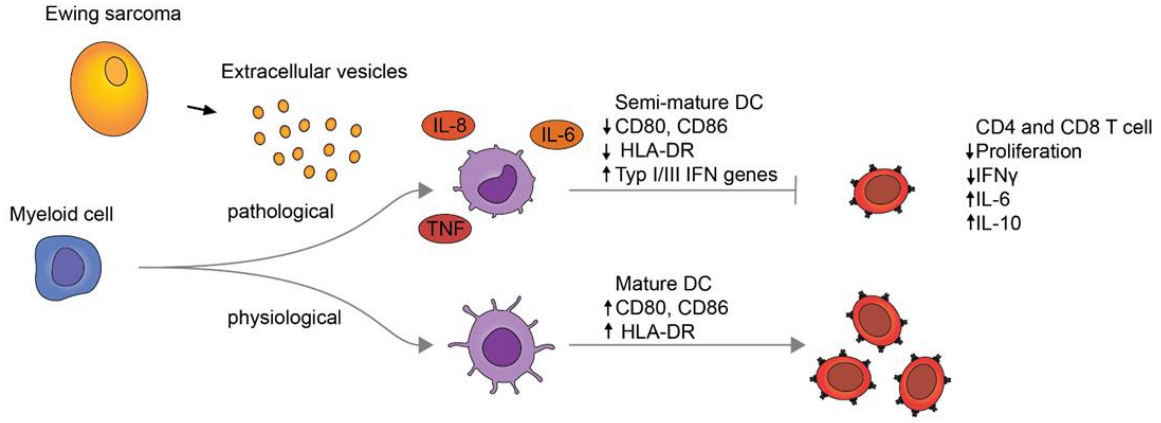

Figure 12 Proposed model: EwS EVs pathologically activate circulating and tumor-infiltrating myeloid cells skewing transcription, maturation and functionality.

6.1 EwS EVs pathologically activate myeloid cells and impair their T cell stimulatory function

This proposed model of pathological activation is based on the following three experimental findings. First, EwS EVs isolated by two independent methods induced expression and release of the pro-inflammatory cytokines IL-6, IL-8 and TNF as well as immunosuppressive IL-10. These findings are in line with results of EVs from various hematological and solid tumors [116,117,243,248]. The release of pro-inflammatory cytokines persisted despite medium change during DC differentiation and in subsequent co-cultures with allogeneic CD14-depleted PBMCs. IL-6 was shown to alter DC differentiation and T cell responses [249], therefore sustained pro-inflammatory cytokine-release induced by EwS EVs may affect the function of tumor-infiltrating myeloid cells in EwS. EwS EVs also induced expression and release of CCL4

from $CD33^+$ and $CD14^+$ myeloid cells. This finding needs further studies, as CCL4 was shown to be required for tumor infiltration of $CD103^+$ DCs and $CD8^+$ T cells in melanoma [250,251].

Second, transcriptomic analysis and flow cytometry demonstrated that EwS EVs impaired the differentiation and maturation of $CD33^+$ and $CD14^+$ myeloid cells towards moDCs. In particular, EwS EVs skewed the transcriptional profile towards macrophages and inhibited the upregulation of the co-stimulatory molecules CD80 and CD86 as well as the antigen-presenting HLA-DR. Similar findings were observed for EVs derived from mice and human adult solid tumor entities [248,252-254]. During moDC differentiation EwS EVs upregulated STAT3 on transcriptome level, which is a hallmark transcription factor of MDSCs [83,255] and contributes to abnormal DC differentiation [249,252,256]. DC maturation of $CD14^+$ and $CD33^+$ myeloid cells was affected when exposed to EwS EVs at an early stage of differentiation, in line with findings of EVs from murine mammary adenocarcinoma [252]. This indicates that particularly immature myeloid cells could be susceptible to tumor-derived EVs and chronic pro-inflammatory signals, leading to an immunosuppressive switch within myeloid cells [84].

Third, in line with their semi-mature phenotype, moDCs differentiated in the presence of EwS exhibited reduced T cell stimulatory capacity, which is a key feature of immature DCs [257] and MDSCs [81].

6.2 EwS EVs trigger an antiviral response, and upregulate RE and satellite repeats in myeloid cells

Although the mechanisms need to be further studied, the present study indicates that the pro-inflammatory response and the impaired maturation and function of myeloid cells could be mediated by the protein and RNA content of EwS EVs. Proteins detected in EwS EVs included Hsp70 and Hsp90, both capable of stimulating pro-inflammatory responses and skewing maturation of myeloid cells via TLR2 and TLR4 [117,243,254,258-260]. EwS EVs induced the inflammatory transcription factor NF-κB in $CD14^+$ cells; however, components of TLR pathways including TLR2, TLR4 and Myd88 were downregulated on transcriptome level. Furthermore, EwS EVs stimulated TNF secretion from MUTZ-3 myeloid cells, which are deficient in TLR4 signaling [244,261,262]. Together, these results suggest that EwS EVs can signal in $CD14^+$ and MUTZ-3 myeloid cells in a TLR4-independent manner.

Transcripts derived from RE and satellite repeats including HERV-K pol, HSAT2 and ACRO1 were detected in EwS cell lines, their corresponding EVs and plasma EVs of EwS patients [121]. In the current study, treatment with EwS EVs lead to accumulation of HERV-K pol, HERV-K pro, LINE-1, HSAT2 and ACRO1 in $CD33^+$ and $CD14^+$ myeloid cells.

RE and satellite repeats contain viral motifs and are under the surveillance of cytosolic and endoplasmatic nucleic acid sensors [174,175]. Consistent with the immunogenic motifs of RE and satellite repeats [139], EwS EVs carrying RE and satellite transcripts induced the RNA-DNA hybrid sensor cGAS, the downstream kinase pTBK1, type I IFNs and the expression of ISGs including the cytosolic dsRNA sensors DDX58/RIG-I and IFIH1/MDA5 in $CD33^+$ and $CD14^+$ myeloid cells. Therefore, EwS EVs might promote the pro-inflammatory response by accumulation of RE and satellite repeats in myeloid cells.

The accumulation of RE and satellite repeats, together with the upregulation of nucleic acid sensors and antiviral effector molecules, suggests that EwS EVs transfer RE and satellite transcripts into myeloid cells. Indeed, carrying transcripts of HERV-K pol and HSAT2, EwS patient plasma EVs and EwS cell line EVs, but not healthy donor plasma EVs or MRC5 EVs, upregulated HERV-K pol, HERV-K pro and HSAT2 in $CD33^+$ and $CD14^+$ myeloid cells. In line with these findings, upregulation of HERV-K6 was observed in human umbilical vein endothelial cells (HUVEC) by medulloblastoma-derived EVs [211].

However, two findings in the current study suggest that EwS EVs may mainly induce the endogenous re-expression of RE and satellite repeats in myeloid cells. First, studies using two independent reporter systems in parenteral and recipient cells demonstrated that a single RNA transcript is transferred only into a minor fraction of the recipient cells by EVs *in vitro*. In particular, de novo retrotransposition of LINE-1 transferred by EVs occurred in less than 1 % of recipient MDA-MB-M231 breast cancer cells and EV-mediated transfer of a guide RNA activated the reporter gene only in 0.2 % of recipient HEK293T cells [212,263]. This is in contrast to the 3–1000-fold increase of HERV-K pro and HSAT2 transcripts in $CD14^+$ myeloid cells and detection of HERV-K pol and HSAT2 in 19–47 % of $CD33^+$ myeloid cells in response to treatment with EwS EVs. Endogenous re-expression could explain the strong increase of HERV-K pol, HERV-K pro and HSAT2 in myeloid cells in response to EwS EVs. Second, RE and satellite repeats are transcriptionally induced by microbes, upon cellular stress or activation of immune cells [264-269]. In addition to EwS EVs, RE and satellite repeats were also upregulated by A673 SEC protein fractions and poly(I:C) in $CD14^+$ cells, indicating responsiveness of RE and satellite repeats to different stimuli. This is consistent with cellular stress upregulating HSAT3 in HeLa cells and poly(I:C) inducing ERVs in mice bone marrow DCs [266,270]. Modulated RE are frequently embedded or located near modulated host genes [245,266,268,271], where the binding of inflammatory transcription factors like IRF3, IRF7, NF-κB and STATs to promoters of RE induces their transcription [148,272]. As EwS EVs

upregulated IRF1, IRF7, NF-κB and STAT3 in $CD14^+$ cells, these inflammatory transcription factors may have contributed to the expression of RE in $CD14^+$ cells in response to EwS EVs.

Of note, recent evidence shows that RE and satellite repeats are constitutively expressed in healthy tissues [268,273-275]. In the present study, EwS EVs, MRC5 EVs and poly(I:C) also downregulated the expression of RE and satellite repeats within $CD14^+$ cells in one of five donors, indicating basal expression of RE and satellite repeats in myeloid cells and donor-specific regulation of RE and satellite activity. Variances in the basal expression of RE and satellite repeats between independent donors may be due to different epigenetic regulation and age [245,247,276]. Further studies are needed to investigate the mechanisms of interpersonal variety of myeloid cells in response to EwS EVs.

The accumulation of RE and satellite repeats may also have an effect on the formation of nuclear compartments and transcriptional condensates, as HERVs and satellite repeats are involved in phase transition and dissociation of transcriptional condensates at heterochromatin sites [277,278]. Altered phase separation is observed in EWS and FET fusion protein positive tumors [279], warranting further studies on the role of upregulated RE, equilibrium of phase transition and transcriptional control.

In summary, EwS EVs lead to accumulation of RE and satellite repeats in myeloid cells accompanied by the activation of antiviral genes and pro-inflammatory cytokine release. Further studies are needed to quantify the EwS EV-mediated transfer of RE and satellite repeats, and if RE and satellites associated with EwS EVs induce the endogenous re-expression of RE and satellite repeats within myeloid cells via nucleic acid sensors and downstream transcription factors. The effect may also be mediated by the protein content of EwS EVs, albeit RNA and protein mechanisms may not be mutually exclusive.

6.3 $CD33^+$ MDSC-like cells are expanded in the blood of EwS patients and harbor increased HERV-K pol and HSAT2 expression

In the present study, PBMCs of EwS patients showed increased levels of $CD33^+$ myeloid cells expressing HERV-K pol and HSAT2 in comparison to healthy donors. These HERV-K pol- and HSAT2-expressing $CD33^+$ myeloid cells displayed an MDSC-like phenotype ($CD33^+HLA\text{-}DR^-$). Basal expression of HERVs in PBMCs has been reported in healthy donors [246,247,280,281], while overexpression was observed in patients with autoimmune muscle and brain disorders [276,282], systemic lupus erythematosus [275] and cancer. For example, HERV-K10-like gag and HERV-K gag were overexpressed in PBMCs of patients with leukemia and

prostate cancer, respectively [283,284]. No data are currently available on satellite repeat expression in blood circulating immune cells.

MDSCs are expanded in adult and pediatric patients with solid cancers [80,88,285], mediate strong immunosuppressive effects and foster tumor growth [82]. The expression of RE and satellite repeats in myeloid cells with a MDSCs-like phenotype has not been reported before. RE and satellites might be linked with MDSCs through pro-inflammatory transcription factors, as C/EBP, NF-κB and STAT3 are involved in the expansion of MDSCs and are predicted to bind to LTR promoters [85,148]. Therefore, sustained pro-inflammatory signals activating pro-inflammatory transcription factors may promote the expression of MDSC genes as well as RE and satellite repeats.

The expression of RE and satellite repeats in tumors and their effect on the immune system is controversial. Subgroups of solid adult and pediatric tumor entities with upregulated RE show viral mimicry, immune infiltration and responsiveness to CPI [166,170,194,196,197]. In line, de-repression of RE in cancer cells by demethylating agents induced viral mimicry and antitumor immunity [184,286]. On the other hand, expression of RE and satellite repeats correlates with reduced immune infiltration and impaired survival in patients with sarcomas and gastrointestinal cancers [195,206,208,210].

EwS is a non-immunogenic tumor expressing RE and satellite repeats, which are released in association with EVs [58,69,121]. In the present study, EwS EVs induced semi-mature DCs with reduced T cell stimulatory function as well as the accumulation of RE and satellite repeats accompanied by antiviral signaling. Therefore, RE and satellite repeats may disseminate from EwS cells via EVs into the TME and blood circulation, contributing to chronic inflammation and in turn immunosuppression in EwS patients.

7 Limitations, perspectives and conclusions

7.1 Limitations and perspectives

Limitations of the current study include the characterization of EVs, the yet to be defined mechanisms by which EwS EVs induced the pro-inflammatory response in myeloid cells, the restriction to *in vitro* models and the narrow analysis of patient PBMCs. These limitations demand further research.

EVs isolated by UC and SEC comprise a heterogeneous population of vesicles with various RNA and protein cargo. Size distribution of EV preparations was quantified by NTA, however also transmission electron microscopy should be applied to verify size and shape, and to identify co-purified non-membranous particles [287]. While the RNA content of plasma EVs from EwS

patients and healthy donors has been characterized by whole transcriptome sequencing [121], the current study compared the protein content of EVs from EwS and MRC5 cell lines as well as EwS patients and healthy donors by immunoblotting, but not by a proteomic approach. Thus, this study potentially left aside proteins able to induce pro-inflammatory responses in myeloid cells. In our attempt to analyze plasma EVs by proteomics, we encountered a strong contamination by immunoglobulins hampering downstream analysis (data not shown). Protocol optimization for proteomics from plasma EVs is a next step. Also, it remains to be studied how RE and satellite repeats are packed and released from EwS cells, as RE and satellite repeats could also be released in RNA-protein complexes independent of EVs.

This study describes pro-inflammatory signaling, impaired maturation as well as accumulation of RE and satellite repeats in myeloid cells in response to EwS EVs. Both, the RNA and protein cargo of EwS EVs may mediate the pro-inflammatory response in myeloid cells, and the mechanisms of the EwS EV-induced pro-inflammatory response and RE accumulation remain to be studied. Mechanistic insights could be obtained by studying the effect of EwS EVs in recipient myeloid cells with knockouts or inhibition of intracellular sensors for pathogenic nucleic acids and proteins. Alternatively, the effect of constituent components of EwS EVs on myeloid cells could be assessed. For example, proteins or RNAs isolated from EwS EVs could be directly transfected into myeloid cells or loaded into synthetic vesicles for the treatment of myeloid cells [288].

Studying the functionality of EVs *in vitro* bears known limitations, as cell culture conditions of parenteral cells and EV-treatment of recipient cells may not recapitulate the *in vivo* situation. To control for *in vitro* artefacts caused by the cell culture conditions or EV isolation method, the non-tumor EVs (from MRC5 fibroblast and healthy donor plasma) were isolated in parallel to EVs from EwS cell lines or patient plasma, and used as negative controls in the treatment of myeloid cells. Still, the concentration of EVs and treatment duration *in vitro* may differ from the dynamic situation in the TME of EwS patients. *In vitro*, 0.05–4 x 10^{10} EV particles were added to 1 x 10^{6} myeloid cells in 1 ml, whereby the EV amount corresponded to 25 % of the total EV particles released from 4 x 10^{8} tumor cells in 18 h. These ratios of EV particles released per tumor cell and EV particles per myeloid cell may not be present in the TME of EwS.

The present study did not assess the effect of EwS EVs on myeloid cells *in vivo*, as the underlying mechanisms of packaging and release of RE and satellite repeats from EwS cells as well as the signaling mechanisms in EwS EV-treated myeloid cells remain to be studied beforehand. Another consideration for *in vivo* experiments is the lack of a syngeneic or transgenic mouse models in EwS [289]. The effect of EwS EVs on myeloid cells could instead

be studied in the established Rag2$^{-/-}$ $\gamma_C^{-/-}$ mice model [46,49,122,290]. In particular, the effect of EwS xenografts or intravenously injected EwS EVs on the phenotype, transcriptome and functionality of myeloid cells or PBMCs could be characterized.

PBMCs of EwS patients and healthy donors were analyzed showing a correlation of HERV-K and HSAT2 expression with a MDSC-like phenotype. Both methods, PrimeFlow RNA assay and sqRT-PCR used in this study are limited to selected surface antigens as well as RE and satellite repeats, therefore scRNAseq, wtRNAseq and multicolor flow cytometry are needed to comprehensively characterize the CD33$^+$HLA-DR$^-$HERVK$^+$/HSAT2$^+$ cells and to cover the expression of families and single elements of RE and satellite repeats. In addition to phenotypical and transcriptional characterization, functionality of patient-derived CD33$^+$HLA-DR$^-$ myeloid cells should be analyzed. Finally, the age of healthy donors differed from EwS patients, which should be addressed in future studies.

7.2 Conclusions

The present study describes that EVs derived from EwS cell lines and patient plasma skew the phenotype, maturation and gene expression of CD14$^+$ and CD33$^+$ myeloid cells and impair their functionality. These *in vitro* findings support a role of EwS EVs in promoting immunosuppressive myeloid cells in TME of EwS. In parallel, EwS EVs lead to the accumulation of RE and satellite repeats in CD14$^+$ and CD33$^+$ myeloid cells *in vitro*, suggesting a transfer or re-expression of repeat elements by EwS EVs. Because repeat elements are upregulated in various cancers, the dissemination of RE and satellite repeats via EVs might be a common mechanism in cancer. HERV-K- and HSAT2-expressing CD33$^+$ myeloid cells with a MDSC-like phenotype were expanded in the blood of EwS patients, indicating that accumulation of RE and satellite repeats may be associated with immunosuppressive myeloid cells.

8 References

1. Parkin, D.M.; Stiller, C.A.; Draper, G.J.; Bieber, C.A. The international incidence of childhood cancer. *Int J Cancer* **1988**, *42*, 511-520, doi:10.1002/ijc.2910420408.

2. Ewing, J. Diffuse endothelioma of bone. *Proc NY Pathol Soc* **1921**, *21*, 17-24.

3. Ambros, I.M.; Ambros, P.F.; Strehl, S.; Kovar, H.; Gadner, H.; Salzer-Kuntschik, M. MIC2 is a specific marker for Ewing's sarcoma and peripheral primitive neuroectodermal tumors. Evidence for a common histogenesis of Ewing's sarcoma and peripheral primitive neuroectodermal tumors from MIC2 expression and specific chromosome aberration. *Cancer* **1991**, *67*, 1886-1893, doi:10.1002/1097-0142(19910401)67:7<1886::aid-cncr2820670712>3.0.co;2-u.

4. Staege, M.S.; Hutter, C.; Neumann, I.; Foja, S.; Hattenhorst, U.E.; Hansen, G.; Afar, D.; Burdach, S.E.G. DNA Microarrays Reveal Relationship of Ewing Family Tumors to Both Endothelial and Fetal Neural Crest-Derived Cells and Define Novel Targets. *Cancer Research* **2004**, *64*, 8213-8221, doi:10.1158/0008-5472.can-03-4059.

5. Schmidt, D.; Harms, D.; Burdach, S. Malignant peripheral neuroectodermal tumours of childhood and adolescence. *Virchows Archiv A* **1985**, *406*, 351-365, doi:10.1007/BF00704304.

6. Grünewald, T.G.P.; Cidre-Aranaz, F.; Surdez, D.; Tomazou, E.M.; de Álava, E.; Kovar, H.; Sorensen, P.H.; Delattre, O.; Dirksen, U. Ewing sarcoma. *Nature Reviews Disease Primers* **2018**, *4*, 5, doi:10.1038/s41572-018-0003-x.

7. Delattre, O.; Zucman, J.; Plougastel, B.; Desmaze, C.; Melot, T.; Peter, M.; Kovar, H.; Joubert, I.; de Jong, P.; Rouleau, G.; et al. Gene fusion with an ETS DNA-binding domain caused by chromosome translocation in human tumours. *Nature* **1992**, *359*, 162-165, doi:10.1038/359162a0.

8. Riggi, N.; Suvà, M.L.; Stamenkovic, I. Ewing's Sarcoma. *New England Journal of Medicine* **2021**, *384*, 154-164, doi:10.1056/NEJMra2028910.

9. Brohl, A.S.; Solomon, D.A.; Chang, W.; Wang, J.; Song, Y.; Sindiri, S.; Patidar, R.; Hurd, L.; Chen, L.; Shern, J.F.; et al. The genomic landscape of the Ewing Sarcoma family of tumors reveals recurrent STAG2 mutation. *PLoS genetics* **2014**, *10*, e1004475, doi:10.1371/journal.pgen.1004475.

10. Crompton, B.D.; Stewart, C.; Taylor-Weiner, A.; Alexe, G.; Kurek, K.C.; Calicchio, M.L.; Kiezun, A.; Carter, S.L.; Shukla, S.A.; Mehta, S.S.; et al. The Genomic Landscape of Pediatric Ewing Sarcoma. *Cancer Discovery* **2014**, *4*, 1326-1341, doi:10.1158/2159-8290.cd-13-1037.

11. Jawad, M.U.; Cheung, M.C.; Min, E.S.; Schneiderbauer, M.M.; Koniaris, L.G.; Scully, S.P. Ewing sarcoma demonstrates racial disparities in incidence-related and sex-related differences in outcome: an analysis of 1631 cases from the SEER database, 1973-2005. *Cancer* **2009**, *115*, 3526-3536, doi:10.1002/cncr.24388.

12. Raney, R.B.; Asmar, L.; Newton, W.A., Jr.; Bagwell, C.; Breneman, J.C.; Crist, W.; Gehan, E.A.; Webber, B.; Wharam, M.; Wiener, E.S.; et al. Ewing's sarcoma of soft tissues in childhood: a report from the Intergroup Rhabdomyosarcoma Study, 1972 to 1991. *Journal of clinical oncology : official journal of the American Society of Clinical Oncology* **1997**, *15*, 574-582, doi:10.1200/jco.1997.15.2.574.

13. Gaspar, N.; Hawkins, D.S.; Dirksen, U.; Lewis, I.J.; Ferrari, S.; Le Deley, M.C.; Kovar, H.; Grimer, R.; Whelan, J.; Claude, L.; et al. Ewing Sarcoma: Current Management and Future Approaches Through Collaboration. *Journal of clinical oncology : official journal of the American Society of Clinical Oncology* **2015**, *33*, 3036-3046, doi:10.1200/jco.2014.59.5256.

14. Esiashvili, N.; Goodman, M.; Marcus, R.B., Jr. Changes in incidence and survival of Ewing sarcoma patients over the past 3 decades: Surveillance Epidemiology and End Results data. *Journal of pediatric hematology/oncology* **2008**, *30*, 425-430, doi:10.1097/MPH.0b013e31816e22f3.

15. Cotterill, S.J.; Ahrens, S.; Paulussen, M.; Jürgens, H.F.; Voûte, P.A.; Gadner, H.; Craft, A.W. Prognostic factors in Ewing's tumor of bone: analysis of 975 patients from the European Intergroup Cooperative

Ewing's Sarcoma Study Group. *Journal of clinical oncology : official journal of the American Society of Clinical Oncology* **2000**, *18*, 3108-3114, doi:10.1200/jco.2000.18.17.3108.

16. Thiel, U.; Wawer, A.; von Luettichau, I.; Bender, H.-U.; Blaeschke, F.; Grunewald, T.G.P.; Steinborn, M.; Röper, B.; Bonig, H.; Klingebiel, T.; et al. Bone marrow involvement identifies a subgroup of advanced Ewing sarcoma patients with fatal outcome irrespective of therapy in contrast to curable patients with multiple bone metastases but unaffected marrow. *Oncotarget* **2016**, *7*.

17. Stahl, M.; Ranft, A.; Paulussen, M.; Bölling, T.; Vieth, V.; Bielack, S.; Görtitz, I.; Braun-Munzinger, G.; Hardes, J.; Jürgens, H.; et al. Risk of recurrence and survival after relapse in patients with Ewing sarcoma. *Pediatr Blood Cancer* **2011**, *57*, 549-553, doi:10.1002/pbc.23040.

18. Juergens, C.; Weston, C.; Lewis, I.; Whelan, J.; Paulussen, M.; Oberlin, O.; Michon, J.; Zoubek, A.; Juergens, H.; Craft, A. Safety assessment of intensive induction with vincristine, ifosfamide, doxorubicin, and etoposide (VIDE) in the treatment of Ewing tumors in the EURO-E.W.I.N.G. 99 clinical trial. *Pediatr Blood Cancer* **2006**, *47*, 22-29, doi:10.1002/pbc.20820.

19. Le Deley, M.C.; Paulussen, M.; Lewis, I.; Brennan, B.; Ranft, A.; Whelan, J.; Le Teuff, G.; Michon, J.; Ladenstein, R.; Marec-Bérard, P.; et al. Cyclophosphamide compared with ifosfamide in consolidation treatment of standard-risk Ewing sarcoma: results of the randomized noninferiority Euro-EWING99-R1 trial. *Journal of clinical oncology : official journal of the American Society of Clinical Oncology* **2014**, *32*, 2440-2448, doi:10.1200/jco.2013.54.4833.

20. Whelan, J.; Deley, M.-C.L.; Dirksen, U.; Judson, I.R.; Hawkins, D.S.; Berg, H.V.D.; Ladenstein, R.; Kruseova, J.; Ranft, A.; Amler, S.; et al. Efficacy of busulfan-melphalan high dose chemotherapy consolidation (BuMel) in localized high-risk Ewing sarcoma (ES): Results of EURO-EWING 99-R2 randomized trial (EE99R2Loc). *Journal of Clinical Oncology* **2016**, *34*, 11000-11000, doi:10.1200/JCO.2016.34.15_suppl.11000.

21. Burdach, S.; van Kaick, B.; Laws, H.J.; Ahrens, S.; Haase, R.; Körholz, D.; Pape, H.; Dunst, J.; Kahn, T.; Willers, R.; et al. Allogeneic and autologous stem-cell transplantation in advanced Ewing tumors. An update after long-term follow-up from two centers of the European Intergroup study EICESS. Stem-Cell Transplant Programs at Düsseldorf University Medical Center, Germany and St. Anna Kinderspital, Vienna, Austria. *Annals of oncology : official journal of the European Society for Medical Oncology* **2000**, *11*, 1451-1462, doi:10.1023/a:1026539908115.

22. Baird, K.; Fry, T.J.; Steinberg, S.M.; Bishop, M.R.; Fowler, D.H.; Delbrook, C.P.; Humphrey, J.L.; Rager, A.; Richards, K.; Wayne, A.S.; et al. Reduced-intensity allogeneic stem cell transplantation in children and young adults with ultrahigh-risk pediatric sarcomas. *Biology of blood and marrow transplantation : journal of the American Society for Blood and Marrow Transplantation* **2012**, *18*, 698-707, doi:10.1016/j.bbmt.2011.08.020.

23. Ladenstein, R.; Pötschger, U.; Le Deley, M.C.; Whelan, J.; Paulussen, M.; Oberlin, O.; van den Berg, H.; Dirksen, U.; Hjorth, L.; Michon, J.; et al. Primary disseminated multifocal Ewing sarcoma: results of the Euro-EWING 99 trial. *Journal of clinical oncology : official journal of the American Society of Clinical Oncology* **2010**, *28*, 3284-3291, doi:10.1200/jco.2009.22.9864.

24. Thiel, U.; Wawer, A.; Wolf, P.; Badoglio, M.; Santucci, A.; Klingebiel, T.; Basu, O.; Borkhardt, A.; Laws, H.J.; Kodera, Y.; et al. No improvement of survival with reduced- versus high-intensity conditioning for allogeneic stem cell transplants in Ewing tumor patients. *Annals of oncology : official journal of the European Society for Medical Oncology* **2011**, *22*, 1614-1621, doi:10.1093/annonc/mdq703.

25. Thiel, U.; Schober, S.J.; Ranft, A.; Gassmann, H.; Jabar, S.; Gall, K.; von Lüttichau, I.; Wawer, A.; Koscielniak, E.; Diaz, M.A.; et al. No difference in survival after HLA mismatched versus HLA matched allogeneic stem cell transplantation in Ewing sarcoma patients with advanced disease. *Bone Marrow Transplantation* **2021**, doi:10.1038/s41409-020-01200-x.

26. Felix, A.; Berlanga, P.; Toulmonde, M.; Landman-Parker, J.; Dumont, S.; Vassal, G.; Le Deley, M.C.; Gaspar, N. Systematic review of phase-I/II trials enrolling refractory and recurrent Ewing sarcoma: Actual knowledge and future directions to optimize the research. *Cancer medicine* **2021**, *10*, 1589-1604, doi:10.1002/cam4.3712.

27. COLEY, W.B. THE TREATMENT OF INOPERABLE SARCOMA WITH THE 'MIXED TOXINS OF ERYSIPELAS AND BACILLUS PRODIGIOSUS.: IMMEDIATE AND FINAL RESULTS IN ONE HUNDRED AND FORTY CASES. *Journal of the American Medical Association* **1898**, *XXXI*, 456-465, doi:10.1001/jama.1898.92450090022001g.

28. Majzner, R.G.; Simon, J.S.; Grosso, J.F.; Martinez, D.; Pawel, B.R.; Santi, M.; Merchant, M.S.; Geoerger, B.; Hezam, I.; Marty, V.; et al. Assessment of programmed death-ligand 1 expression and tumor-associated immune cells in pediatric cancer tissues. *Cancer* **2017**, *123*, 3807-3815, doi:https://doi.org/10.1002/cncr.30724.

29. Spurny, C.; Kailayangiri, S.; Jamitzky, S.; Altvater, B.; Wardelmann, E.; Dirksen, U.; Hardes, J.; Hartmann, W.; Rossig, C. Programmed cell death ligand 1 (PD-L1) expression is not a predominant feature in Ewing sarcomas. *Pediatr Blood Cancer* **2018**, *65*, doi:10.1002/pbc.26719.

30. van Erp, A.E.M.; Versleijen-Jonkers, Y.M.H.; Hillebrandt-Roeffen, M.H.S.; van Houdt, L.; Gorris, M.A.J.; van Dam, L.S.; Mentzel, T.; Weidema, M.E.; Savci-Heijink, C.D.; Desar, I.M.E.; et al. Expression and clinical association of programmed cell death-1, programmed death-ligand-1 and CD8(+) lymphocytes in primary sarcomas is subtype dependent. *Oncotarget* **2017**, *8*, 71371-71384, doi:10.18632/oncotarget.19071.

31. Davis, K.L.; Fox, E.; Merchant, M.S.; Reid, J.M.; Kudgus, R.A.; Liu, X.; Minard, C.G.; Voss, S.; Berg, S.L.; Weigel, B.J.; et al. Nivolumab in children and young adults with relapsed or refractory solid tumours or lymphoma (ADVL1412): a multicentre, open-label, single-arm, phase 1-2 trial. *The Lancet. Oncology* **2020**, *21*, 541-550, doi:10.1016/s1470-2045(20)30023-1.

32. Machado, I.; López-Guerrero, J.A.; Scotlandi, K.; Picci, P.; Llombart-Bosch, A. Immunohistochemical analysis and prognostic significance of PD-L1, PD-1, and CD8+ tumor-infiltrating lymphocytes in Ewing's sarcoma family of tumors (ESFT). *Virchows Archiv : an international journal of pathology* **2018**, *472*, 815-824, doi:10.1007/s00428-018-2316-2.

33. Tawbi, H.A.; Burgess, M.; Bolejack, V.; Van Tine, B.A.; Schuetze, S.M.; Hu, J.; D'Angelo, S.; Attia, S.; Riedel, R.F.; Priebat, D.A.; et al. Pembrolizumab in advanced soft-tissue sarcoma and bone sarcoma (SARC028): a multicentre, two-cohort, single-arm, open-label, phase 2 trial. *The Lancet. Oncology* **2017**, *18*, 1493-1501, doi:10.1016/s1470-2045(17)30624-1.

34. D'Angelo, S.P.; Mahoney, M.R.; Van Tine, B.A.; Atkins, J.; Milhem, M.M.; Jahagirdar, B.N.; Antonescu, C.R.; Horvath, E.; Tap, W.D.; Schwartz, G.K.; et al. Nivolumab with or without ipilimumab treatment for metastatic sarcoma (Alliance A091401): two open-label, non-comparative, randomised, phase 2 trials. *The Lancet. Oncology* **2018**, *19*, 416-426, doi:10.1016/s1470-2045(18)30006-8.

35. Rosenberg, S.A.; Packard, B.S.; Aebersold, P.M.; Solomon, D.; Topalian, S.L.; Toy, S.T.; Simon, P.; Lotze, M.T.; Yang, J.C.; Seipp, C.A.; et al. Use of Tumor-Infiltrating Lymphocytes and Interleukin-2 in the Immunotherapy of Patients with Metastatic Melanoma. *New England Journal of Medicine* **1988**, *319*, 1676-1680, doi:10.1056/NEJM198812223192527.

36. June, C.H.; O'Connor, R.S.; Kawalekar, O.U.; Ghassemi, S.; Milone, M.C. CAR T cell immunotherapy for human cancer. *Science (New York, N.Y.)* **2018**, *359*, 1361-1365, doi:doi:10.1126/science.aar6711.

37. Rosenberg, S.A.; Restifo, N.P. Adoptive cell transfer as personalized immunotherapy for human cancer. *Science (New York, N.Y.)* **2015**, *348*, 62-68, doi:10.1126/science.aaa4967.

38. Kalos, M.; Levine Bruce, L.; Porter David, L.; Katz, S.; Grupp Stephan, A.; Bagg, A.; June Carl, H. T Cells with Chimeric Antigen Receptors Have Potent Antitumor Effects and Can Establish Memory in Patients with Advanced Leukemia. *Science Translational Medicine* **2011**, *3*, 95ra73-95ra73, doi:10.1126/scitranslmed.3002842.

39. Melenhorst, J.J.; Chen, G.M.; Wang, M.; Porter, D.L.; Chen, C.; Collins, M.A.; Gao, P.; Bandyopadhyay, S.; Sun, H.; Zhao, Z.; et al. Decade-long leukaemia remissions with persistence of CD4+ CAR T cells. *Nature* **2022**, *602*, 503-509, doi:10.1038/s41586-021-04390-6.

40. Maude, S.L.; Frey, N.; Shaw, P.A.; Aplenc, R.; Barrett, D.M.; Bunin, N.J.; Chew, A.; Gonzalez, V.E.; Zheng, Z.; Lacey, S.F.; et al. Chimeric antigen receptor T cells for sustained remissions in leukemia. *The New England journal of medicine* **2014**, *371*, 1507-1517, doi:10.1056/NEJMoa1407222.

41. Lee, D.W.; Kochenderfer, J.N.; Stetler-Stevenson, M.; Cui, Y.K.; Delbrook, C.; Feldman, S.A.; Fry, T.J.; Orentas, R.; Sabatino, M.; Shah, N.N.; et al. T cells expressing CD19 chimeric antigen receptors for acute lymphoblastic leukaemia in children and young adults: a phase 1 dose-escalation trial. *The Lancet* **2015**, *385*, 517-528, doi:10.1016/S0140-6736(14)61403-3.

42. Majzner, R.G.; Theruvath, J.L.; Nellan, A.; Heitzeneder, S.; Cui, Y.; Mount, C.W.; Rietberg, S.P.; Linde, M.H.; Xu, P.; Rota, C.; et al. CAR T Cells Targeting B7-H3, a Pan-Cancer Antigen, Demonstrate Potent Preclinical Activity Against Pediatric Solid Tumors and Brain Tumors. *Clinical Cancer Research* **2019**, *25*, 2560-2574, doi:10.1158/1078-0432.ccr-18-0432.

43. Huang, X.; Park, H.; Greene, J.; Pao, J.; Mulvey, E.; Zhou, S.X.; Albert, C.M.; Moy, F.; Sachdev, D.; Yee, D.; et al. IGF1R- and ROR1-Specific CAR T Cells as a Potential Therapy for High Risk Sarcomas. *PloS one* **2015**, *10*, e0133152, doi:10.1371/journal.pone.0133152.

44. Englisch, A.; Altvater, B.; Kailayangiri, S.; Hartmann, W.; Rossig, C. VEGFR2 as a target for CAR T cell therapy of Ewing sarcoma. *Pediatric Blood & Cancer* **2020**, *67*, e28313, doi:https://doi.org/10.1002/pbc.28313.

45. Ahmed, N.; Brawley, V.S.; Hegde, M.; Robertson, C.; Ghazi, A.; Gerken, C.; Liu, E.; Dakhova, O.; Ashoori, A.; Corder, A.; et al. Human Epidermal Growth Factor Receptor 2 (HER2) –Specific Chimeric Antigen Receptor–Modified T Cells for the Immunotherapy of HER2-Positive Sarcoma. *Journal of Clinical Oncology* **2015**, *33*, 1688-1696, doi:10.1200/jco.2014.58.0225.

46. Thiel, U.; Pirson, S.; Müller-Spahn, C.; Conrad, H.; Busch, D.H.; Bernhard, H.; Burdach, S.; Richter, G.H.S. Specific recognition and inhibition of Ewing tumour growth by antigen-specific allo-restricted cytotoxic T cells. *British Journal of Cancer* **2011**, *104*, 948-956, doi:10.1038/bjc.2011.54.

47. Kirschner, A.; Thiede, M.; Grünewald, T.G.; Alba Rubio, R.; Richter, G.H.; Kirchner, T.; Busch, D.H.; Burdach, S.; Thiel, U. Pappalysin-1 T cell receptor transgenic allo-restricted T cells kill Ewing sarcoma in vitro and in vivo. *Oncoimmunology* **2017**, *6*, e1273301, doi:10.1080/2162402x.2016.1273301.

48. Schirmer, D.; Grünewald, T.G.; Klar, R.; Schmidt, O.; Wohlleber, D.; Rubío, R.A.; Uckert, W.; Thiel, U.; Bohne, F.; Busch, D.H.; et al. Transgenic antigen-specific, HLA-A*02:01-allo-restricted cytotoxic T cells recognize tumor-associated target antigen STEAP1 with high specificity. *Oncoimmunology* **2016**, *5*, e1175795, doi:10.1080/2162402x.2016.1175795.

49. Blaeschke, F.; Thiel, U.; Kirschner, A.; Thiede, M.; Rubio, R.A.; Schirmer, D.; Kirchner, T.; Richter, G.H.S.; Mall, S.; Klar, R.; et al. Human HLA-A*02:01/CHM1+ allo-restricted T cell receptor transgenic CD8+ T cells specifically inhibit Ewing sarcoma growth in vitro and in vivo. *Oncotarget* **2016**, *7*, 43267-43280, doi:10.18632/oncotarget.9218.

50. Thiel, U.; Schober, S.J.; Einspieler, I.; Kirschner, A.; Thiede, M.; Schirmer, D.; Gall, K.; Blaeschke, F.; Schmidt, O.; Jabar, S.; et al. Ewing sarcoma partial regression without GvHD by chondromodulin-I/HLA-A*02:01-specific allorestricted T cell receptor transgenic T cells. *Oncoimmunology* **2017**, *6*, e1312239-e1312239, doi:10.1080/2162402X.2017.1312239.

51. Russell, S.J.; Peng, K.W. Viruses as anticancer drugs. *Trends in pharmacological sciences* **2007**, *28*, 326-333, doi:10.1016/j.tips.2007.05.005.

52. Schober, S.J.; Thiel, U.; Thiede, M.; Ehrenfeld, M.; Nawroth, R.; Richter, G.H.; Burdach, S.E.G.; Holm, P.S. Abstract A48: YB-1-based oncolytic virotherapy in combination with CDK4/6-inhibitors against Ewing sarcoma. *Cancer Research* **2020**, *80*, A48-A48, doi:10.1158/1538-7445.pedca19-a48.

53. Koch, J.; Schober, S.J.; Hindupur, S.V.; Schöning, C.; Klein, F.G.; Mantwill, K.; Ehrenfeld, M.; Schillinger, U.; Hohnecker, T.; Qi, P.; et al. Targeting the Retinoblastoma/E2F repressive complex by CDK4/6 inhibitors amplifies oncolytic potency of an oncolytic adenovirus. *Nature Communications* **2022**, *13*, 4689, doi:10.1038/s41467-022-32087-5.

54. Morales, E.; Olson, M.; Iglesias, F.; Dahiya, S.; Luetkens, T.; Atanackovic, D. Role of immunotherapy in Ewing sarcoma. *J Immunother Cancer* **2020**, *8*, e000653, doi:10.1136/jitc-2020-000653.

55. Atretkhany, K.N.; Drutskaya, M.S.; Nedospasov, S.A.; Grivennikov, S.I.; Kuprash, D.V. Chemokines, cytokines and exosomes help tumors to shape inflammatory microenvironment. *Pharmacology & therapeutics* **2016**, *168*, 98-112, doi:10.1016/j.pharmthera.2016.09.011.

56. Binnewies, M.; Roberts, E.W.; Kersten, K.; Chan, V.; Fearon, D.F.; Merad, M.; Coussens, L.M.; Gabrilovich, D.I.; Ostrand-Rosenberg, S.; Hedrick, C.C.; et al. Understanding the tumor immune microenvironment (TIME) for effective therapy. *Nat Med* **2018**, *24*, 541-550, doi:10.1038/s41591-018-0014-x.

57. Brohl, A.S.; Sindiri, S.; Wei, J.S.; Milewski, D.; Chou, H.-C.; Song, Y.K.; Wen, X.; Kumar, J.; Reardon, H.V.; Mudunuri, U.S.; et al. Immuno-transcriptomic profiling of extracranial pediatric solid malignancies. *Cell Reports* **2021**, *37*, doi:10.1016/j.celrep.2021.110047.

58. Gröbner, S.N.; Worst, B.C.; Weischenfeldt, J.; Buchhalter, I.; Kleinheinz, K.; Rudneva, V.A.; Johann, P.D.; Balasubramanian, G.P.; Segura-Wang, M.; Brabetz, S.; et al. The landscape of genomic alterations across childhood cancers. *Nature* **2018**, *555*, 321-327, doi:10.1038/nature25480.

59. Lawrence, M.S.; Stojanov, P.; Polak, P.; Kryukov, G.V.; Cibulskis, K.; Sivachenko, A.; Carter, S.L.; Stewart, C.; Mermel, C.H.; Roberts, S.A.; et al. Mutational heterogeneity in cancer and the search for new cancer-associated genes. *Nature* **2013**, *499*, 214-218, doi:10.1038/nature12213.

60. Berghuis, D.; de Hooge, A.S.; Santos, S.J.; Horst, D.; Wiertz, E.J.; van Eggermond, M.C.; van den Elsen, P.J.; Taminiau, A.H.; Ottaviano, L.; Schaefer, K.L.; et al. Reduced human leukocyte antigen expression in advanced-stage Ewing sarcoma: implications for immune recognition. *The Journal of pathology* **2009**, *218*, 222-231, doi:10.1002/path.2537.

61. Yabe, H.; Tsukahara, T.; Kawaguchi, S.; Wada, T.; Torigoe, T.; Sato, N.; Terai, C.; Aoki, M.; Hirose, S.; Morioka, H.; et al. Prognostic significance of HLA class I expression in Ewing's sarcoma family of tumors. *Journal of surgical oncology* **2011**, *103*, 380-385, doi:10.1002/jso.21829.

62. Altvater, B.; Kailayangiri, S.; Pérez Lanuza, L.F.; Urban, K.; Greune, L.; Flügge, M.; Meltzer, J.; Farwick, N.; König, S.; Görlich, D.; et al. HLA-G and HLA-E Immune Checkpoints Are Widely Expressed in Ewing Sarcoma but Have Limited Functional Impact on the Effector Functions of Antigen-Specific CAR T Cells. *Cancers* **2021**, *13*, 2857.

63. Spurny, C.; Kailayangiri, S.; Altvater, B.; Jamitzky, S.; Hartmann, W.; Wardelmann, E.; Ranft, A.; Dirksen, U.; Amler, S.; Hardes, J.; et al. T cell infiltration into Ewing sarcomas is associated with local expression of immune-inhibitory HLA-G. *Oncotarget* **2018**, *9*, 6536-6549, doi:10.18632/oncotarget.23815.

64. Berghuis, D.; Santos, S.J.; Baelde, H.J.; Taminiau, A.H.M.; Maarten Egeler, R.; Schilham, M.W.; Hogendoorn, P.C.W.; Lankester, A.C. Pro-inflammatory chemokine–chemokine receptor interactions within the Ewing sarcoma microenvironment determine CD8+ T-lymphocyte infiltration and affect tumour progression. *The Journal of pathology* **2011**, *223*, 347-357, doi:https://doi.org/10.1002/path.2819.

65. Stahl, D.; Gentles, A.J.; Thiele, R.; Gütgemann, I. Prognostic profiling of the immune cell microenvironment in Ewing´s Sarcoma Family of Tumors. *Oncoimmunology* **2019**, *8*, e1674113-e1674113, doi:10.1080/2162402X.2019.1674113.

66. Brinkrolf, P.; Landmeier, S.; Altvater, B.; Chen, C.; Pscherer, S.; Rosemann, A.; Ranft, A.; Dirksen, U.; Juergens, H.; Rossig, C. A high proportion of bone marrow T cells with regulatory phenotype (CD4+CD25hiFoxP3+) in Ewing sarcoma patients is associated with metastatic disease. *Int J Cancer* **2009**, *125*, 879-886, doi:10.1002/ijc.24461.

67. Vakkila, J.; Jaffe, R.; Michelow, M.; Lotze, M.T. Pediatric cancers are infiltrated predominantly by macrophages and contain a paucity of dendritic cells: a major nosologic difference with adult tumors. *Clinical cancer research : an official journal of the American Association for Cancer Research* **2006**, *12*, 2049-2054, doi:10.1158/1078-0432.ccr-05-1824.

68. Wculek, S.K.; Cueto, F.J.; Mujal, A.M.; Melero, I.; Krummel, M.F.; Sancho, D. Dendritic cells in cancer immunology and immunotherapy. *Nature Reviews Immunology* **2020**, *20*, 7-24, doi:10.1038/s41577-019-0210-z.

69. Gentles, A.J.; Newman, A.M.; Liu, C.L.; Bratman, S.V.; Feng, W.; Kim, D.; Nair, V.S.; Xu, Y.; Khuong, A.; Hoang, C.D.; et al. The prognostic landscape of genes and infiltrating immune cells across human cancers. *Nat Med* **2015**, *21*, 938-945, doi:10.1038/nm.3909.

70. Fujiwara, T.; Fukushi, J.; Yamamoto, S.; Matsumoto, Y.; Setsu, N.; Oda, Y.; Yamada, H.; Okada, S.; Watari, K.; Ono, M.; et al. Macrophage infiltration predicts a poor prognosis for human ewing sarcoma. *The American journal of pathology* **2011**, *179*, 1157-1170, doi:10.1016/j.ajpath.2011.05.034.

71. Qian, B.-Z.; Li, J.; Zhang, H.; Kitamura, T.; Zhang, J.; Campion, L.R.; Kaiser, E.A.; Snyder, L.A.; Pollard, J.W. CCL2 recruits inflammatory monocytes to facilitate breast-tumour metastasis. *Nature* **2011**, *475*, 222-225, doi:10.1038/nature10138.

72. Wynn, T.A.; Chawla, A.; Pollard, J.W. Macrophage biology in development, homeostasis and disease. *Nature* **2013**, *496*, 445-455, doi:10.1038/nature12034.

73. Hesketh, A.J.; Maloney, C.; Behr, C.A.; Edelman, M.C.; Glick, R.D.; Al-Abed, Y.; Symons, M.; Soffer, S.Z.; Steinberg, B.M. The Macrophage Inhibitor CNI-1493 Blocks Metastasis in a Mouse Model of Ewing Sarcoma through Inhibition of Extravasation. *PloS one* **2016**, *10*, e0145197, doi:10.1371/journal.pone.0145197.

74. Beatty, G.L.; Winograd, R.; Evans, R.A.; Long, K.B.; Luque, S.L.; Lee, J.W.; Clendenin, C.; Gladney, W.L.; Knoblock, D.M.; Guirnalda, P.D.; et al. Exclusion of T Cells From Pancreatic Carcinomas in Mice Is Regulated by Ly6C(low) F4/80(+) Extratumoral Macrophages. *Gastroenterology* **2015**, *149*, 201-210, doi:10.1053/j.gastro.2015.04.010.

75. Rodriguez, P.C.; Quiceno, D.G.; Zabaleta, J.; Ortiz, B.; Zea, A.H.; Piazuelo, M.B.; Delgado, A.; Correa, P.; Brayer, J.; Sotomayor, E.M.; et al. Arginase I production in the tumor microenvironment by mature myeloid cells inhibits T-cell receptor expression and antigen-specific T-cell responses. *Cancer Res* **2004**, *64*, 5839-5849, doi:10.1158/0008-5472.can-04-0465.

76. Handl, M.; Hermanova, M.; Hotarkova, S.; Jarkovsky, J.; Mudry, P.; Shatokhina, T.; Vesela, M.; Sterba, J.; Zambo, I. Clinicopathological correlation of tumor-associated macrophages in Ewing sarcoma. *Biomedical papers* **2018**, *162*, 54-60, doi:10.5507/bp.2017.049.

77. Denton, N.L.; Chen, C.Y.; Hutzen, B.; Currier, M.A.; Scott, T.; Nartker, B.; Leddon, J.L.; Wang, P.Y.; Srinivas, R.; Cassady, K.A.; et al. Myelolytic Treatments Enhance Oncolytic Herpes Virotherapy in Models of Ewing Sarcoma by Modulating the Immune Microenvironment. *Molecular therapy oncolytics* **2018**, *11*, 62-74, doi:10.1016/j.omto.2018.10.001.

78. Volchenboum, S.L.; Andrade, J.; Huang, L.; Barkauskas, D.A.; Krailo, M.; Womer, R.B.; Ranft, A.; Potratz, J.; Dirksen, U.; Triche, T.J.; et al. Gene expression profiling of Ewing sarcoma tumours reveals the prognostic importance of tumour–stromal interactions: a report from the Children's Oncology Group. *The Journal of Pathology: Clinical Research* **2015**, *1*, 83-94, doi:https://doi.org/10.1002/cjp2.9.

79. Lissat, A.; Joerschke, M.; Shinde, D.A.; Braunschweig, T.; Meier, A.; Makowska, A.; Bortnick, R.; Henneke, P.; Herget, G.; Gorr, T.A.; et al. IL6 secreted by Ewing sarcoma tumor microenvironment confers anti-apoptotic and cell-disseminating paracrine responses in Ewing sarcoma cells. *BMC Cancer* **2015**, *15*, 552, doi:10.1186/s12885-015-1564-7.

80. Zhang, H.; Maric, I.; DiPrima, M.J.; Khan, J.; Orentas, R.J.; Kaplan, R.N.; Mackall, C.L. Fibrocytes represent a novel MDSC subset circulating in patients with metastatic cancer. *Blood* **2013**, *122*, 1105-1113, doi:10.1182/blood-2012-08-449413.

81. Bronte, V.; Brandau, S.; Chen, S.-H.; Colombo, M.P.; Frey, A.B.; Greten, T.F.; Mandruzzato, S.; Murray, P.J.; Ochoa, A.; Ostrand-Rosenberg, S.; et al. Recommendations for myeloid-derived suppressor cell nomenclature and characterization standards. *Nature Communications* **2016**, *7*, 12150, doi:10.1038/ncomms12150.

82. Veglia, F.; Perego, M.; Gabrilovich, D. Myeloid-derived suppressor cells coming of age. *Nature immunology* **2018**, *19*, 108-119, doi:10.1038/s41590-017-0022-x.

83. Veglia, F.; Sanseviero, E.; Gabrilovich, D.I. Myeloid-derived suppressor cells in the era of increasing myeloid cell diversity. *Nat Rev Immunol* **2021**, *21*, 485-498, doi:10.1038/s41577-020-00490-y.

84. Gabrilovich, D.I.; Ostrand-Rosenberg, S.; Bronte, V. Coordinated regulation of myeloid cells by tumours. *Nature Reviews Immunology* **2012**, *12*, 253-268, doi:10.1038/nri3175.

85. Condamine, T.; Mastio, J.; Gabrilovich, D.I. Transcriptional regulation of myeloid-derived suppressor cells. *J Leukoc Biol* **2015**, *98*, 913-922, doi:10.1189/jlb.4RI0515-204R.

86. Gabrilovich, D.I. The Dawn of Myeloid-Derived Suppressor Cells: Identification of Arginase I as the Mechanism of Immune Suppression. *Cancer Research* **2021**, *81*, 3953-3955, doi:10.1158/0008-5472.CAN-21-1237.

87. Long, A.H.; Highfill, S.L.; Cui, Y.; Smith, J.P.; Walker, A.J.; Ramakrishna, S.; El-Etriby, R.; Galli, S.; Tsokos, M.G.; Orentas, R.J.; et al. Reduction of MDSCs with All-trans Retinoic Acid Improves CAR Therapy Efficacy for Sarcomas. *Cancer Immunology Research* **2016**, *4*, 869-880, doi:10.1158/2326-6066.cir-15-0230.

88. Hingorani, P.; Maas, M.L.; Gustafson, M.P.; Dickman, P.; Adams, R.H.; Watanabe, M.; Eshun, F.; Williams, J.; Seidel, M.J.; Dietz, A.B. Increased CTLA-4(+) T cells and an increased ratio of monocytes with loss of class II (CD14(+) HLA-DR(lo/neg)) found in aggressive pediatric sarcoma patients. *J Immunother Cancer* **2015**, *3*, 35-35, doi:10.1186/s40425-015-0082-0.

89. Robbins, P.D.; Morelli, A.E. Regulation of immune responses by extracellular vesicles. *Nature Reviews Immunology* **2014**, *14*, 195-208, doi:10.1038/nri3622.

90. Kalluri, R.; LeBleu, V.S. The biology, function, and biomedical applications of exosomes. *Science* **2020**, *367*, doi:10.1126/science.aau6977.

91. van Niel, G.; Carter, D.R.F.; Clayton, A.; Lambert, D.W.; Raposo, G.; Vader, P. Challenges and directions in studying cell–cell communication by extracellular vesicles. *Nature Reviews Molecular Cell Biology* **2022**, doi:10.1038/s41580-022-00460-3.

92. Cocucci, E.; Meldolesi, J. Ectosomes and exosomes: shedding the confusion between extracellular vesicles. *Trends Cell Biol* **2015**, *25*, 364-372, doi:10.1016/j.tcb.2015.01.004.

93. van Niel, G.; D'Angelo, G.; Raposo, G. Shedding light on the cell biology of extracellular vesicles. *Nature reviews. Molecular cell biology* **2018**, *19*, 213-228, doi:10.1038/nrm.2017.125.

94. Baietti, M.F.; Zhang, Z.; Mortier, E.; Melchior, A.; Degeest, G.; Geeraerts, A.; Ivarsson, Y.; Depoortere, F.; Coomans, C.; Vermeiren, E.; et al. Syndecan–syntenin–ALIX regulates the biogenesis of exosomes. *Nature Cell Biology* **2012**, *14*, 677-685, doi:10.1038/ncb2502.

95. van Niel, G.; Charrin, S.; Simoes, S.; Romao, M.; Rochin, L.; Saftig, P.; Marks, Michael S.; Rubinstein, E.; Raposo, G. The Tetraspanin CD63 Regulates ESCRT-Independent and -Dependent Endosomal Sorting during Melanogenesis. *Developmental Cell* **2011**, *21*, 708-721, doi:10.1016/j.devcel.2011.08.019.

96. Tóth, E.; Turiák, L.; Visnovitz, T.; Cserép, C.; Mázló, A.; Sódar, B.W.; Försönits, A.I.; Petővári, G.; Sebestyén, A.; Komlósi, Z.; et al. Formation of a protein corona on the surface of extracellular vesicles in blood plasma. *J Extracell Vesicles* **2021**, *10*, e12140, doi:10.1002/jev2.12140.

97. Mathieu, M.; Martin-Jaular, L.; Lavieu, G.; Théry, C. Specificities of secretion and uptake of exosomes and other extracellular vesicles for cell-to-cell communication. *Nature Cell Biology* **2019**, *21*, 9-17, doi:10.1038/s41556-018-0250-9.

98. Zhang, H.; Freitas, D.; Kim, H.S.; Fabijanic, K.; Li, Z.; Chen, H.; Mark, M.T.; Molina, H.; Martin, A.B.; Bojmar, L.; et al. Identification of distinct nanoparticles and subsets of extracellular vesicles by asymmetric flow field-flow fractionation. *Nature Cell Biology* **2018**, *20*, 332-343, doi:10.1038/s41556-018-0040-4.

99. Zhang, Q.; Higginbotham, J.N.; Jeppesen, D.K.; Yang, Y.-P.; Li, W.; McKinley, E.T.; Graves-Deal, R.; Ping, J.; Britain, C.M.; Dorsett, K.A.; et al. Transfer of Functional Cargo in Exomeres. *Cell Reports* **2019**, *27*, 940-954.e946, doi:10.1016/j.celrep.2019.01.009.

100. Zhang, Q.; Jeppesen, D.K.; Higginbotham, J.N.; Graves-Deal, R.; Trinh, V.Q.; Ramirez, M.A.; Sohn, Y.; Neininger, A.C.; Taneja, N.; McKinley, E.T.; et al. Supermeres are functional extracellular nanoparticles replete with disease biomarkers and therapeutic targets. *Nat Cell Biol* **2021**, *23*, 1240-1254, doi:10.1038/s41556-021-00805-8.

101. Willms, E.; Cabañas, C.; Mäger, I.; Wood, M.J.A.; Vader, P. Extracellular Vesicle Heterogeneity: Subpopulations, Isolation Techniques, and Diverse Functions in Cancer Progression. *Front Immunol* **2018**, *9*, doi:10.3389/fimmu.2018.00738.

102. Mulcahy, L.A.; Pink, R.C.; Carter, D.R. Routes and mechanisms of extracellular vesicle uptake. *J Extracell Vesicles* **2014**, *3*, doi:10.3402/jev.v3.24641.

103. Chevillet, J.R.; Kang, Q.; Ruf, I.K.; Briggs, H.A.; Vojtech, L.N.; Hughes, S.M.; Cheng, H.H.; Arroyo, J.D.; Meredith, E.K.; Gallichotte, E.N.; et al. Quantitative and stoichiometric analysis of the microRNA content of exosomes. *Proceedings of the National Academy of Sciences of the United States of America* **2014**, *111*, 14888-14893, doi:10.1073/pnas.1408301111.

104. Dellar, E.R.; Hill, C.; Melling, G.E.; Carter, D.R.F.; Baena-Lopez, L.A. Unpacking extracellular vesicles: RNA cargo loading and function. *Journal of Extracellular Biology* **2022**, *1*, e40, doi:https://doi.org/10.1002/jex2.40.

105. Valadi, H.; Ekström, K.; Bossios, A.; Sjöstrand, M.; Lee, J.J.; Lötvall, J.O. Exosome-mediated transfer of mRNAs and microRNAs is a novel mechanism of genetic exchange between cells. *Nat Cell Biol* **2007**, *9*, 654-659, doi:10.1038/ncb1596.

106. Pegtel, D.M.; Cosmopoulos, K.; Thorley-Lawson, D.A.; van Eijndhoven, M.A.; Hopmans, E.S.; Lindenberg, J.L.; de Gruijl, T.D.; Würdinger, T.; Middeldorp, J.M. Functional delivery of viral miRNAs via exosomes. *Proceedings of the National Academy of Sciences of the United States of America* **2010**, *107*, 6328-6333, doi:10.1073/pnas.0914843107.

107. Pucci, F.; Garris, C.; Lai, C.P.; Newton, A.; Pfirschke, C.; Engblom, C.; Alvarez, D.; Sprachman, M.; Evavold, C.; Magnuson, A.; et al. SCS macrophages suppress melanoma by restricting tumor-derived vesicle-B cell interactions. *Science* **2016**, *352*, 242-246, doi:doi:10.1126/science.aaf1328.

108. Ridder, K.; Sevko, A.; Heide, J.; Dams, M.; Rupp, A.-K.; Macas, J.; Starmann, J.; Tjwa, M.; Plate, K.H.; Sültmann, H.; et al. Extracellular vesicle-mediated transfer of functional RNA in the tumor microenvironment. *Oncoimmunology* **2015**, *4*, e1008371, doi:10.1080/2162402X.2015.1008371.

109. Zomer, A.; Maynard, C.; Verweij, Frederik J.; Kamermans, A.; Schäfer, R.; Beerling, E.; Schiffelers, Raymond M.; de Wit, E.; Berenguer, J.; Ellenbroek, Saskia Inge J.; et al. In Vivo Imaging Reveals Extracellular Vesicle-Mediated Phenocopying of Metastatic Behavior. *Cell* **2015**, *161*, 1046-1057, doi:https://doi.org/10.1016/j.cell.2015.04.042.

110. Cheng, M.; Yang, J.; Zhao, X.; Zhang, E.; Zeng, Q.; Yu, Y.; Yang, L.; Wu, B.; Yi, G.; Mao, X.; et al. Circulating myocardial microRNAs from infarcted hearts are carried in exosomes and mobilise bone marrow progenitor cells. *Nature Communications* **2019**, *10*, 959, doi:10.1038/s41467-019-08895-7.

111. Kamerkar, S.; LeBleu, V.S.; Sugimoto, H.; Yang, S.; Ruivo, C.F.; Melo, S.A.; Lee, J.J.; Kalluri, R. Exosomes facilitate therapeutic targeting of oncogenic KRAS in pancreatic cancer. *Nature* **2017**, *546*, 498-503, doi:10.1038/nature22341.

112. Hyenne, V.; Ghoroghi, S.; Collot, M.; Bons, J.; Follain, G.; Harlepp, S.; Mary, B.; Bauer, J.; Mercier, L.; Busnelli, I.; et al. Studying the Fate of Tumor Extracellular Vesicles at High Spatiotemporal Resolution Using the Zebrafish Embryo. *Dev Cell* **2019**, *48*, 554-572.e557, doi:10.1016/j.devcel.2019.01.014.

113. Verweij, F.J.; Revenu, C.; Arras, G.; Dingli, F.; Loew, D.; Pegtel, D.M.; Follain, G.; Allio, G.; Goetz, J.G.; Zimmermann, P.; et al. Live Tracking of Inter-organ Communication by Endogenous Exosomes In Vivo. *Dev Cell* **2019**, *48*, 573-589.e574, doi:10.1016/j.devcel.2019.01.004.

114. Arkhypov, I.; Lasser, S.; Petrova, V.; Weber, R.; Groth, C.; Utikal, J.; Altevogt, P.; Umansky, V. Myeloid Cell Modulation by Tumor-Derived Extracellular Vesicles. *International journal of molecular sciences* **2020**, *21*, doi:10.3390/ijms21176319.

115. Gabrusiewicz, K.; Li, X.; Wei, J.; Hashimoto, Y.; Marisetty, A.L.; Ott, M.; Wang, F.; Hawke, D.; Yu, J.; Healy, L.M.; et al. Glioblastoma stem cell-derived exosomes induce M2 macrophages and PD-L1 expression on human monocytes. *Oncoimmunology* **2018**, *7*, e1412909, doi:10.1080/2162402x.2017.1412909.

116. Haderk, F.; Schulz, R.; Iskar, M.; Cid, L.L.; Worst, T.; Willmund, K.V.; Schulz, A.; Warnken, U.; Seiler, J.; Benner, A.; et al. Tumor-derived exosomes modulate PD-L1 expression in monocytes. *Science Immunology* **2017**, *2*, eaah5509, doi:10.1126/sciimmunol.aah5509.

117. Fleming, V.; Hu, X.; Weller, C.; Weber, R.; Groth, C.; Riester, Z.; Hüser, L.; Sun, Q.; Nagibin, V.; Kirschning, C.; et al. Melanoma Extracellular Vesicles Generate Immunosuppressive Myeloid Cells by Upregulating PD-L1 via TLR4 Signaling. *Cancer Research* **2019**, *79*, 4715-4728, doi:10.1158/0008-5472.can-19-0053.

118. Villasante, A.; Marturano-Kruik, A.; Ambati, S.R.; Liu, Z.; Godier-Furnemont, A.; Parsa, H.; Lee, B.W.; Moore, M.A.S.; Vunjak-Novakovic, G. Recapitulating the Size and Cargo of Tumor Exosomes in a Tissue-Engineered Model. *Theranostics* **2016**, *6*, 1119-1130, doi:10.7150/thno.13944.

119. Miller, I.V.; Raposo, G.; Welsch, U.; Prazeres da Costa, O.; Thiel, U.; Lebar, M.; Maurer, M.; Bender, H.U.; von Luettichau, I.; Richter, G.H.; et al. First identification of Ewing's sarcoma-derived extracellular vesicles and exploration of their biological and potential diagnostic implications. *Biology of the cell* **2013**, *105*, 289-303, doi:10.1111/boc.201200086.

120. Samuel, G.; Crow, J.; Klein, J.B.; Merchant, M.L.; Nissen, E.; Koestler, D.C.; Laurence, K.; Liang, X.; Neville, K.; Staggs, V.; et al. Ewing sarcoma family of tumors-derived small extracellular vesicle proteomics identify potential clinical biomarkers. *Oncotarget* **2020**, *11*, 2995-3012, doi:10.18632/oncotarget.27678.

121. Evdokimova, V.; Ruzanov, P.; Gassmann, H.; Zaidi, S.H.; Peltekova, V.; Heisler, L.E.; McPherson, J.D.; Orlic-Milacic, M.; Specht, K.; Steiger, K.; et al. Exosomes transmit retroelement RNAs to drive inflammation and immunosuppression in Ewing Sarcoma. *bioRxiv* **2019**, 806851, doi:10.1101/806851.

122. Richter, G.H.S.; Plehm, S.; Fasan, A.; Rössler, S.; Unland, R.; Bennani-Baiti, I.M.; Hotfilder, M.; Löwel, D.; Luettichau, I.v.; Mossbrugger, I.; et al. EZH2 is a mediator of EWS/FLI1 driven tumor growth and metastasis blocking endothelial and neuro-ectodermal differentiation. *Proceedings of the National Academy of Sciences* **2009**, *106*, 5324-5329, doi:doi:10.1073/pnas.0810759106.

123. Kling, M.J.; Chaturvedi, N.K.; Kesherwani, V.; Coulter, D.W.; McGuire, T.R.; Sharp, J.G.; Joshi, S.S. Exosomes secreted under hypoxia enhance stemness in Ewing´s sarcoma through miR-210 delivery. *Oncotarget* **2020**, *11*.

124. Ventura, S.; Aryee, D.N.T.; Felicetti, F.; De Feo, A.; Mancarella, C.; Manara, M.C.; Picci, P.; Colombo, M.P.; Kovar, H.; Carè, A.; et al. CD99 regulates neural differentiation of Ewing sarcoma cells through miR-34a-Notch-mediated control of NF-κB signaling. *Oncogene* **2016**, *35*, 3944-3954, doi:10.1038/onc.2015.463.

125. De Feo, A.; Sciandra, M.; Ferracin, M.; Felicetti, F.; Astolfi, A.; Pignochino, Y.; Picci, P.; Carè, A.; Scotlandi, K. Exosomes from CD99-deprived Ewing sarcoma cells reverse tumor malignancy by inhibiting

cell migration and promoting neural differentiation. *Cell Death & Disease* **2019**, *10*, 471, doi:10.1038/s41419-019-1675-1.

126. Tsugita, M.; Yamada, N.; Noguchi, S.; Yamada, K.; Moritake, H.; Shimizu, K.; Akao, Y.; Ohno, T. Ewing Sarcoma Cells Secrete EWS/Fli-1 Fusion mRNA via Microvesicles. *PloS one* **2013**, *8*, e77416, doi:10.1371/journal.pone.0077416.

127. Djebali, S.; Davis, C.A.; Merkel, A.; Dobin, A.; Lassmann, T.; Mortazavi, A.; Tanzer, A.; Lagarde, J.; Lin, W.; Schlesinger, F.; et al. Landscape of transcription in human cells. *Nature* **2012**, *489*, 101-108, doi:10.1038/nature11233.

128. Lander, E.S.; Linton, L.M.; Birren, B.; Nusbaum, C.; Zody, M.C.; Baldwin, J.; Devon, K.; Dewar, K.; Doyle, M.; FitzHugh, W.; et al. Initial sequencing and analysis of the human genome. *Nature* **2001**, *409*, 860-921, doi:10.1038/35057062.

129. Dunham, I.; Kundaje, A.; Aldred, S.F.; Collins, P.J.; Davis, C.A.; Doyle, F.; Epstein, C.B.; Frietze, S.; Harrow, J.; Kaul, R.; et al. An integrated encyclopedia of DNA elements in the human genome. *Nature* **2012**, *489*, 57-74, doi:10.1038/nature11247.

130. Kazazian, H.H., Jr.; Moran, J.V. Mobile DNA in Health and Disease. *The New England journal of medicine* **2017**, *377*, 361-370, doi:10.1056/NEJMra1510092.

131. Elbarbary, R.A.; Lucas, B.A.; Maquat, L.E. Retrotransposons as regulators of gene expression. *Science (New York, N.Y.)* **2016**, *351*, aac7247, doi:10.1126/science.aac7247.

132. Rebollo, R.; Romanish, M.T.; Mager, D.L. Transposable elements: an abundant and natural source of regulatory sequences for host genes. *Annual review of genetics* **2012**, *46*, 21-42, doi:10.1146/annurev-genet-110711-155621.

133. Grow, E.J.; Flynn, R.A.; Chavez, S.L.; Bayless, N.L.; Wossidlo, M.; Wesche, D.J.; Martin, L.; Ware, C.B.; Blish, C.A.; Chang, H.Y.; et al. Intrinsic retroviral reactivation in human preimplantation embryos and pluripotent cells. *Nature* **2015**, *522*, 221-225, doi:10.1038/nature14308.

134. Ting, D.T.; Lipson, D.; Paul, S.; Brannigan, B.W.; Akhavanfard, S.; Coffman, E.J.; Contino, G.; Deshpande, V.; Iafrate, A.J.; Letovsky, S.; et al. Aberrant Overexpression of Satellite Repeats in Pancreatic and Other Epithelial Cancers. *Science (New York, N.Y.)* **2011**, *331*, 593-596, doi:doi:10.1126/science.1200801.

135. Volkman, H.E.; Stetson, D.B. The enemy within: endogenous retroelements and autoimmune disease. *Nature immunology* **2014**, *15*, 415-422, doi:10.1038/ni.2872.

136. Bannert, N.; Kurth, R. Retroelements and the human genome: New perspectives on an old relation. *Proceedings of the National Academy of Sciences* **2004**, *101*, 14572-14579, doi:10.1073/pnas.0404838101.

137. Katoh, I.; Kurata, S.-i. Association of Endogenous Retroviruses and Long Terminal Repeats with Human Disorders. *Frontiers in Oncology* **2013**, *3*.

138. Miga, K.H. Centromeric Satellite DNAs: Hidden Sequence Variation in the Human Population. *Genes* **2019**, *10*, 352, doi:10.3390/genes10050352.

139. Kassiotis, G.; Stoye, J.P. Immune responses to endogenous retroelements: taking the bad with the good. *Nature reviews. Immunology* **2016**, *16*, 207-219, doi:10.1038/nri.2016.27.

140. Deniz, Ö.; Frost, J.M.; Branco, M.R. Regulation of transposable elements by DNA modifications. *Nature Reviews Genetics* **2019**, *20*, 417-431, doi:10.1038/s41576-019-0106-6.

141. Molaro, A.; Malik, H.S. Hide and seek: how chromatin-based pathways silence retroelements in the mammalian germline. *Current opinion in genetics & development* **2016**, *37*, 51-58, doi:10.1016/j.gde.2015.12.001.

142. Fueyo, R.; Judd, J.; Feschotte, C.; Wysocka, J. Roles of transposable elements in the regulation of mammalian transcription. *Nature Reviews Molecular Cell Biology* **2022**, doi:10.1038/s41580-022-00457-y.

143. Frank, J.A.; Feschotte, C. Co-option of endogenous viral sequences for host cell function. *Current opinion in virology* **2017**, *25*, 81-89, doi:10.1016/j.coviro.2017.07.021.

144. Thompson, Peter J.; Macfarlan, Todd S.; Lorincz, Matthew C. Long Terminal Repeats: From Parasitic Elements to Building Blocks of the Transcriptional Regulatory Repertoire. *Molecular Cell* **2016**, *62*, 766-776, doi:10.1016/j.molcel.2016.03.029.

145. Friedli, M.; Trono, D. The developmental control of transposable elements and the evolution of higher species. *Annual review of cell and developmental biology* **2015**, *31*, 429-451, doi:10.1146/annurev-cellbio-100814-125514.

146. Babaian, A.; Mager, D.L. Endogenous retroviral promoter exaptation in human cancer. *Mob DNA* **2016**, *7*, 24, doi:10.1186/s13100-016-0080-x.

147. Chuong, E.B.; Elde, N.C.; Feschotte, C. Regulatory evolution of innate immunity through co-option of endogenous retroviruses. *Science (New York, N.Y.)* **2016**, *351*, 1083-1087, doi:10.1126/science.aad5497.

148. Manghera, M.; Douville, R.N. Endogenous retrovirus-K promoter: a landing strip for inflammatory transcription factors? *Retrovirology* **2013**, *10*, 16, doi:10.1186/1742-4690-10-16.

149. Andersson, G.; Svensson, A.-C.; Setterblad, N.; Rask, L. Retroelements in the human MHC class II region. *Trends in Genetics* **1998**, *14*, 109-114, doi:https://doi.org/10.1016/S0168-9525(97)01359-0.

150. Mayer, J.; Blomberg, J.; Seal, R.L. A revised nomenclature for transcribed human endogenous retroviral loci. *Mob DNA* **2011**, *2*, 7-7, doi:10.1186/1759-8753-2-7.

151. Hohn, O.; Hanke, K.; Bannert, N. HERV-K(HML-2), the Best Preserved Family of HERVs: Endogenization, Expression, and Implications in Health and Disease. *Frontiers in Oncology* **2013**, *3*.

152. Burns, K.H.; Boeke, J.D. Human transposon tectonics. *Cell* **2012**, *149*, 740-752, doi:10.1016/j.cell.2012.04.019.

153. Jakobsson, J.; Vincendeau, M. SnapShot: Human endogenous retroviruses. *Cell* **2022**, *185*, 400-400.e401, doi:10.1016/j.cell.2021.12.028.

154. Payer, L.M.; Burns, K.H. Transposable elements in human genetic disease. *Nature Reviews Genetics* **2019**, *20*, 760-772, doi:10.1038/s41576-019-0165-8.

155. Saksouk, N.; Simboeck, E.; Déjardin, J. Constitutive heterochromatin formation and transcription in mammals. *Epigenetics & Chromatin* **2015**, *8*, 3, doi:10.1186/1756-8935-8-3.

156. Garrido-Ramos, M.A. Satellite DNA: An Evolving Topic. *Genes* **2017**, *8*, doi:10.3390/genes8090230.

157. Corless, S.; Höcker, S.; Erhardt, S. Centromeric RNA and Its Function at and Beyond Centromeric Chromatin. *Journal of molecular biology* **2020**, *432*, 4257-4269, doi:10.1016/j.jmb.2020.03.027.

158. Smurova, K.; De Wulf, P. Centromere and Pericentromere Transcription: Roles and Regulation … in Sickness and in Health. *Frontiers in Genetics* **2018**, *9*, doi:10.3389/fgene.2018.00674.

159. Altemose, N.; Miga, K.H.; Maggioni, M.; Willard, H.F. Genomic Characterization of Large Heterochromatic Gaps in the Human Genome Assembly. *PLOS Computational Biology* **2014**, *10*, e1003628, doi:10.1371/journal.pcbi.1003628.

160. Boots, J.L.; von Pelchrzim, F.; Weiss, A.; Zimmermann, B.; Friesacher, T.; Radtke, M.; Żywicki, M.; Chen, D.; Matylla-Kulińska, K.; Zagrovic, B.; et al. RNA polymerase II-binding aptamers in human ACRO1

satellites disrupt transcription in cis. *Transcription* **2020**, *11*, 217-229, doi:10.1080/21541264.2020.1790990.

161. Sengupta, S.; Parihar, R.; Ganesh, S. Satellite III non-coding RNAs show distinct and stress-specific patterns of induction. *Biochemical and Biophysical Research Communications* **2009**, *382*, 102-107, doi:https://doi.org/10.1016/j.bbrc.2009.02.137.

162. Hall, L.L.; Byron, M.; Carone, D.M.; Whitfield, T.W.; Pouliot, G.P.; Fischer, A.; Jones, P.; Lawrence, J.B. Demethylated HSATII DNA and HSATII RNA Foci Sequester PRC1 and MeCP2 into Cancer-Specific Nuclear Bodies. *Cell Rep* **2017**, *18*, 2943-2956, doi:10.1016/j.celrep.2017.02.072.

163. Tasselli, L.; Xi, Y.; Zheng, W.; Tennen, R.I.; Odrowaz, Z.; Simeoni, F.; Li, W.; Chua, K.F. SIRT6 deacetylates H3K18ac at pericentric chromatin to prevent mitotic errors and cellular senescence. *Nature structural & molecular biology* **2016**, *23*, 434-440, doi:10.1038/nsmb.3202.

164. De Cecco, M.; Ito, T.; Petrashen, A.P.; Elias, A.E.; Skvir, N.J.; Criscione, S.W.; Caligiana, A.; Brocculi, G.; Adney, E.M.; Boeke, J.D.; et al. L1 drives IFN in senescent cells and promotes age-associated inflammation. *Nature* **2019**, *566*, 73-78, doi:10.1038/s41586-018-0784-9.

165. Tilman, G.; Arnoult, N.; Lenglez, S.; Van Beneden, A.; Loriot, A.; De Smet, C.; Decottignies, A. Cancer-linked satellite 2 DNA hypomethylation does not regulate Sat2 non-coding RNA expression and is initiated by heat shock pathway activation. *Epigenetics* **2012**, *7*, 903-913, doi:10.4161/epi.21107.

166. Topham, J.T.; Titmuss, E.; Pleasance, E.D.; Williamson, L.M.; Karasinska, J.M.; Culibrk, L.; Lee, M.K.C.; Mendis, S.; Denroche, R.E.; Jang, G.H.; et al. Endogenous Retrovirus Transcript Levels Are Associated with Immunogenic Signatures in Multiple Metastatic Cancer Types. *Molecular cancer therapeutics* **2020**, *19*, 1889-1897, doi:10.1158/1535-7163.mct-20-0094.

167. Rodriguez-Martin, B.; Alvarez, E.G.; Baez-Ortega, A.; Zamora, J.; Supek, F.; Demeulemeester, J.; Santamarina, M.; Ju, Y.S.; Temes, J.; Garcia-Souto, D.; et al. Pan-cancer analysis of whole genomes identifies driver rearrangements promoted by LINE-1 retrotransposition. *Nature Genetics* **2020**, *52*, 306-319, doi:10.1038/s41588-019-0562-0.

168. Eymery, A.; Horard, B.; El Atifi-Borel, M.; Fourel, G.; Berger, F.; Vitte, A.L.; Van den Broeck, A.; Brambilla, E.; Fournier, A.; Callanan, M.; et al. A transcriptomic analysis of human centromeric and pericentric sequences in normal and tumor cells. *Nucleic acids research* **2009**, *37*, 6340-6354, doi:10.1093/nar/gkp639.

169. Ho, X.D.; Nguyen, H.G.; Trinh, L.H.; Reimann, E.; Prans, E.; Kõks, G.; Maasalu, K.; Le, V.Q.; Nguyen, V.H.; Le, N.T.N.; et al. Analysis of the Expression of Repetitive DNA Elements in Osteosarcoma. *Frontiers in Genetics* **2017**, *8*, doi:10.3389/fgene.2017.00193.

170. Leruste, A.; Tosello, J.; Ramos, R.N.; Tauziède-Espariat, A.; Brohard, S.; Han, Z.Y.; Beccaria, K.; Andrianteranagna, M.; Caudana, P.; Nikolic, J.; et al. Clonally Expanded T Cells Reveal Immunogenicity of Rhabdoid Tumors. *Cancer cell* **2019**, *36*, 597-612.e598, doi:10.1016/j.ccell.2019.10.008.

171. Ho, X.D.; Nguyen, H.G.; Trinh, L.H.; Reimann, E.; Prans, E.; Kõks, G.; Maasalu, K.; Le, V.Q.; Nguyen, V.H.; Le, N.T.N.; et al. Analysis of the Expression of Repetitive DNA Elements in Osteosarcoma. *Frontiers in genetics* **2017**, *8*, 193-193, doi:10.3389/fgene.2017.00193.

172. Bersani, F.; Lee, E.; Kharchenko, P.V.; Xu, A.W.; Liu, M.; Xega, K.; MacKenzie, O.C.; Brannigan, B.W.; Wittner, B.S.; Jung, H.; et al. Pericentromeric satellite repeat expansions through RNA-derived DNA intermediates in cancer. *Proceedings of the National Academy of Sciences* **2015**, *112*, 15148-15153, doi:10.1073/pnas.1518008112.

173. Shadle, S.C.; Bennett, S.R.; Wong, C.J.; Karreman, N.A.; Campbell, A.E.; van der Maarel, S.M.; Bass, B.L.; Tapscott, S.J. DUX4-induced bidirectional HSATII satellite repeat transcripts form intranuclear double-stranded RNA foci in human cell models of FSHD. *Human molecular genetics* **2019**, *28*, 3997-4011, doi:10.1093/hmg/ddz242.

174. Tanne, A.; Muniz, L.R.; Puzio-Kuter, A.; Leonova, K.I.; Gudkov, A.V.; Ting, D.T.; Monasson, R.; Cocco, S.; Levine, A.J.; Bhardwaj, N.; et al. Distinguishing the immunostimulatory properties of noncoding RNAs expressed in cancer cells. *Proceedings of the National Academy of Sciences* **2015**, *112*, 15154-15159, doi:10.1073/pnas.1517584112.

175. Mu, X.; Ahmad, S.; Hur, S. Endogenous Retroelements and the Host Innate Immune Sensors. *Advances in immunology* **2016**, *132*, 47-69, doi:10.1016/bs.ai.2016.07.001.

176. Gázquez-Gutiérrez, A.; Witteveldt, J.; Heras, S.R.; Macias, S. Sensing of transposable elements by the antiviral innate immune system. *RNA* **2021**, *27*, 735-752, doi:10.1261/rna.078721.121.

177. Rajshekar, S.; Yao, J.; Arnold, P.K.; Payne, S.G.; Zhang, Y.; Bowman, T.V.; Schmitz, R.J.; Edwards, J.R.; Goll, M. Pericentromeric hypomethylation elicits an interferon response in an animal model of ICF syndrome. *eLife* **2018**, *7*, e39658, doi:10.7554/eLife.39658.

178. Yu, P.; Lübben, W.; Slomka, H.; Gebler, J.; Konert, M.; Cai, C.; Neubrandt, L.; Prazeres da Costa, O.; Paul, S.; Dehnert, S.; et al. Nucleic acid-sensing Toll-like receptors are essential for the control of endogenous retrovirus viremia and ERV-induced tumors. *Immunity* **2012**, *37*, 867-879, doi:10.1016/j.immuni.2012.07.018.

179. Young, G.R.; Eksmond, U.; Salcedo, R.; Alexopoulou, L.; Stoye, J.P.; Kassiotis, G. Resurrection of endogenous retroviruses in antibody-deficient mice. *Nature* **2012**, *491*, 774-778, doi:10.1038/nature11599.

180. Rehwinkel, J.; Gack, M.U. RIG-I-like receptors: their regulation and roles in RNA sensing. *Nature Reviews Immunology* **2020**, *20*, 537-551, doi:10.1038/s41577-020-0288-3.

181. Schlee, M.; Hartmann, G. Discriminating self from non-self in nucleic acid sensing. *Nature Reviews Immunology* **2016**, *16*, 566-580, doi:10.1038/nri.2016.78.

182. Hornung, V.; Ellegast, J.; Kim, S.; Brzózka, K.; Jung, A.; Kato, H.; Poeck, H.; Akira, S.; Conzelmann, K.K.; Schlee, M.; et al. 5'-Triphosphate RNA is the ligand for RIG-I. *Science (New York, N.Y.)* **2006**, *314*, 994-997, doi:10.1126/science.1132505.

183. Sun, L.; Wu, J.; Du, F.; Chen, X.; Chen, Z.J. Cyclic GMP-AMP Synthase Is a Cytosolic DNA Sensor That Activates the Type I Interferon Pathway. *Science (New York, N.Y.)* **2013**, *339*, 786-791, doi:doi:10.1126/science.1232458.

184. Chiappinelli, Katherine B.; Strissel, Pamela L.; Desrichard, A.; Li, H.; Henke, C.; Akman, B.; Hein, A.; Rote, Neal S.; Cope, Leslie M.; Snyder, A.; et al. Inhibiting DNA Methylation Causes an Interferon Response in Cancer via dsRNA Including Endogenous Retroviruses. *Cell* **2015**, *162*, 974-986, doi:10.1016/j.cell.2015.07.011.

185. Zhao, K.; Du, J.; Peng, Y.; Li, P.; Wang, S.; Wang, Y.; Hou, J.; Kang, J.; Zheng, W.; Hua, S.; et al. LINE1 contributes to autoimmunity through both RIG-I- and MDA5-mediated RNA sensing pathways. *Journal of autoimmunity* **2018**, *90*, 105-115, doi:10.1016/j.jaut.2018.02.007.

186. Ivashkiv, L.B.; Donlin, L.T. Regulation of type I interferon responses. *Nature Reviews Immunology* **2014**, *14*, 36-49, doi:10.1038/nri3581.

187. Schoggins, J.W.; Rice, C.M. Interferon-stimulated genes and their antiviral effector functions. *Current opinion in virology* **2011**, *1*, 519-525, doi:10.1016/j.coviro.2011.10.008.

188. Schoggins, J.W. Interferon-Stimulated Genes: What Do They All Do? *Annual Review of Virology* **2019**, *6*, 567-584, doi:10.1146/annurev-virology-092818-015756.

189. Diamond, M.S.; Farzan, M. The broad-spectrum antiviral functions of IFIT and IFITM proteins. *Nature Reviews Immunology* **2013**, *13*, 46-57, doi:10.1038/nri3344.

190. Alcazer, V.; Bonaventura, P.; Depil, S. Human Endogenous Retroviruses (HERVs): Shaping the Innate Immune Response in Cancers. *Cancers* **2020**, *12*, 610, doi:10.3390/cancers12030610.

191. Kassiotis, G. Endogenous retroviruses and the development of cancer. *J Immunol* **2014**, *192*, 1343-1349, doi:10.4049/jimmunol.1302972.

192. Bannert, N.; Hofmann, H.; Block, A.; Hohn, O. HERVs New Role in Cancer: From Accused Perpetrators to Cheerful Protectors. *Frontiers in microbiology* **2018**, *9*, 178-178, doi:10.3389/fmicb.2018.00178.

193. Chen, R.; Ishak, C.A.; De Carvalho, D.D. Endogenous Retroelements and the Viral Mimicry Response in Cancer Therapy and Cellular Homeostasis. *Cancer Discovery* **2021**, *11*, 2707-2725, doi:10.1158/2159-8290.CD-21-0506.

194. Kong, Y.; Rose, C.M.; Cass, A.A.; Williams, A.G.; Darwish, M.; Lianoglou, S.; Haverty, P.M.; Tong, A.-J.; Blanchette, C.; Albert, M.L.; et al. Transposable element expression in tumors is associated with immune infiltration and increased antigenicity. *Nature Communications* **2019**, *10*, 5228, doi:10.1038/s41467-019-13035-2.

195. Solovyov, A.; Vabret, N.; Arora, K.S.; Snyder, A.; Funt, S.A.; Bajorin, D.F.; Rosenberg, J.E.; Bhardwaj, N.; Ting, D.T.; Greenbaum, B.D. Global Cancer Transcriptome Quantifies Repeat Element Polarization between Immunotherapy Responsive and T Cell Suppressive Classes. *Cell Rep* **2018**, *23*, 512-521, doi:10.1016/j.celrep.2018.03.042.

196. Panda, A.; de Cubas, A.A.; Stein, M.; Riedlinger, G.; Kra, J.; Mayer, T.; Smith, C.C.; Vincent, B.G.; Serody, J.S.; Beckermann, K.E.; et al. Endogenous retrovirus expression is associated with response to immune checkpoint blockade in clear cell renal cell carcinoma. *JCI insight* **2018**, *3*, doi:10.1172/jci.insight.121522.

197. Rooney, Michael S.; Shukla, Sachet A.; Wu, Catherine J.; Getz, G.; Hacohen, N. Molecular and Genetic Properties of Tumors Associated with Local Immune Cytolytic Activity. *Cell* **2015**, *160*, 48-61, doi:10.1016/j.cell.2014.12.033.

198. Au, L.; Hatipoglu, E.; Robert de Massy, M.; Litchfield, K.; Beattie, G.; Rowan, A.; Schnidrig, D.; Thompson, R.; Byrne, F.; Horswell, S.; et al. Determinants of anti-PD-1 response and resistance in clear cell renal cell carcinoma. *Cancer cell* **2021**, *39*, 1497-1518.e1411, doi:10.1016/j.ccell.2021.10.001.

199. Diesch, J.; Zwick, A.; Garz, A.-K.; Palau, A.; Buschbeck, M.; Götze, K.S. A clinical-molecular update on azanucleoside-based therapy for the treatment of hematologic cancers. *Clinical Epigenetics* **2016**, *8*, 71, doi:10.1186/s13148-016-0237-y.

200. Srinivasan, U.; Reaman, G.H.; Poplack, D.G.; Glaubiger, D.L.; LeVine, A.S. Phase II study of 5-azacytidine in sarcomas of bone. *American journal of clinical oncology* **1982**, *5*, 411-415, doi:10.1097/00000421-198208000-00011.

201. Zhou, X.; Singh, M.; Sanz Santos, G.; Guerlavais, V.; Carvajal, L.A.; Aivado, M.; Zhan, Y.; Oliveira, M.M.S.; Westerberg, L.S.; Annis, D.A.; et al. Pharmacologic Activation of p53 Triggers Viral Mimicry Response Thereby Abolishing Tumor Immune Evasion and Promoting Antitumor Immunity. *Cancer Discov* **2021**, *11*, 3090-3105, doi:10.1158/2159-8290.cd-20-1741.

202. Goel, S.; DeCristo, M.J.; Watt, A.C.; BrinJones, H.; Sceneay, J.; Li, B.B.; Khan, N.; Ubellacker, J.M.; Xie, S.; Metzger-Filho, O.; et al. CDK4/6 inhibition triggers anti-tumour immunity. *Nature* **2017**, *548*, 471-475, doi:10.1038/nature23465.

203. Jones, P.A.; Ohtani, H.; Chakravarthy, A.; De Carvalho, D.D. Epigenetic therapy in immune-oncology. *Nature Reviews Cancer* **2019**, *19*, 151-161, doi:10.1038/s41568-019-0109-9.

204. Jayabal, P.; Ma, X.; Shiio, Y. EZH2 suppresses endogenous retroviruses and an interferon response in cancers. *Genes & cancer* **2021**, *12*, 96-105, doi:10.18632/genesandcancer.218.

205. Ishak, C.A.; Marshall, A.E.; Passos, D.T.; White, C.R.; Kim, S.J.; Cecchini, M.J.; Ferwati, S.; MacDonald, W.A.; Howlett, C.J.; Welch, I.D.; et al. An RB-EZH2 Complex Mediates Silencing of Repetitive DNA Sequences. *Mol Cell* **2016**, *64*, 1074-1087, doi:10.1016/j.molcel.2016.10.021.

206. Kosumi, K.; Baba, Y.; Okadome, K.; Yagi, T.; Kiyozumi, Y.; Yoshida, N.; Watanabe, M.; Baba, H. Tumor Long-interspersed Nucleotide Element-1 Methylation Level and Immune Response to Esophageal Cancer. *Annals of surgery* **2020**, *272*, 1025-1034, doi:10.1097/sla.0000000000003264.

207. Jung, H.; Choi, J.K.; Lee, E.A. Immune signatures correlate with L1 retrotransposition in gastrointestinal cancers. *Genome research* **2018**, *28*, 1136-1146, doi:10.1101/gr.231837.117.

208. Giebler, M.; Staege, M.S.; Blauschmidt, S.; Ohm, L.I.; Kraus, M.; Würl, P.; Taubert, H.; Greither, T. Elevated HERV-K Expression in Soft Tissue Sarcoma Is Associated with Worsened Relapse-Free Survival. *Frontiers in Microbiology* **2018**, *9*, doi:10.3389/fmicb.2018.00211.

209. Cañadas, I.; Thummalapalli, R.; Kim, J.W.; Kitajima, S.; Jenkins, R.W.; Christensen, C.L.; Campisi, M.; Kuang, Y.; Zhang, Y.; Gjini, E.; et al. Tumor innate immunity primed by specific interferon-stimulated endogenous retroviruses. *Nature Medicine* **2018**, *24*, 1143-1150, doi:10.1038/s41591-018-0116-5.

210. Espinet, E.; Gu, Z.; Imbusch, C.D.; Giese, N.A.; Büscher, M.; Safavi, M.; Weisenburger, S.; Klein, C.; Vogel, V.; Falcone, M.; et al. Aggressive PDACs Show Hypomethylation of Repetitive Elements and the Execution of an Intrinsic IFN Program Linked to a Ductal Cell of Origin. *Cancer Discovery* **2021**, *11*, 638-659, doi:10.1158/2159-8290.CD-20-1202.

211. Balaj, L.; Lessard, R.; Dai, L.; Cho, Y.-J.; Pomeroy, S.L.; Breakefield, X.O.; Skog, J. Tumour microvesicles contain retrotransposon elements and amplified oncogene sequences. *Nature Communications* **2011**, *2*, 180, doi:10.1038/ncomms1180.

212. Kawamura, Y.; Sanchez Calle, A.; Yamamoto, Y.; Sato, T.-A.; Ochiya, T. Extracellular vesicles mediate the horizontal transfer of an active LINE-1 retrotransposon. *Journal of Extracellular Vesicles* **2019**, *8*, 1643214, doi:10.1080/20013078.2019.1643214.

213. Ferrari, L.; Cafora, M.; Rota, F.; Hoxha, M.; Iodice, S.; Tarantini, L.; Dolci, M.; Delbue, S.; Pistocchi, A.; Bollati, V. Extracellular Vesicles Released by Colorectal Cancer Cell Lines Modulate Innate Immune Response in Zebrafish Model: The Possible Role of Human Endogenous Retroviruses. *International journal of molecular sciences* **2019**, *20*, 3669, doi:10.3390/ijms20153669.

214. Li, Y.; Chen, Y.; Zhang, N.; Fan, D. Human endogenous retrovirus K (HERV-K) env in neuronal extracellular vesicles: a new biomarker of motor neuron disease. *Amyotrophic lateral sclerosis & frontotemporal degeneration* **2021**, 1-8, doi:10.1080/21678421.2021.1936061.

215. Cambier, L.; Stachelek, K.; Triska, M.; Jubran, R.; Huang, M.; Li, W.; Zhang, J.; Li, J.; Cobrinik, D. Extracellular vesicle-associated repetitive element DNAs as candidate osteosarcoma biomarkers. *Scientific Reports* **2021**, *11*, 94, doi:10.1038/s41598-020-77398-z.

216. Morozov, V.A.; Morozov, A.V. A Comprehensive Analysis of Human Endogenous Retroviruses HERV-K (HML.2) from Teratocarcinoma Cell Lines and Detection of Viral Cargo in Microvesicles. *International journal of molecular sciences* **2021**, *22*, doi:10.3390/ijms222212398.

217. Jiang, Z.; Wei, F.; Zhang, Y.; Wang, T.; Gao, W.; Yu, S.; Sun, H.; Pu, J.; Sun, Y.; Wang, M.; et al. IFI16 directly senses viral RNA and enhances RIG-I transcription and activation to restrict influenza virus infection. *Nature Microbiology* **2021**, *6*, 932-945, doi:10.1038/s41564-021-00907-x.

218. Imaizumi, T.; Yano, C.; Numata, A.; Tsugawa, K.; Hayakari, R.; Matsumiya, T.; Yoshida, H.; Watanabe, S.; Tsuruga, K.; Kawaguchi, S.; et al. Interferon (IFN)-Induced Protein 35 (IFI35), a Type I Interferon-Dependent Transcript, Upregulates Inflammatory Signaling Pathways by Activating Toll-Like Receptor 3 in Human Mesangial Cells. *Kidney and Blood Pressure Research* **2016**, *41*, 635-642, doi:10.1159/000447932.

219. Yin, X.; Yang, J.; Chen, J.; Ni, R.; Zhou, Y.; Song, H.; Jin, L.; Tang, T.; Pan, Y. LncRNA CTD-3252C9.4 modulates pancreatic cancer cell survival and apoptosis through regulating IFI6 transcription. *Cancer Cell International* **2021**, *21*, 433, doi:10.1186/s12935-021-02142-0.

220. Kelemen, A.; Carmi, I.; Oszvald, Á.; Lőrincz, P.; Petővári, G.; Tölgyes, T.; Dede, K.; Bursics, A.; Buzás, E.I.; Wiener, Z. IFITM1 expression determines extracellular vesicle uptake in colorectal cancer. *Cellular and Molecular Life Sciences* **2021**, *78*, 7009-7024, doi:10.1007/s00018-021-03949-w.

221. Meischel, T.; Fritzlar, S.; Villalon-Letelier, F.; Tessema, M.B.; Brooks, A.G.; Reading, P.C.; Londrigan, S.L. IFITM Proteins That Restrict the Early Stages of Respiratory Virus Infection Do Not Influence Late-Stage Replication. *Journal of Virology* **2021**, *95*, e00837-00821, doi:doi:10.1128/JVI.00837-21.

222. Safley, S.A.; Villinger, F.; Jackson, E.H.; Tucker-Burden, C.; Cohen, C.; Weber, C.J. Interleukin-6 production and secretion by human parathyroids. *Clinical and experimental immunology* **2004**, *136*, 145-156, doi:10.1111/j.1365-2249.2004.02419.x.

223. Mandal, P.K.; Ewing, A.D.; Hancks, D.C.; Kazazian, H.H., Jr. Enrichment of processed pseudogene transcripts in L1-ribonucleoprotein particles. *Human molecular genetics* **2013**, *22*, 3730-3748, doi:10.1093/hmg/ddt225.

224. Théry, C.; Witwer, K.W.; Aikawa, E.; Alcaraz, M.J.; Anderson, J.D.; Andriantsitohaina, R.; Antoniou, A.; Arab, T.; Archer, F.; Atkin-Smith, G.K.; et al. Minimal information for studies of extracellular vesicles 2018 (MISEV2018): a position statement of the International Society for Extracellular Vesicles and update of the MISEV2014 guidelines. *Journal of extracellular vesicles* **2018**, *7*, 1535750-1535750, doi:10.1080/20013078.2018.1535750.

225. Ramirez, M.I.; Amorim, M.G.; Gadelha, C.; Milic, I.; Welsh, J.A.; Freitas, V.M.; Nawaz, M.; Akbar, N.; Couch, Y.; Makin, L.; et al. Technical challenges of working with extracellular vesicles. *Nanoscale* **2018**, *10*, 881-906, doi:10.1039/C7NR08360B.

226. Fricke, F.; Buschmann, D.; Pfaffl, M.W. Isolation and characterization of extracellular vesicles. *Trillium Extracellular Vesicles* **2019**, *1*, doi:https://doi.org/10.47184/tev.2019.01.02.

227. Coumans, F.A.W.; Brisson, A.R.; Buzas, E.I.; Dignat-George, F.; Drees, E.E.E.; El-Andaloussi, S.; Emanueli, C.; Gasecka, A.; Hendrix, A.; Hill, A.F.; et al. Methodological Guidelines to Study Extracellular Vesicles. *Circulation Research* **2017**, *120*, 1632-1648, doi:10.1161/CIRCRESAHA.117.309417.

228. Théry, C.; Amigorena, S.; Raposo, G.; Clayton, A. Isolation and characterization of exosomes from cell culture supernatants and biological fluids. *Current protocols in cell biology* **2006**, *Chapter 3*, Unit 3.22, doi:10.1002/0471143030.cb0322s30.

229. Schober, S.J.; Thiede, M.; Gassmann, H.; Prexler, C.; Xue, B.; Schirmer, D.; Wohlleber, D.; Stein, S.; Grunewald, T.G.P.; Busch, D.H.; et al. MHC Class I-Restricted TCR-Transgenic CD4(+) T Cells Against STEAP1 Mediate Local Tumor Control of Ewing Sarcoma In Vivo. *Cells* **2020**, *9*, doi:10.3390/cells9071581.

230. Meyer-Wentrup, F.; Burdach, S. Efficacy of dendritic cell generation for clinical use: recovery and purity of monocytes and mature dendritic cells after immunomagnetic sorting or adherence selection of CD14+ starting populations. *Journal of hematotherapy & stem cell research* **2003**, *12*, 289-299, doi:10.1089/152581603322023025.

231. Bruger, A.M.; Vanhaver, C.; Bruderek, K.; Amodio, G.; Tavukçuoğlu, E.; Esendagli, G.; Gregori, S.; Brandau, S.; van der Bruggen, P. Protocol to assess the suppression of T-cell proliferation by human MDSC. *Methods in enzymology* **2020**, *632*, 155-192, doi:10.1016/bs.mie.2019.05.046.

232. Fuchs, N.V.; Loewer, S.; Daley, G.Q.; Izsvák, Z.; Löwer, J.; Löwer, R. Human endogenous retrovirus K (HML-2) RNA and protein expression is a marker for human embryonic and induced pluripotent stem cells. *Retrovirology* **2013**, *10*, 115-115, doi:10.1186/1742-4690-10-115.

233. Enukashvily, N.I.; Donev, R.; Waisertreiger, I.S.; Podgornaya, O.I. Human chromosome 1 satellite 3 DNA is decondensed, demethylated and transcribed in senescent cells and in A431 epithelial carcinoma cells. *Cytogenetic and genome research* **2007**, *118*, 42-54, doi:10.1159/000106440.

234. Shu, S.L.; Yang, Y.; Allen, C.L.; Hurley, E.; Tung, K.H.; Minderman, H.; Wu, Y.; Ernstoff, M.S. Purity and yield of melanoma exosomes are dependent on isolation method. *Journal of Extracellular Vesicles* **2020**, *9*, 1692401, doi:10.1080/20013078.2019.1692401.

235. Sedger, L.M.; McDermott, M.F. TNF and TNF-receptors: From mediators of cell death and inflammation to therapeutic giants – past, present and future. *Cytokine & Growth Factor Reviews* **2014**, *25*, 453-472, doi:https://doi.org/10.1016/j.cytogfr.2014.07.016.

236. Brandt, K.; Bulfone-Paus, S.; Foster, D.C.; Rückert, R. Interleukin-21 inhibits dendritic cell activation and maturation. *Blood* **2003**, *102*, 4090-4098, doi:10.1182/blood-2003-03-0669.

237. Wang, S.; Miyazaki, Y.; Shinozaki, Y.; Yoshida, H. Augmentation of antigen-presenting and Th1-promoting functions of dendritic cells by WSX-1(IL-27R) deficiency. *Journal of immunology (Baltimore, Md. : 1950)* **2007**, *179*, 6421-6428, doi:10.4049/jimmunol.179.10.6421.

238. Lecavalier-Barsoum, M.; Chaudary, N.; Han, K.; Pintilie, M.; Hill, R.P.; Milosevic, M. Targeting CXCL12/CXCR4 and myeloid cells to improve the therapeutic ratio in patient-derived cervical cancer models treated with radio-chemotherapy. *British Journal of Cancer* **2019**, *121*, 249-256, doi:10.1038/s41416-019-0497-3.

239. Kochan, G.; Escors, D.; Breckpot, K.; Guerrero-Setas, D. Role of non-classical MHC class I molecules in cancer immunosuppression. *OncoImmunology* **2013**, *2*, e26491, doi:10.4161/onci.26491.

240. Su, Y.-L.; Banerjee, S.; White, S.V.; Kortylewski, M. STAT3 in Tumor-Associated Myeloid Cells: Multitasking to Disrupt Immunity. *Int J Mol Sci* **2018**, *19*, 1803, doi:10.3390/ijms19061803.

241. Satoh, T.; Kidoya, H.; Naito, H.; Yamamoto, M.; Takemura, N.; Nakagawa, K.; Yoshioka, Y.; Morii, E.; Takakura, N.; Takeuchi, O.; et al. Critical role of Trib1 in differentiation of tissue-resident M2-like macrophages. *Nature* **2013**, *495*, 524-528, doi:10.1038/nature11930.

242. Masterson, A.J.; Sombroek, C.C.; de Gruijl, T.D.; Graus, Y.M.F.; van der Vliet, H.J.J.; Lougheed, S.a.M.; van den Eertwegh, A.J.M.; Pinedo, H.M.; Scheper, R.J. MUTZ-3, a human cell line model for the cytokine-induced differentiation of dendritic cells from CD34+precursors. *Blood* **2002**, *100*, 701-703, doi:10.1182/blood.V100.2.701.

243. Bretz, N.P.; Ridinger, J.; Rupp, A.K.; Rimbach, K.; Keller, S.; Rupp, C.; Marmé, F.; Umansky, L.; Umansky, V.; Eigenbrod, T.; et al. Body fluid exosomes promote secretion of inflammatory cytokines in monocytic cells via Toll-like receptor signaling. *The Journal of biological chemistry* **2013**, *288*, 36691-36702, doi:10.1074/jbc.M113.512806.

244. Kim, K.D.; Choi, S.-C.; Noh, Y.-W.; Kim, J.W.; Paik, S.-G.; Yang, Y.; Kim, K.I.; Lim, J.-S. Impaired responses of leukemic dendritic cells derived from a human myeloid cell line to LPS stimulation. *Experimental & Molecular Medicine* **2006**, *38*, 72-84, doi:10.1038/emm.2006.9.

245. Pisano, M.P.; Tabone, O.; Bodinier, M.; Grandi, N.; Textoris, J.; Mallet, F.; Tramontano, E. RNA-Seq Transcriptome Analysis Reveals Long Terminal Repeat Retrotransposon Modulation in Human Peripheral Blood Mononuclear Cells after In Vivo Lipopolysaccharide Injection. *J Virol* **2020**, *94*, doi:10.1128/jvi.00587-20.

246. Andersson, M.L.; Medstrand, P.; Yin, H.; Blomberg, J. Differential expression of human endogenous retroviral sequences similar to mouse mammary tumor virus in normal peripheral blood mononuclear cells. *AIDS research and human retroviruses* **1996**, *12*, 833-840, doi:10.1089/aid.1996.12.833.

247. Balestrieri, E.; Pica, F.; Matteucci, C.; Zenobi, R.; Sorrentino, R.; Argaw-Denboba, A.; Cipriani, C.; Bucci, I.; Sinibaldi-Vallebona, P. Transcriptional activity of human endogenous retroviruses in human peripheral blood mononuclear cells. *Biomed Res Int* **2015**, *2015*, 164529-164529, doi:10.1155/2015/164529.

248. Valenti, R.; Huber, V.; Filipazzi, P.; Pilla, L.; Sovena, G.; Villa, A.; Corbelli, A.; Fais, S.; Parmiani, G.; Rivoltini, L. Human tumor-released microvesicles promote the differentiation of myeloid cells with

transforming growth factor-beta-mediated suppressive activity on T lymphocytes. *Cancer Res* **2006**, *66*, 9290-9298, doi:10.1158/0008-5472.can-06-1819.

249. Park, S.J.; Nakagawa, T.; Kitamura, H.; Atsumi, T.; Kamon, H.; Sawa, S.; Kamimura, D.; Ueda, N.; Iwakura, Y.; Ishihara, K.; et al. IL-6 regulates in vivo dendritic cell differentiation through STAT3 activation. *Journal of immunology (Baltimore, Md. : 1950)* **2004**, *173*, 3844-3854, doi:10.4049/jimmunol.173.6.3844.

250. Spranger, S.; Bao, R.; Gajewski, T.F. Melanoma-intrinsic β-catenin signalling prevents anti-tumour immunity. *Nature* **2015**, *523*, 231-235, doi:10.1038/nature14404.

251. Williford, J.-M.; Ishihara, J.; Ishihara, A.; Mansurov, A.; Hosseinchi, P.; Marchell, T.M.; Potin, L.; Swartz, M.A.; Hubbell, J.A. Recruitment of CD103(+) dendritic cells via tumor-targeted chemokine delivery enhances efficacy of checkpoint inhibitor immunotherapy. *Sci Adv* **2019**, *5*, eaay1357-eaay1357, doi:10.1126/sciadv.aay1357.

252. Yu, S.; Liu, C.; Su, K.; Wang, J.; Liu, Y.; Zhang, L.; Li, C.; Cong, Y.; Kimberly, R.; Grizzle, W.E.; et al. Tumor Exosomes Inhibit Differentiation of Bone Marrow Dendritic Cells. *The Journal of Immunology* **2007**, *178*, 6867-6875, doi:10.4049/jimmunol.178.11.6867.

253. Maus, R.L.G.; Jakub, J.W.; Nevala, W.K.; Christensen, T.A.; Noble-Orcutt, K.; Sachs, Z.; Hieken, T.J.; Markovic, S.N. Human Melanoma-Derived Extracellular Vesicles Regulate Dendritic Cell Maturation. *Front Immunol* **2017**, *8*, 358-358, doi:10.3389/fimmu.2017.00358.

254. Ning, Y.; Shen, K.; Wu, Q.; Sun, X.; Bai, Y.; Xie, Y.; Pan, J.; Qi, C. Tumor exosomes block dendritic cells maturation to decrease the T cell immune response. *Immunology Letters* **2018**, *199*, 36-43, doi:https://doi.org/10.1016/j.imlet.2018.05.002.

255. Trovato, R.; Fiore, A.; Sartori, S.; Canè, S.; Giugno, R.; Cascione, L.; Paiella, S.; Salvia, R.; De Sanctis, F.; Poffe, O.; et al. Immunosuppression by monocytic myeloid-derived suppressor cells in patients with pancreatic ductal carcinoma is orchestrated by STAT3. *Journal for ImmunoTherapy of Cancer* **2019**, *7*, 255, doi:10.1186/s40425-019-0734-6.

256. Nefedova, Y.; Huang, M.; Kusmartsev, S.; Bhattacharya, R.; Cheng, P.; Salup, R.; Jove, R.; Gabrilovich, D. Hyperactivation of STAT3 is involved in abnormal differentiation of dendritic cells in cancer. *Journal of immunology (Baltimore, Md. : 1950)* **2004**, *172*, 464-474, doi:10.4049/jimmunol.172.1.464.

257. Schmidt, S.V.; Nino-Castro, A.C.; Schultze, J.L. Regulatory dendritic cells: there is more than just immune activation. *Front Immunol* **2012**, *3*, 274, doi:10.3389/fimmu.2012.00274.

258. Chalmin, F.; Ladoire, S.; Mignot, G.; Vincent, J.; Bruchard, M.; Remy-Martin, J.-P.; Boireau, W.; Rouleau, A.; Simon, B.; Lanneau, D.; et al. Membrane-associated Hsp72 from tumor-derived exosomes mediates STAT3-dependent immunosuppressive function of mouse and human myeloid-derived suppressor cells. *The Journal of Clinical Investigation* **2010**, *120*, 457-471, doi:10.1172/JCI40483.

259. Shen, Y.; Guo, D.; Weng, L.; Wang, S.; Ma, Z.; Yang, Y.; Wang, P.; Wang, J.; Cai, Z. Tumor-derived exosomes educate dendritic cells to promote tumor metastasis via HSP72/HSP105-TLR2/TLR4 pathway. *Oncoimmunology* **2017**, *6*, e1362527, doi:10.1080/2162402x.2017.1362527.

260. Diao, J.; Yang, X.; Song, X.; Chen, S.; He, Y.; Wang, Q.; Chen, G.; Luo, C.; Wu, X.; Zhang, Y. Exosomal Hsp70 mediates immunosuppressive activity of the myeloid-derived suppressor cells via phosphorylation of Stat3. *Medical oncology (Northwood, London, England)* **2015**, *32*, 453, doi:10.1007/s12032-014-0453-2.

261. Santegoets, S.J.A.M.; van den Eertwegh, A.J.M.; van de Loosdrecht, A.A.; Scheper, R.J.; de Gruijl, T.D. Human dendritic cell line models for DC differentiation and clinical DC vaccination studies. *Journal of Leukocyte Biology* **2008**, *84*, 1364-1373, doi:10.1189/jlb.0208092.

262. Rasaiyaah, J.; Noursadeghi, M.; Kellam, P.; Chain, B. Transcriptional and functional defects of dendritic cells derived from the MUTZ-3 leukaemia line. *Immunology* **2009**, *127*, 429-441, doi:10.1111/j.1365-2567.2008.03018.x.

263. de Jong, O.G.; Murphy, D.E.; Mäger, I.; Willms, E.; Garcia-Guerra, A.; Gitz-Francois, J.J.; Lefferts, J.; Gupta, D.; Steenbeek, S.C.; van Rheenen, J.; et al. A CRISPR-Cas9-based reporter system for single-cell detection of extracellular vesicle-mediated functional transfer of RNA. *Nature Communications* **2020**, *11*, 1113, doi:10.1038/s41467-020-14977-8.

264. Moroni, C.; Stoye, J.P.; DeLamarter, J.F.; Erb, P.; Jay, F.A.; Jongstra, J.; Martin, D.; Schumann, G. Normal B-cell activation involves endogenous retroviral antigen expression: implications for leukemogenesis. *Cold Spring Harbor symposia on quantitative biology* **1980**, *44 Pt 2*, 1205-1210, doi:10.1101/sqb.1980.044.01.130.

265. Stoye, J.P.; Moroni, C. Endogenous retrovirus expression in stimulated murine lymphocytes. Identification of a new locus controlling mitogen induction of a defective virus. *Journal of Experimental Medicine* **1983**, *157*, 1660-1674, doi:10.1084/jem.157.5.1660.

266. Young, G.R.; Mavrommatis, B.; Kassiotis, G. Microarray analysis reveals global modulation of endogenous retroelement transcription by microbes. *Retrovirology* **2014**, *11*, 59, doi:10.1186/1742-4690-11-59.

267. Hung, T.; Pratt, G.A.; Sundararaman, B.; Townsend, M.J.; Chaivorapol, C.; Bhangale, T.; Graham, R.R.; Ortmann, W.; Criswell, L.A.; Yeo, G.W.; et al. The Ro60 autoantigen binds endogenous retroelements and regulates inflammatory gene expression. *Science (New York, N.Y.)* **2015**, *350*, 455-459, doi:10.1126/science.aac7442.

268. Mommert, M.; Tabone, O.; Oriol, G.; Cerrato, E.; Guichard, A.; Naville, M.; Fournier, P.; Volff, J.-N.; Pachot, A.; Monneret, G.; et al. LTR-retrotransposon transcriptome modulation in response to endotoxin-induced stress in PBMCs. *BMC Genomics* **2018**, *19*, 522, doi:10.1186/s12864-018-4901-9.

269. Nogalski, M.T.; Solovyov, A.; Kulkarni, A.S.; Desai, N.; Oberstein, A.; Levine, A.J.; Ting, D.T.; Shenk, T.; Greenbaum, B.D. A tumor-specific endogenous repetitive element is induced by herpesviruses. *Nature Communications* **2019**, *10*, 90, doi:10.1038/s41467-018-07944-x.

270. Valgardsdottir, R.; Chiodi, I.; Giordano, M.; Rossi, A.; Bazzini, S.; Ghigna, C.; Riva, S.; Biamonti, G. Transcription of Satellite III non-coding RNAs is a general stress response in human cells. *Nucleic acids research* **2008**, *36*, 423-434, doi:10.1093/nar/gkm1056.

271. Wang, M.; Wang, L.; Liu, H.; Chen, J.; Liu, D. Transcriptome Analyses Implicate Endogenous Retroviruses Involved in the Host Antiviral Immune System through the Interferon Pathway. *Virologica Sinica* **2021**, *36*, 1315-1326, doi:10.1007/s12250-021-00370-2.

272. Manghera, M.; Ferguson-Parry, J.; Lin, R.; Douville, R.N. NF-κB and IRF1 Induce Endogenous Retrovirus K Expression via Interferon-Stimulated Response Elements in Its 5′ Long Terminal Repeat. *Journal of Virology* **2016**, *90*, 9338-9349, doi:10.1128/jvi.01503-16.

273. Larouche, J.-D.; Trofimov, A.; Hesnard, L.; Ehx, G.; Zhao, Q.; Vincent, K.; Durette, C.; Gendron, P.; Laverdure, J.-P.; Bonneil, É.; et al. Widespread and tissue-specific expression of endogenous retroelements in human somatic tissues. *Genome Medicine* **2020**, *12*, 40, doi:10.1186/s13073-020-00740-7.

274. Bergallo, M.; Loiacono, E.; Galliano, I.; Montanari, P.; Peruzzi, L.; Tovo, P.A.; Coppo, R. HERV-K and W expression in peripheral mononuclear cells of children with Henoch-Schönlein purpura and relation with TLRs activation. *Minerva pediatrica* **2017**, doi:10.23736/s0026-4946.17.04717-x.

275. Tokuyama, M.; Kong, Y.; Song, E.; Jayewickreme, T.; Kang, I.; Iwasaki, A. ERVmap analysis reveals genome-wide transcription of human endogenous retroviruses. *Proceedings of the National Academy of Sciences* **2018**, *115*, 12565-12572, doi:10.1073/pnas.1814589115.

276. Krieg, A.M.; Gourley, M.F.; Klinman, D.M.; Perl, A.; Steinberg, A.D. Heterogeneous expression and coordinate regulation of endogenous retroviral sequences in human peripheral blood mononuclear cells. *AIDS research and human retroviruses* **1992**, *8*, 1991-1998, doi:10.1089/aid.1992.8.1991.

277. Asimi, V.; Sampath Kumar, A.; Niskanen, H.; Riemenschneider, C.; Hetzel, S.; Naderi, J.; Fasching, N.; Popitsch, N.; Du, M.; Kretzmer, H.; et al. Hijacking of transcriptional condensates by endogenous retroviruses. *Nature Genetics* **2022**, *54*, 1238-1247, doi:10.1038/s41588-022-01132-w.

278. Novo, C.L.; Wong, E.V.; Hockings, C.; Poudel, C.; Sheekey, E.; Wiese, M.; Okkenhaug, H.; Boulton, S.J.; Basu, S.; Walker, S.; et al. Satellite repeat transcripts modulate heterochromatin condensates and safeguard chromosome stability in mouse embryonic stem cells. *Nature Communications* **2022**, *13*, 3525, doi:10.1038/s41467-022-31198-3.

279. Zuo, L.; Zhang, G.; Massett, M.; Cheng, J.; Guo, Z.; Wang, L.; Gao, Y.; Li, R.; Huang, X.; Li, P.; et al. Loci-specific phase separation of FET fusion oncoproteins promotes gene transcription. *Nature Communications* **2021**, *12*, 1491, doi:10.1038/s41467-021-21690-7.

280. Medstrand, P.; Lindeskog, M.; Blomberg, J. Expression of human endogenous retroviral sequences in peripheral blood mononuclear cells of healthy individuals. *The Journal of general virology* **1992**, *73 (Pt 9)*, 2463-2466, doi:10.1099/0022-1317-73-9-2463.

281. Seifarth, W.; Frank, O.; Zeilfelder, U.; Spiess, B.; Greenwood, A.D.; Hehlmann, R.; Leib-Mösch, C. Comprehensive analysis of human endogenous retrovirus transcriptional activity in human tissues with a retrovirus-specific microarray. *J Virol* **2005**, *79*, 341-352, doi:10.1128/jvi.79.1.341-352.2005.

282. Johnston, J.B.; Silva, C.; Holden, J.; Warren, K.G.; Clark, A.W.; Power, C. Monocyte activation and differentiation augment human endogenous retrovirus expression: implications for inflammatory brain diseases. *Annals of neurology* **2001**, *50*, 434-442, doi:10.1002/ana.1131.

283. Depil, S.; Roche, C.; Dussart, P.; Prin, L. Expression of a human endogenous retrovirus, HERV-K, in the blood cells of leukemia patients. *Leukemia* **2002**, *16*, 254-259, doi:10.1038/sj.leu.2402355.

284. Wallace, T.A.; Downey, R.F.; Seufert, C.J.; Schetter, A.; Dorsey, T.H.; Johnson, C.A.; Goldman, R.; Loffredo, C.A.; Yan, P.; Sullivan, F.J.; et al. Elevated HERV-K mRNA expression in PBMC is associated with a prostate cancer diagnosis particularly in older men and smokers. *Carcinogenesis* **2014**, *35*, 2074-2083, doi:10.1093/carcin/bgu114.

285. Cassetta, L.; Bruderek, K.; Skrzeczynska-Moncznik, J.; Osiecka, O.; Hu, X.; Rundgren, I.M.; Lin, A.; Santegoets, K.; Horzum, U.; Godinho-Santos, A.; et al. Differential expansion of circulating human MDSC subsets in patients with cancer, infection and inflammation. *Journal for ImmunoTherapy of Cancer* **2020**, *8*, e001223, doi:10.1136/jitc-2020-001223.

286. Roulois, D.; Loo Yau, H.; Singhania, R.; Wang, Y.; Danesh, A.; Shen, Shu Y.; Han, H.; Liang, G.; Jones, Peter A.; Pugh, Trevor J.; et al. DNA-Demethylating Agents Target Colorectal Cancer Cells by Inducing Viral Mimicry by Endogenous Transcripts. *Cell* **2015**, *162*, 961-973, doi:10.1016/j.cell.2015.07.056.

287. Lötvall, J.; Hill, A.F.; Hochberg, F.; Buzás, E.I.; Di Vizio, D.; Gardiner, C.; Gho, Y.S.; Kurochkin, I.V.; Mathivanan, S.; Quesenberry, P.; et al. Minimal experimental requirements for definition of extracellular vesicles and their functions: a position statement from the International Society for Extracellular Vesicles. *Journal of extracellular vesicles* **2014**, *3*, 26913-26913, doi:10.3402/jev.v3.26913.

288. Staufer, O.; Dietrich, F.; Rimal, R.; Schröter, M.; Fabritz, S.; Boehm, H.; Singh, S.; Möller, M.; Platzman, I.; Spatz, J.P. Bottom-up assembly of biomedical relevant fully synthetic extracellular vesicles. *Science Advances* **2021**, *7*, eabg6666, doi:doi:10.1126/sciadv.abg6666.

289. Minas, T.Z.; Surdez, D.; Javaheri, T.; Tanaka, M.; Howarth, M.; Kang, H.-J.; Han, J.; Han, Z.-Y.; Sax, B.; Kream, B.E.; et al. Combined experience of six independent laboratories attempting to create an Ewing sarcoma mouse model. *Oncotarget* **2016**, *8*.

290. von Freeden-Jeffry, U.; Davidson, N.; Wiler, R.; Fort, M.; Burdach, S.; Murray, R. IL-7 Deficiency Prevents Development of a Non-T Cell Non-B Cell-Mediated Colitis. *The Journal of Immunology* **1998**, *161*, 5673-5680.

291. Gassmann, H.; Schneider, K.; Evdokimova, V.; Ruzanov, P.; Schober, S.J.; Xue, B.; von Heyking, K.; Thiede, M.; Richter, G.H.S.; Pfaffl, M.W.; et al. Ewing Sarcoma-Derived Extracellular Vesicles Impair Dendritic Cell Maturation and Function. *Cells* **2021**, *10*, 2081.

9 Appendix

9.1 Supplementary figures

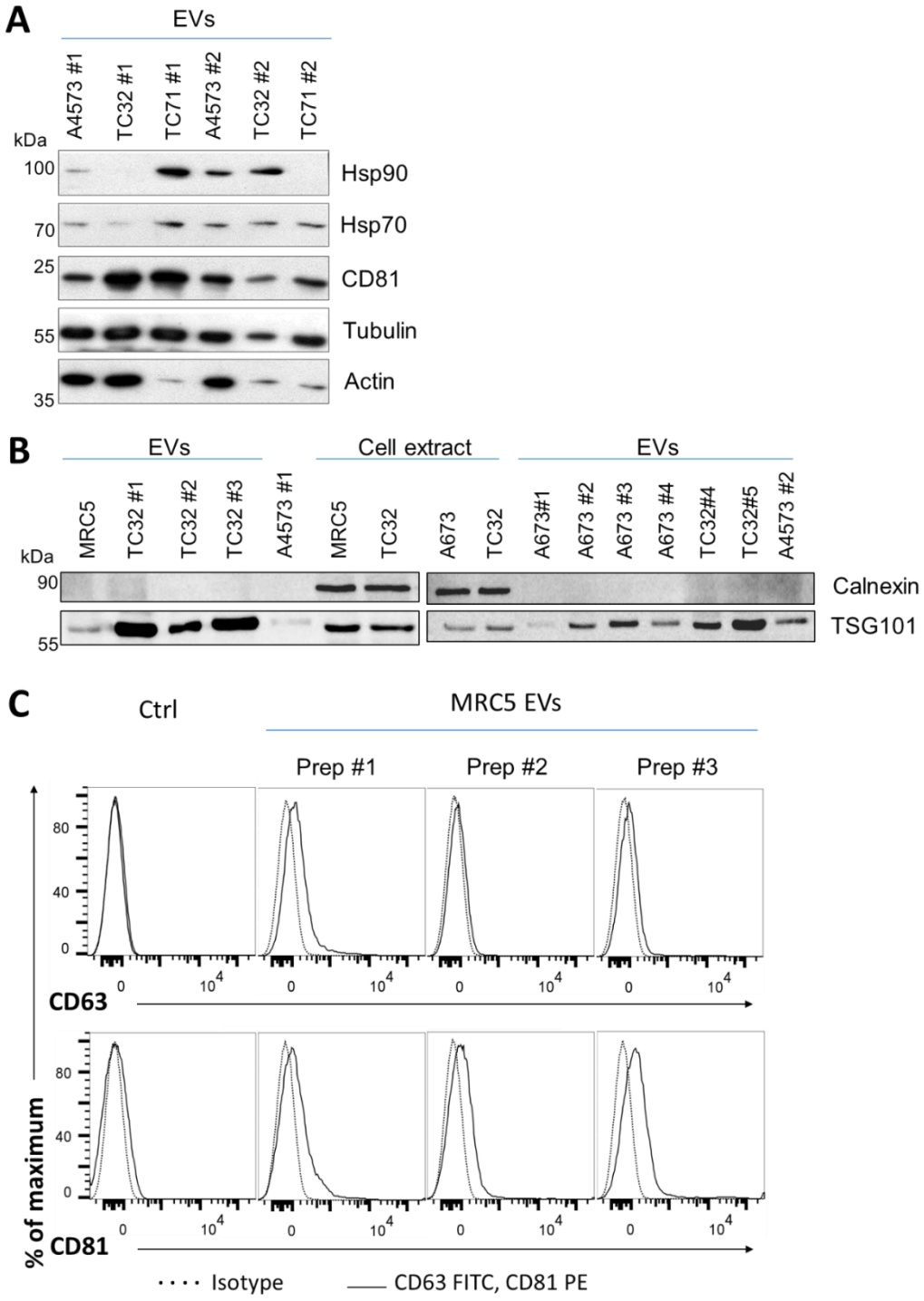

Supplementary Figure 1 Extended characterization of EV preparations from EwS and fibroblast cell lines.

(**A**) Immunoblotting of EV preparations from EwS A4573, TC32 and TC71 cell lines for EV marker CD81, chaperone proteins Hsp70 and Hsp90, and cytoskeleton proteins actin and tubulin. (**B**) Immunoblotting of EV preparations and respective parental A4573, A673 and TC32 and MRC5 fibroblasts cell lines for EV marker TSG101 and the negative marker Calnexin. (**C**) Flow cytometry of MRC5 EV preparations coupled to 4.0 µm latex beads for EV markers CD63 and CD81 (solid line) as well as the corresponding isotype controls (dotted line). Data from indicated number of independent EV preparations are shown.

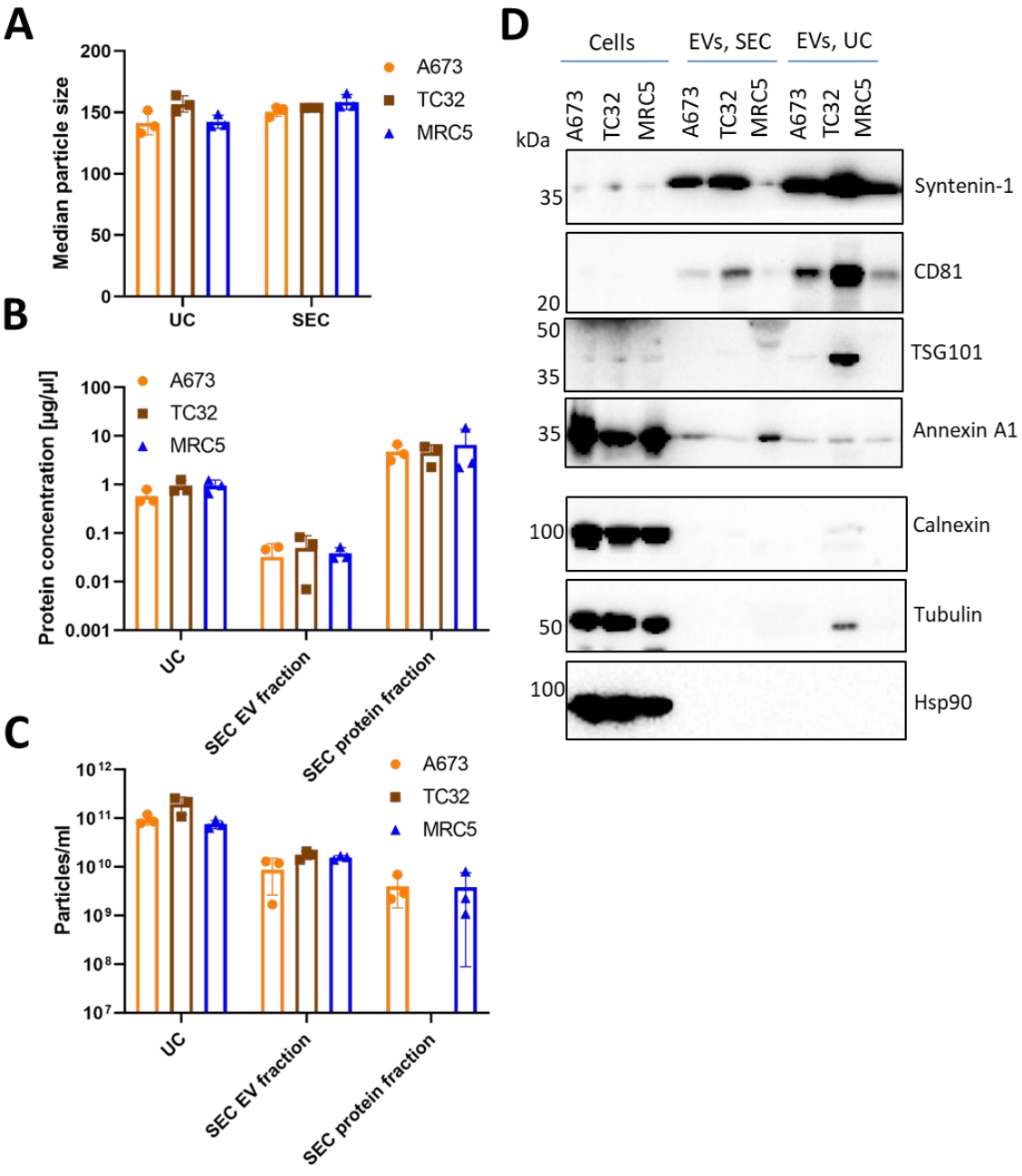

Supplementary Figure 2 EVs isolated by UC and SEC exhibit similar size distribution and EV markers.

(**A–D**) EVs were isolated in parallel by UC and SEC from the conditioned medium of A673, TC32 and MRC5. (**A**) NTA for size distribution, (**B**) BCA assay for protein concentration and (**C**) NTA for particle concentration of EV preparations and protein fractions isolated by UC and SEC are shown. (**D**) Immunoblots of one representative EV preparation from (A–C) and respective cell lysates for EV markers Syntenin-1, CD81, TSG101 and Annexin A1, Hsp90, and tubulin, and the negative marker Calnexin. Results of three independent biological replicates are displayed in A–C. Data are presented as mean ± SD and were statistically tested using two-way ANOVA with multiple comparison Tukey test. Results were not significant, $p > 0.05$.

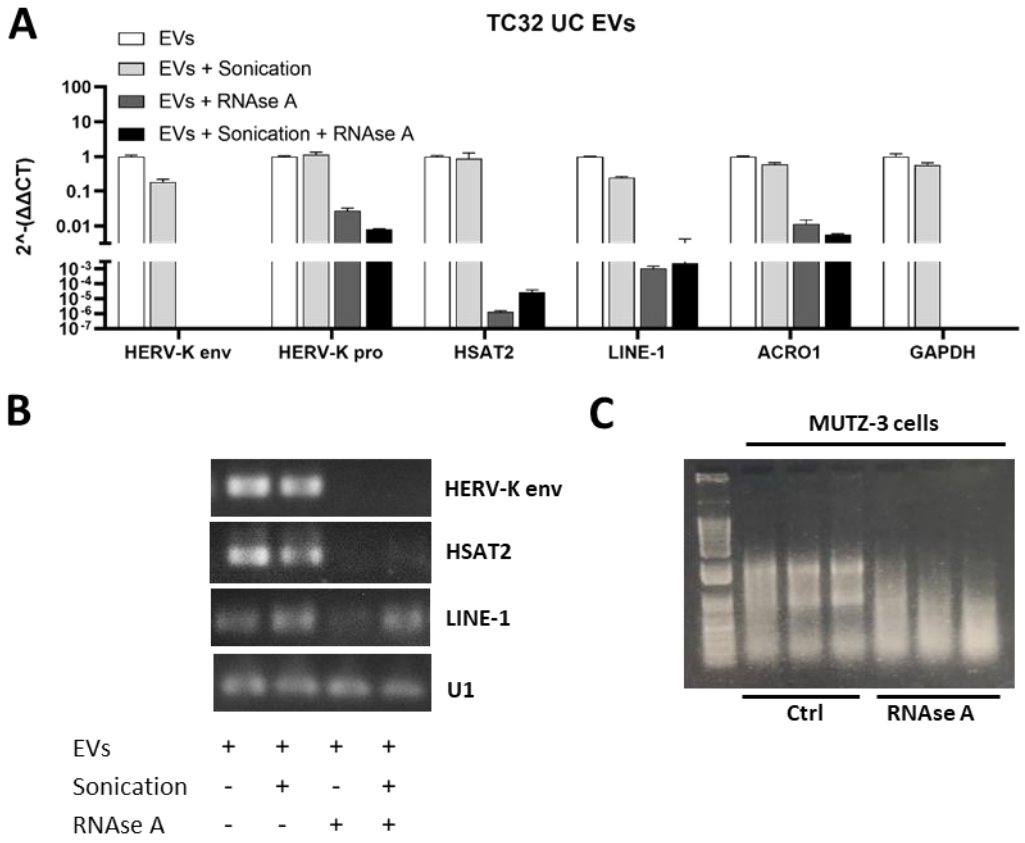

Supplementary Figure 3 RNAse A degrades RE and satellite transcripts of TC32 EV preparations irrespective of sonication.

(**A, B**) Freshly isolated TC32 UC EVs were equally split on four aliquots and treated either with sonication, RNAse A, sonication and RNAse A or left untreated. (**A**) qRT-PCR results for HERV-K env, HERV-K pro, HSAT2, LINE-1, ACRO1 and GAPDH are shown. U1, a spliceosomal RNA, was used for normalization in EVs, as U1 was not degraded by RNAse A in contrast to GAPDH. (**B**) DNA gel image of HERV-K env, HSAT2, LINE-1 and U1 products after 44 cycles of PCR. (**C**) DNA gel image of total RNA isolated from MUTZ-3 cells using the mirVana isolation kit. PBS as control or RNAse A were added before total RNA isolation. Results of one independent experiment are shown for (A,B) and (C). Data in (A) are presented as mean ± SD of three technical replicates.

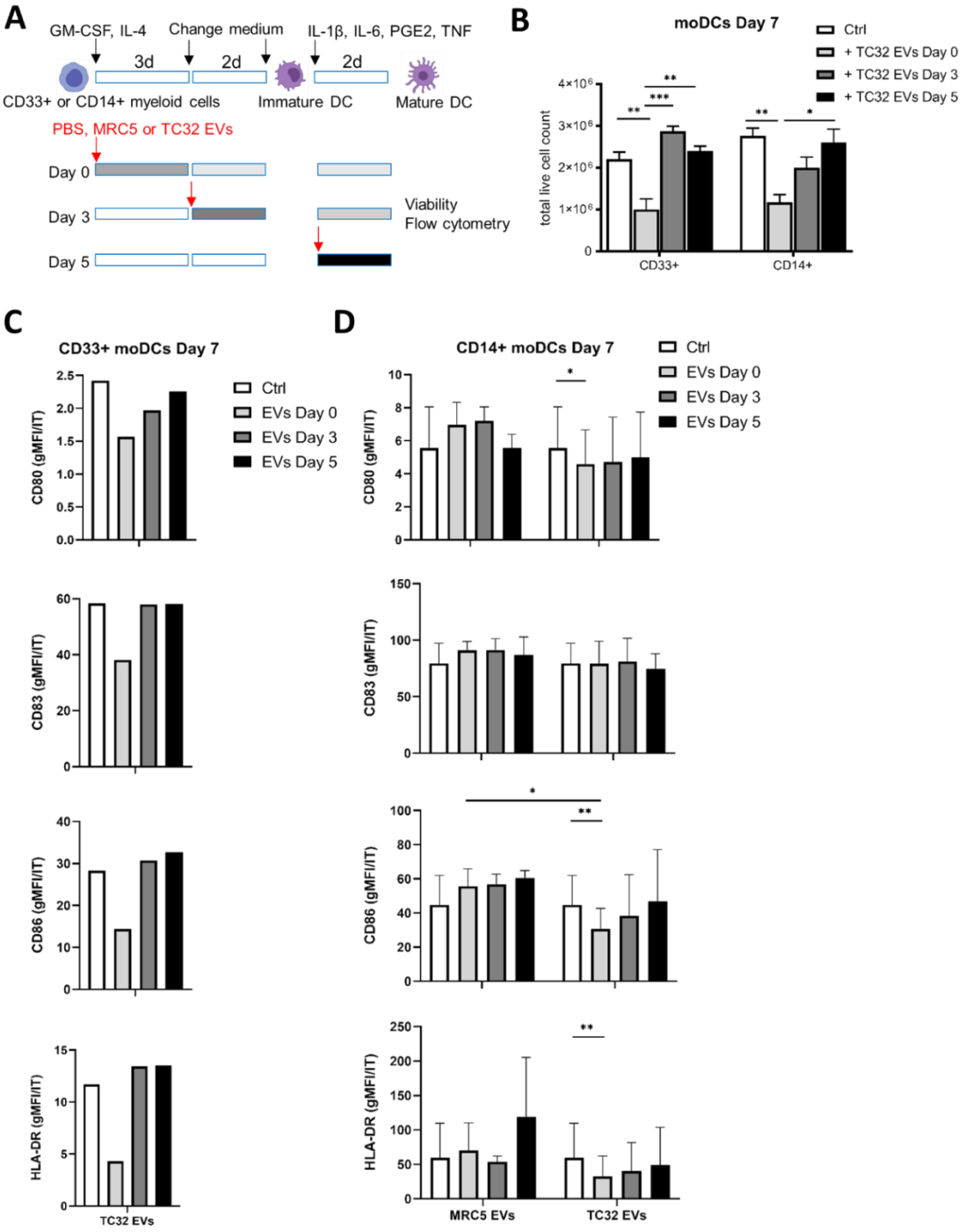

Supplementary Figure 4 EwS EVs affect viability and maturation of CD33$^+$ and CD14$^+$ myeloid cells at an early stage.

(**A**) Experimental layout (B–D). Healthy donor-derived CD14$^+$ or CD33$^+$ myeloid cells were differentiated by GM-CSF and IL-4 for 5 days and matured to moDCs by IL-1β, IL-6, PGE_2 and TNF for 2 additional days. 3 x 10^9 EV particles/ml from TC32 or MRC5 cells or PBS as control (Ctrl) were added on day 0 or 3 during differentiation or day 5 during maturation. At day 7, surface expression of CD80, CD83, CD86 and HLA-DR was assessed by flow cytometry. (**B**) Viability of CD14$^+$ or CD33$^+$ myeloid cells treated with indicated EVs or PBS as Ctrl was quantified by Trypan blue staining. Geometric mean fluorescence intensity (gMFI) normalized to the respective isotype (IT) control of CD80, CD83, CD86 and HLA-DR on (**C**) CD33$^+$ or (**D**) CD14$^+$ myeloid cells. Results were derived from one (B, C) or six (D) independent donors with one (B, C) three (D, MRC5) or five (D, TC32 EVs) independent EV preparations. Data are presented as mean ± SD. Unpaired (B) and paired (D) two-tailed t-tests were used to calculate p values. * $p \leq 0.05$, ** $p \leq 0.01$ and *** $p \leq 0.001$.

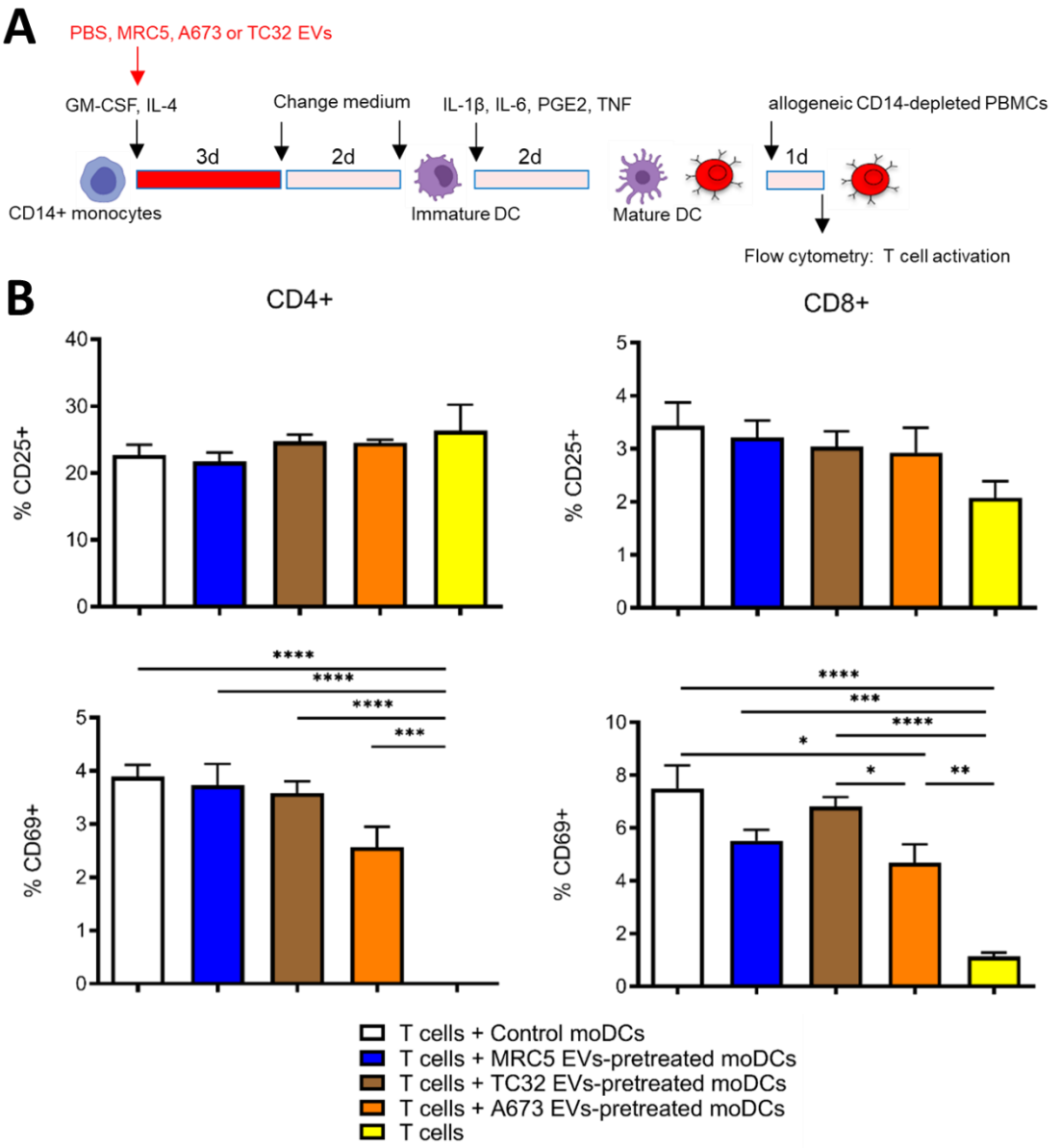

Supplementary Figure 5 CD8$^+$ T cells upregulate less CD69 (but not CD25) activation marker when co-cultured with allogeneic CD14$^+$ monocytes differentiated in the presence of EwS EVs.

(**A**) Experimental layout (B). Healthy donor-derived CD14$^+$ monocytes cells were differentiated by GM-CSF and IL-4 for 5 days and matured to moDCs by IL-1β, IL-6, PGE_2 and TNF for 2 additional days. 3 x 10^9 EV particles/ml from A673, TC32 or MRC5 cells or PBS as control were added on day 0. At day 7, EV-pretreated CD14$^+$ moDCs were co-cultured with CD14-depleted PBMCs at a ratio of 1:2 for 24 h. (**B**) CD25 and CD69 surface expression on CD3$^+$CD4$^+$ and CD3$^+$CD8$^+$ T cells was assessed by flow cytometry. Isotype (IT) controls were used to gate on positive events. Representative result from two independent donors with three independent EV preparations are shown. Data are presented as mean ± SD. One-way ANOVA with multiple comparison Tukey test (C) was used to calculate p values. * $p \leq 0.05$, ** $p \leq 0.01$, *** $p \leq 0.001$ and *** $p \leq 0.0001$.

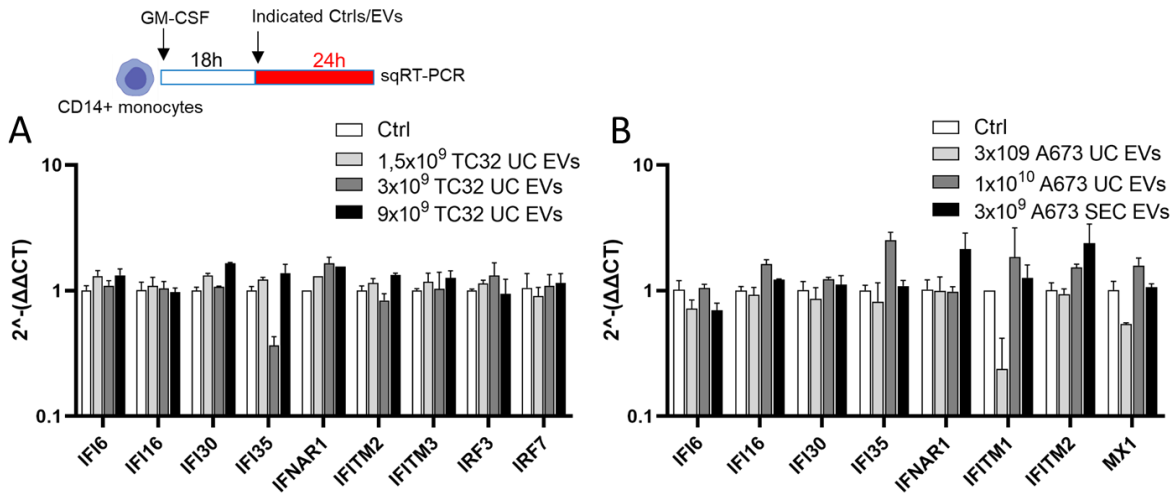

Supplementary Figure 6 Unchanged ISGs in response to EwS EVs in CD14$^+$ monocytes.

(**A, B**) CD14$^+$ monocytes were seeded for 18 h in X-VIVO medium containing 1 % human AB serum and GM-CSF (80 U/ml), and treated for 24 h with PBS as control (Ctrl) or indicated amount of EVs from TC32 (**A**) or A673 (**B**). Gene expression was quantified by sqRT-PCR. Representative results from two independent donors are shown. Data are presented as mean ± SD.

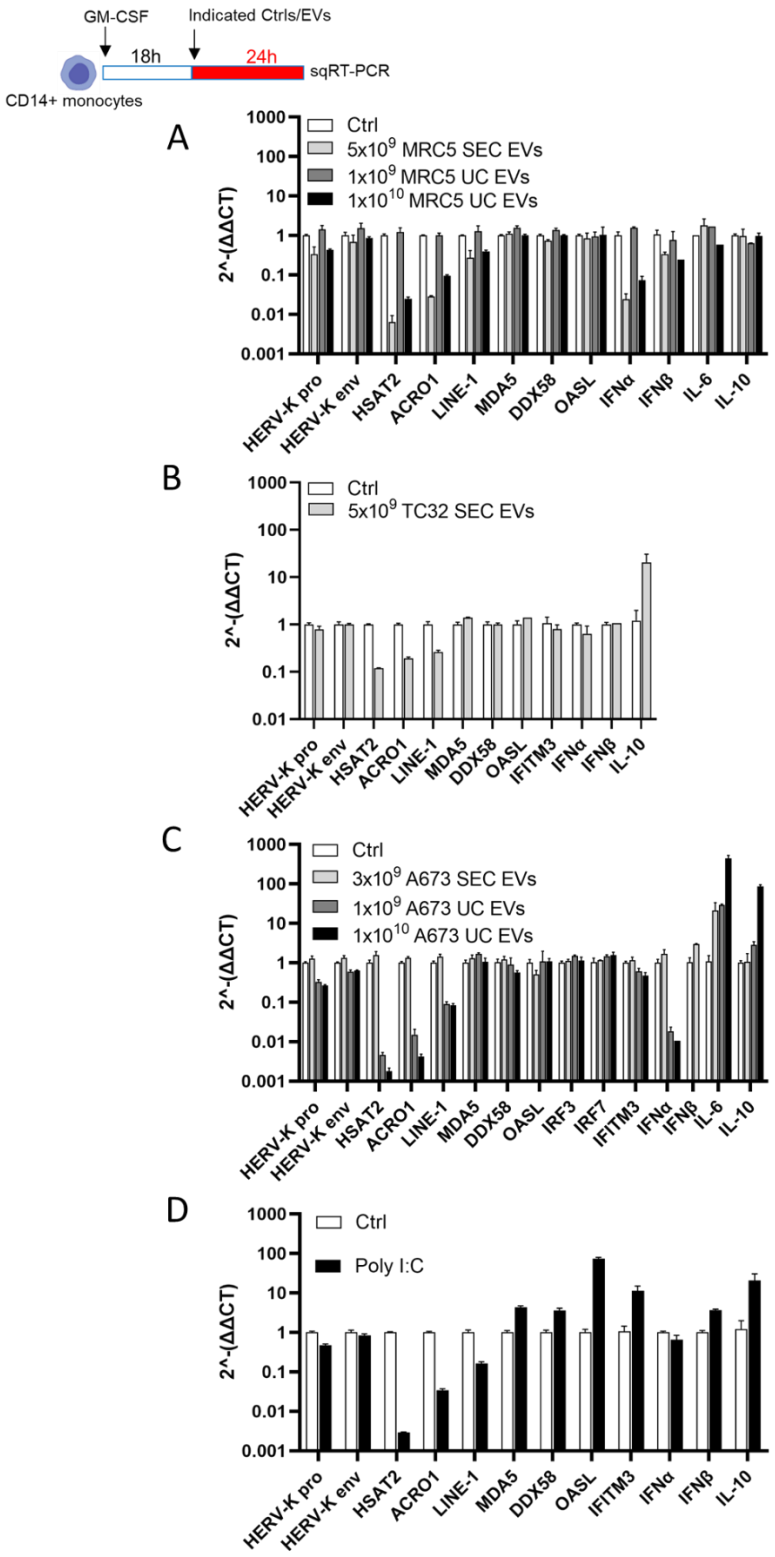

Supplementary Figure 7 EwS EVs downregulate RE and ISGs in CD14⁺ monocytes in one of five healthy donors.

(**A**–**D**) CD14⁺ monocytes were seeded for 18 h in X-VIVO medium containing 1 % human AB serum and GM-CSF (80 U/ml), and treated for 24 h with indicated amount of EVs isolated by UC and SEC from MRC5(**A**), TC32 (**B**), A673 (**C**), or PBS as control (Ctrl). Poly(I:C) (2 µg/ml) was used as positive controls (**D**). Gene expression was quantified by sqRT-PCR. Results were obtained from one independent donor. Data are presented as mean ± SD.

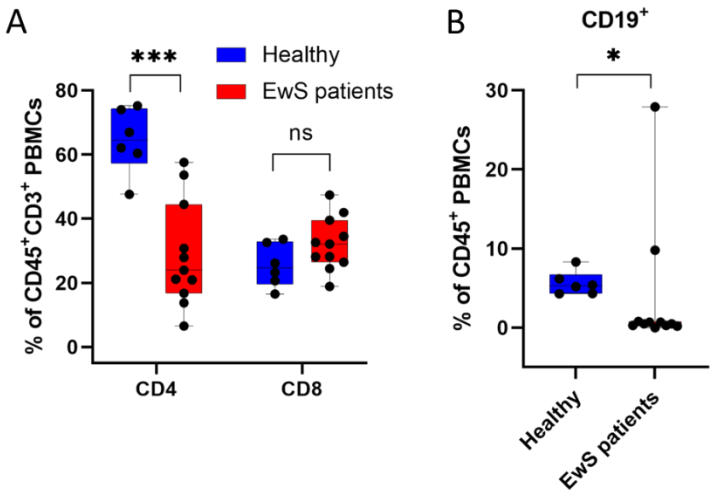

Supplementary Figure 8 Reduced frequencies of CD4$^+$ T cells and CD19$^+$ B cells in CD45$^+$ PBMCs of EwS patients compared to healthy donors.

(**A, B**) PrimeFlow RNA assay of PBMCs from healthy donors and EwS patients. (**A**) Frequency of CD4$^+$ and CD8$^+$ T cells among CD45$^+$CD3$^+$ PBMCs of healthy donors (n = 6) or EwS patients (n = 11). (**B**) Frequency of CD19$^+$ B cells among CD45$^+$ PBMCs of healthy donors (n = 6) or EwS patients (n = 11). Data are presented as box plots with min, median and max. Mann-Whitney U test (A,B) was used to calculate p values. * $p \leq 0.05$ and *** $p \leq 0.001$.

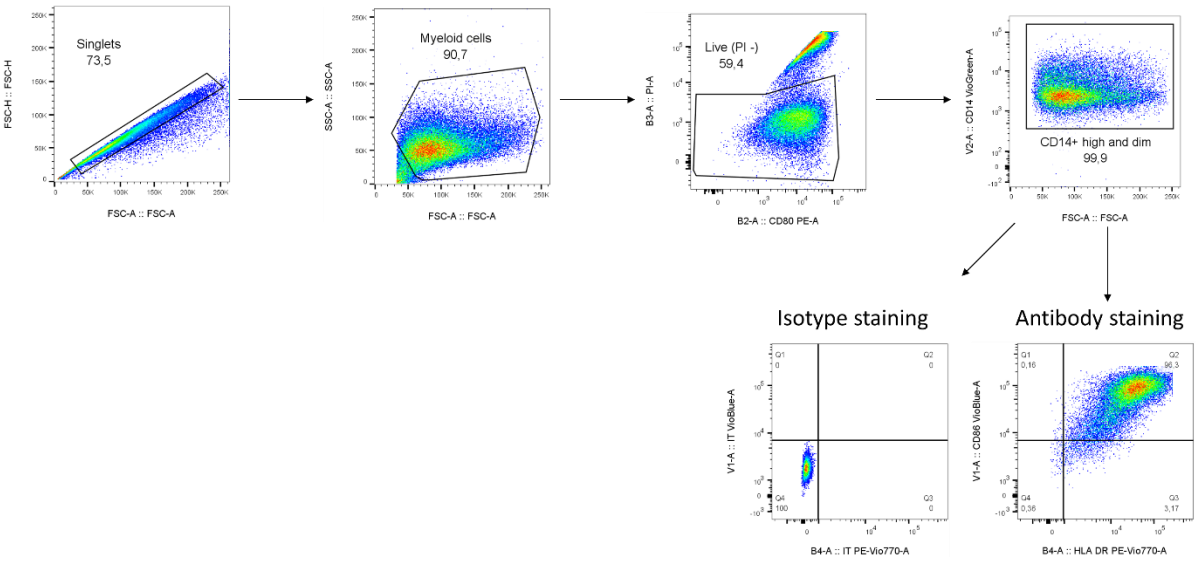

Supplementary Figure 9 Flow cytometry gating strategy of myeloid cells.

9.2 Abbreviations

AF	Alexa Fluor
ANOVA	Analysis of variance
APS	Ammonium persulfate
ARG1	Arginase 1
Aza	Azacytidine
Bp	Base pair
BSA	Bovine serum albumin
C/EBP	CCAAT-Enhancer Binding Protein
cGAS	Cyclic GMP-AMP synthase
CAR	Chimeric antigen receptor
CCL2	(C-C motif) ligand 2
CCR	Childhood Cancer Repository
CCR2	C-C chemokine receptor type 2
CD	Cluster of differentiation
CDKs	Cyclin-dependent kinases
cDNA	Complementary DNA
Ctrl	Control
CPI	Checkpoint inhibitors
CTLA-4	Cytotoxic T lymphocyte antigen-4
CXCL9/10	C-X-C Motif Chemokine Ligand 9/10
CXCR3	C-X-C Motif Chemokine Receptor 3
DAMPs	Danger associated patterns
DAPI	4',6-diamidino-2-phenylindole
ddH_20	Double-distilled H_20
DMSO	Dimethylsulfoxide
DMEM	Dulbecco's Modified Eagle's Medium
DNMTi	DNA methyltransferase inhibitors
DTT	Dithiothreitol
EDTA	Ethylenediaminetetraacetic acid
Env	(Retroviral) envelope protein
ESCRT	Endosomal sorting complex required for transport
ETS	E-twenty-six
EVs	Extracellular vesicles
EwS	Ewing sarcoma
EWSR1	Ewing's sarcoma breakpoint region 1
EZH2	Enhancer of Zeste, *Drosophila*, Homolog 2
FBS	Fetal bovine serum
FLI1	Friend leukemia virus integration 1
FMO	Fluorescence minus one
FPKM	Fragments per kilobase of transcript per million mapped reads
FUS	Fused in sarcoma
Gag	(Retroviral) structural proteins
GAPDH	Glyceraldehyde 3-phosphate dehydrogenase
G-CSF	Granulocyte colony-stimulating factor
GM-CSF	Granulocyte-macrophage colony-stimulating factor
gMFI	Geometric mean fluorescence intensity
HER2	Human epidermal growth factor receptor 2
HLA	Human leukocyte antigen
HSAT	Human satellite

Hsp	Heat shock protein
HUVEC	Human umbilical vein endothelial cells
IDO	Indoleamine 2,3-dioxygenase
IFITM	Interferon-induced transmembrane protein
IFN	Interferon
IFNARs	Interferon-α/β receptors
IGF1R	Type I insulin-like growth factor receptor
IKKε	IκB kinase-ε
ILVs	Intraluminal vesicles
IL	Interleukin
IRF	Interferon-regulatory factor
ISGs	Interferon-stimulated genes
ISREs	Interferon-stimulated response elements
IT	Isotype
KRAB-ZNF	Krüppel-associated box domain zinc finger
LINEs	Long interspersed nuclear elements
LPS	Lipopolysaccharide
LTR	Long terminal repeat
MaLR	Mammalian apparent LTR retrotransposons
MAVS	Mitochondrial antiviral signaling protein
MDA5	Melanoma differentiation associated gene 5
MDSCs	Myeloid-derived suppressor cells
MEM	Minimum Essential Medium
MHC	Major histocompatibility complex
M-MDSCs	Monocytic-MDSCs
MoDCs	Monocytic-derived dendritic cells
MSigDB	Molecular Signature Database
MVE	Multivesicular endosome
MYD88	Myeloid differentiation primary response 88 protein
NF-κB	Nuclear factor kappa B
NGFR	Nerve growth factor receptor
ns	Not significant
NTA	Nanoparticle Tracking Analysis
OAS	Oligoadenylate synthase
ORF	Open reading frame
PAMPs	Pathogen associated patterns
PBMCs	Peripheral blood mononuclear cells
PBS	Phosphate-buffered saline
PD-1	Programmed cell death protein 1
PDAC	Pancreatic ductal adenocarcinoma
PD-L1	Programmed death ligand 1
PGE_2	Prostaglandin E2
PhD	Doctor of philosophy
PI	Propidium iodide
PMSF	Phenylmethylsulfonyl fluoride
Pol	Polymerase
Poly(I:C)	Polyinosinic–polycytidylic acid
Pro	(Retroviral) protease
PRRs	Pattern recognition receptors
RE	Endogenous retroelements
rh	Recombinant human

RIG-I	Retinoic acid-inducible gene I
RLRs	RIG-I-like receptors
ROR1	Receptor tyrosine kinase-like orphan receptor 1
RPMI	Roswell Park Memorial Institute Medium
RT	Reverse transcriptase
SCT	Stem cell transplantation
SD	Standard deviation
SDS	Sodium dodecyl sulfate
SEM	Standard error of the mean
SINEs	Short interspersed nuclear elements
STAG2	Cohesin subunit SA-2
sqRT-PCR	Semi-quantitative real-time polymerase chain reaction
STAT	Signal transducer and activator of transcription
STEAP1	Six-transmembrane epithelial antigen of the prostate 1
STING	Stimulator of IFN genes
TAE	Tris-acetate-EDTA
TAF15	TATA-binding protein-associated factor 15
TAMs	Tumor-associated macrophages
TBK1	TANK-binding kinase 1
TCR	T cell receptor
TLR	Toll-like receptor
TME	Tumor microenvironment
TMED	Tetramethylethylenediamine
TNF	Tumor necrosis factor
TP53	Tumor suppressor p53
TRIF	TIR-domain-containing adapter-inducing interferon-β
Tris	Tris(hydroxymethyl)aminomethane
TSG101	Tumor susceptibility gene 101
UC	Ultracentrifugation
UTR	Untranslated region
VEGFR2	Vascular endothelial growth factor receptor 2

9.3 List of figures and supplementary figures

9.3.1 List of figures

9.3.2 List of supplementary figures

9.4 List of tables

10 Declaration of shared data in two dissertations

Data from the following sections presented in this Ph.D. thesis were generated together with Kira Schneider and will also be published in her MD thesis (Dr. med.):

5.1 Isolation and characterization of EVs from cell culture supernatant and human plasma
5.2 EwS cell line EVs induce a pro-inflammatory response in myeloid cells
5.3 EwS cell line EVs impair the differentiation and maturation of myeloid cells towards moDCs
5.4 EwS cell line EVs modulate gene expression of myeloid cells associated with inflammatory responses and semi-mature phenotype
5.5 EwS cell line EVs reduce the T cell stimulatory capacity of moDCs

The data of the above sections have been published in the peer-reviewed journal *Cells* with Hendrik Maximilian Gaßmann and Kira Schneider as shared first authors. Cells 2021, 10, 2081. https://doi.org/10.3390/cells10082081 [291].

Hereby both parties confirm that aforementioned data were compiled in collaboration and contributions are mutually agreed.

_____	_____
Location and date	Location and date
_____	_____
Kira Schneider (signature)	Hendrik M. Gaßmann (signature)

11 Publications related to this PhD thesis

Original articles (peer-reviewed)

Schober, S.J.; Hallmen, E.; Reßle, F.; Gassmann, H.; Prexler, C.; Wawer, A.; von Luettichau, I.; Ladenstein, R.; Kazanowska, B.; Ljungman, G.; et al. No Improvement of Survival for Alveolar Rhabdomyosarcoma Patients After HLA-Matched Versus -Mismatched Allogeneic Hematopoietic Stem Cell Transplantation Compared to Standard-of-Care Therapy. Front Oncol 2022, 12.

Gassmann, H.; Schneider, K.; Evdokimova, V.; Ruzanov, P.; Schober, S.J.; Xue, B.; von Heyking, K.; Thiede, M.; Richter, G.H.S.; Pfaffl, M.W.; Noessner, E.; Stein, L.D.; Sorensen, P.H.; Burdach, S.E.G.; Thiel, U. Ewing Sarcoma-Derived Extracellular Vesicles Impair Dendritic Cell Maturation and Function. Cells 2021, 10, 208.

Biele, E.; Schober, S.J.; Prexler, C.; Thiede, M.; Heyking, K.V.; Gassmann, H.; Eck, J.; Xue, B.; Burdach, S.; Thiel, U. Monocyte Maturation Mediators Upregulate CD83, ICAM-1 and MHC Class 1 Expression on Ewing's Sarcoma, Enhancing T Cell Cytotoxicity. Cells 2021, 10.

Thiel U., Schober S.J., Ranft A., Gassmann H., Jabar S., Gall K., von Lüttichau I., Wawer A., Koscielniak E., Diaz M.A., Ussowicz M., Kazantsev I., Afanasyev B., Merker M., Klingebiel T., Prete A., Gruhn B., Bader P., Jürgens H., Dirksen U., Handgretinger R., Burdach S., Lang P. No difference in survival after HLA mismatched versus HLA matched allogeneic stem cell transplantation in Ewing sarcoma patients with advanced disease. Bone Marrow Transplantation 2021.

Schober, S.J.; Thiede, M.; Gassmann, H.; Prexler, C.; Xue, B.; Schirmer, D.; Wohlleber, D.; Stein, S.; Grünewald, T.G.P.; Busch, D.H.; Richter, G.H.S.; Burdach, S.E.G.; Thiel, U.: „MHC Class I-Restricted TCR-Transgenic CD4+ T Cells Against STEAP1 Mediate Local Tumor Control of Ewing Sarcoma In Vivo.“ Cells 2020, 9, 1581.

Preprint articles (not peer-reviewed)

Evdokimova V., Ruzanov P., Gassmann H., Zaidi S.H., Peltekova V., Heisler L.E., McPherson J.D., Orlic-Milacic M., Specht K., Steiger K., Schober S.J., Thiel U., McKee T.D., Zaidi M, Spring C.M., Lapouble E., Delattre O., Burdach S., Stein L.D., Sorensen P.H.: „Exosomes transmit retroelement RNAs to drive inflammation and immunosuppression in Ewing Sarcoma.“ bioRxiv 2019, 806851.

Conference contributions

Gassmann H., Schneider K., Evdokimova V., Ruzanov P., Xue B., von Heyking K., Thiede M., Schober S.J., Stein L.D., Sorensen P.H. , Thiel U. and Burdach S. Ewing Sarcoma-Derived Extracellular Vesicles Impair Dendritic Cell Maturation and Function. ePoster Title(s): #1318, 53rd Congress of the International Society of Paediatric Oncology (SIOP).

Gassmann H., Schneider K., Evdokimova V., Ruzanov P., Schober S.J., Xue B., von Heyking, K.; Thiede, M.; Richter, G.H.S.; Pfaffl, M.W.; Noessner, E.; Stein, L.D.; Sorensen, P.H.; Burdach, S.E.G.; Thiel, U. Ewing Sarcoma-Derived Extracellular Vesicles Impair Dendritic Cell Maturation and Function. Poster abstract P8, 4th Autmn Meeting of the German Society for Extracellular vesicles.

12 Acknowledgements

I would like to express special thanks to Prof. Dr. med. Stefan Burdach for his encouraging supervision and scientific input. He provided a broad scientific picture and drove progress in the project, for which he connected scientists from Vancouver, Toronto and Munich. These collaborations were pivotal, fruitful and productive.

I am very grateful to PD Dr. med. Uwe Thiel, who supported me as a scientific mentor with straightforward experimental suggestions and focus on the translational relevance. But he also backed me up in difficult times, made me question decision, and provided a productive, welcoming and pleasant environment.

I especially like to thank Prof. Dr. rer. nat. Elfriede Nößner for her mentorship and expert knowledge in immunology. She taught me to realistically approach time schedules for experiments, to enquire the relevance of experimental data and to look for further implications in results.

I thank Dr. Dr. med. Sebastian J. Schober, who introduced me to the fascination of translational immunology research and history of cancer therapy, encouraging me to pursue cancer immunology together with him. We had many great discussions, troubleshootings and fine moments outside of the lab.

Valentina Evdokimova, PhD and Peter Ruzanov, PhD for your true friendship, the time in Toronto, your hospitality, the introduction into the world of science and the curiosity for the unknown. Furthermore, I thank Lincoln Stein, MD, PhD, Poul Sorensen MD, PhD and Laszlo Radvanyi, PhD for the scientific discussions and the opportunity to join OICR, Toronto, Canada as a visiting scientist.

I am particularly thankful to our team in the lab, which is always happy, friendly and helpful. Kira Schneider for enduring the challenges of our project and her contributions solving them. Busheng Xue for significantly improving my lab techniques, his support even into the night, our scientific discussions and the time we spent outside the lab. Melanie Thiede, Jennifer Eck, Laetitia von Bismarck and Dr. rer. nat. Kristina von Heyking who helped to establish methods, perform experiments and deal with machines and experiments not working as intended. I want to thank Prof. Dr. rer. nat. Günther Richter supporting the first steps of the project.

I also thank Prof. Dr. rer. nat. Michael Pfaffl, Christian Gätz und Dapi Meng-Lin Chiang. They warmly welcomed me at the Division of Animal Physiology and Immunology, TUM. Their expert technical advices and suggestions were critical to obtain reliable data.

Lastly, I am indebted to my family, which always fully supports me. Thank you! My gratefulness goes to Caterina for your love, empathy, patience, support and wonderful nature.